Blocking necroptosis through a genetic point mutation of MLKL mitigates obesity, MASLD and MetALD progression

Von der Fakultät für Mathematik und Naturwissenschaften der RWTH Aachen University zur Erlangung des akademischen Grades eines Doktors der Naturwissenschaften genehmigte Dissertation

vorgelegt von

Master of Science

Michael Thaddäus Singer

aus Isny im Allgäu

Berichter: Prof. Dr. med. Mathias Walter Hornef
Prof. Dr. med. Tom Lüdde, PhD
Prof. Dr. Lars Mathias Blank

Tag der mündlichen Prüfung: 25.02.2026

Diese Dissertation ist auf den Internetseiten der Universitätsbibliothek verfügbar.

Abstract

Obesity and chronic liver disease nowadays affect about 30% of the population, especially in western countries, tendency rising, already putting health systems under extreme pressure. A sedentary life style combined with a surplus of calories can lead to widespread changes throughout the body, including excessive expansion of adipose tissue, inflammatory processes, disturbances in glucose and insulin signaling, steatotic liver and cardiovascular diseases, and even certain types of cancer. Despite the severity of metabolic diseases, their pharmaceutical treatments are still limited, highlighting the ever increasing importance of research in this field.

Chronic liver diseases are often associated with increased levels of programmed cell death such as apoptosis (non-immunogenic) and necroptosis (immunogenic). Studies could show, that effector proteins of necroptosis show upregulation in patients suffering from MASH, suggesting active involvement of necroptosis in the progression of MASLD. Animal studies that were using KO models of necroptosis executer MLKL were showing ambiguous results. While some claimed that MLKL deletion protects animals from diet-induced body weight gain, liver steatosis and insulin resistance, others could not see any protection at all.

Due to indecisive literature, we decided to apply a novel MLKL point mutation (K219R), which expresses a full-length MLKL protein, while fully blocking its oligomerization, and thereby, necroptosis execution. We further applied three different feeding cohorts to animals: high caloric western diet alone (MASH) or in combination with alcohol (MetALD) as well as a control diet (NCD).

While we could not observe a complete rescue in MLKL^{K219R} animals from diet- and alcohol-induced changes, we show significant improvements of metabolic markers in these animals when compared to controls. These improvements are reflected by reduced body weight gain and adipose tissue mass, decreased levels of liver steatosis as well as liver damage associated serum markers. We could show mild effects on lipid metabolism in MLKL^{K219R} livers, and we were able to show significantly reduced inflammation in epididymal adipose tissue as well as reduced differentiation potential of primary adipocytes from inguinal adipose tissue. Furthermore, animals on control diet did not show any spontaneous phenotype differences when compared to WT animals, but they displayed increased physical activity, potentially suggesting higher energy expenditure of MLKLK^{K219R} animals.

By applying another point mutation to the upstream kinase and activator of necroptosis, RIPK1, we failed to observe any protective effects on diet-induced metabolic changes, suggesting that MLKL acts independent of RIPK1. Due to the fact, that we were not able to detect the phosphorylated form of MLKL, we suggest, that MLKL, in a metabolic context, acts cell-type specific as well as independent of necroptosis and its upstream kinases RIPK1/3.

Consequently, this study makes a significant contribution to the ongoing scientific discourse around MLKL and its role in metabolic processes.

Zusammenfassung

Übergewicht und chronische Lebererkrankungen betreffen heutzutage etwa 30% der Bevölkerung, insbesondere in westlichen Ländern. Die steigende Tendenz dieser Erkrankungen setzen die Gesundheitssysteme damit bereits heute massiv unter Druck. Ein sedativer Lebensstil in Kombination mit einem Kalorienüberschuss kann zu weitreichenden Veränderungen im gesamten Körper führen. Dazu zählen eine übermäßige Expansion des Fettgewebes, entzündliche Prozesse, Störungen in der Glukose- und Insulinsignalübertragung, steatotische Leber-, sowie kardiovaskuläre Erkrankungen und bestimmte Krebsarten. Trotz der Schwere metabolischer Erkrankungen sind pharmakologische Behandlungsmöglichkeiten nach wie vor begrenzt, was die zunehmende Bedeutung der Forschung in diesem Bereich unterstreicht.

Chronische Lebererkrankungen gehen häufig mit einem erhöhten Vorkommen von programmiertem Zelltod einher, wie z.B. Apoptose (nicht-immunogen) und Nekroptose (immunogen). Studien konnten zeigen, dass Effektoren der Nekroptose bei PatientInnen mit MASH hochreguliert sind, was auf eine aktive Beteiligung der Nekroptose an der Progression von MASLD hindeutet. Tierstudien mit Knockout-Modellen des Proteins MLKL, welches für die Ausführung der Nekroptose verantwortlich ist, lieferten bislang uneindeutige Ergebnisse. Während einige Studien zeigten, dass ein Fehlen von MLKL Tiere vor diätinduzierter Gewichtszunahme, Lebersteatose und Insulinresistenz schützt, konnten andere Studien diese Effekte nicht beobachten.

Aufgrund dieser widersprüchlichen Datenlage haben wir beschlossen, eine neuartige Punktmutation in MLKL (K219R) zu verwenden, die ein voll funktionsfähiges, nicht-oligomerisierbares MLKL-Protein exprimiert und somit die Nekroptose vollständig blockiert. Wir haben drei verschiedene Fütterungskohorten auf Versuchstiere angewandt: eine hochkalorische „Western Diet“ allein (MASH), oder in Kombination mit Alkohol (MetALD), sowie eine Standarddiät (NCD) zur Kontrolle.

Obwohl wir bei $MLKL^{K219R}$-Tieren keine vollständige Rettung vor diät- oder alkoholinduzierten Veränderungen beobachten konnten, zeigen unsere Ergebnisse im Vergleich zu Kontrolltieren signifikante Verbesserungen metabolischer Marker. Diese Verbesserungen äußern sich in einer reduzierten Gewichtszunahme, reduzierten Fettmasse, verminderten Lebersteatose sowie einem geringeren Level an leberschadenassoziierten Serummarkern. Während wir in den Lebern der $MLKL^{K219R}$-Tiere nur geringe Effekte auf den Lipidstoffwechsel feststellen konnten, zeigte das epididymale Fettgewebe deutlich weniger Entzündungen, sowie ein verringertes Differenzierungspotential primärer Adipozyten aus inguinalem Fettgewebe. Tiere, die eine Kontrolldiät erhielten, zeigten im Vergleich zu WT-Tieren keine phänotypischen Unterschiede, wiesen jedoch eine gesteigerte körperliche Aktivität auf, was auf einen erhöhten Energieverbrauch von $MLKL^{K219R}$-Tieren hinweisen könnte.

Bei Anwendung einer weiteren Punktmutation in der Upstream-Kinase RIPK1, unter anderem einem Aktivator der Nekroptose, konnten wir hingegen keine protektiven Effekte hinsichtlich diätinduzierter metabolischer Veränderungen feststellen, was darauf hindeutet, dass MLKL unabhängig von RIPK1 agiert. Da wir zudem keine phosphorylierte Form von MLKL nachweisen konnten, schlagen wir vor, dass MLKL im metabolischen Kontext nicht

nur zelltypspezifisch, sondern auch unabhängig von der klassischen Nekroptose und ihren upstream-Kinasen RIPK1/3 agiert.

Somit leistet diese Studie einen wichtigen Beitrag zur laufenden wissenschaftlichen Diskussion über die Rolle von MLKL in metabolischen Kontext.

Contents

List of Abbreviations

ALD	alcoholic liver disease
AP	alkaline phosphatase
Apaf-1	apoptotic protease activating factor-1
ALT	alanine transaminase
AMPK	AMP-activated protein kinase
AST	aspartate transferase
ATP	adenosine triphosphate
AUC	area under the curve
BAT	brown adipose tissue
BMI	body mass index
BSA	bovine serum albumin
$CaCl_2$	calcium chloride
caspase	cysteine-dependent aspartate-directed protease
CCL2	chemokine C-C-motif ligand 2
cDNA	complementary deoxyribonucleic acid
cIAP	cellular inhibitor of apoptosis protein
Cidea	cell death-inducing DFFA-like effector A
CLD	chronic liver disease
CLS	crown-like structures
CoA	co-enzyme A
CO_2	carbon dioxide
Cpt1	carnitin-palmitoyltransferase 1
Ct	cycle threshold
CVD	cardiovascular disease
CYLD	cylindromatosis
CytC	cytochrome C
DAMP	damage-associated molecular patterns
DED	death effector domain
Dgat1	diacylglycerol-O-acyltransferase 1
DISC	death-inducing Signaling complex
DNA	deoxyribonucleic acid
DR	death receptor
dH2O	distilled Water
EBSS	Earle’s balanced salt solution
ECL	enhanced chemoluminescence
EDTA	ethylenediaminetetraacetic acid
ELISA	enzyme-linked immunosorbent assay
ER	endoplasmic reticulum
ESCRT	endosomal sorting complexes required for transport
EtOH	ethanol
EV	extracellular vesicle
eWAT	epididymal/visceral WAT

FA	fatty acids
Fabp4	fatty acid binding protein 4
FADD	Fas-associated protein with death-domain
Fas	FS-7-associated cell surface antigen
FasL	Fas ligand
Fasn	fatty acid synthesis
FBS	fetal bovine serum
FFA	free fatty acid
FGF21	fibroblast growth factor 21
FLIP	FLICE-like inhibitory protein
GAPDH	glyceraldehyde-3-phosphate dehydrogenase
GLDH	glutamate dehydrogenase
GLUT2	glucose transporter 2
GM-CSF	granulocyte-macrophage colony-stimulating factor
GTT	glucose tolerance test
HBSS	Hank's balanced salt solution
HCC	hepatocellular carcinoma
HCV	hepatitis C virus
HDL	high density lipoprotein
H&E	hematoxilin & eosin
HEPES	4-(2-hydroxyethyl)-1-piperazineethanesulfonic acid
HFD	high-fat diet
HIF1	hypoxia inducible factor 1
HPRT	hypoxanthine guanine phosphoribosyltransferase
HRP	horse radish peroxidase
IBMX	3-isobutyl-1-methylxanthine
IFNR	interferon receptor
iWAT	inguinal/subcutaneous WAT
IHC	immunohistochemical
IKK	IκB kinase
IL	interleukin
IR	insulin resistance
JAK	Janus kinase
KO	knock out
LCL	N-[(1S)-1-cyclohexyl-2-[(2S)-2-[4-(4-fluorobenzoyl)-2-thiazolyl]-1-pyrrolidinyl]-2-oxoethyl]-2S-(methylamino)-propanamide
LD	lipid droplets
LDL	low density lipoprotein
LPS	lipopolysaccharide
LSD	least significant difference
LUBAC	linear ubiquitin chain (M1) assembly complex
MAPK	mitogen-activated protein kinase
MASH	metabolic dysfunction-associated steatohepatitis

MASLD	metabolic dysfunction-associated steatoic liver disease
MetALD	metabolic dysfunction and alcohol associated liver disease
MLKL	mixed lineage kinase domaine like
MOMP	mitochondrial outer membrane permeabilization
mRNA	messenger RNA
NaCl	natrium chloride
NAS	NAFLD activity score
NAFLD	nonalcoholic fatty liver disease
NASH	nonalcoholic steatohepatitis
NCD	normal chow diet
Nec1s	necrostatin-1s
NEFA	non-esterified fatty acid
NEMO	NF-κB essential modulator
NF-κB	nuclear factor kappa-light-chain-enhancer of activated B-cells
NLRP3	NOD-like receptor protein 3
PBS	phosphate buffered saline
PCD	programmed cell death
PCR	polymerase chain reaction
PI	propidium iodide
pMLKL	phosphorylated mixed lineage kinase domain-Like
PPARα	peroxisome proliferator-activated receptor α
PRDM16	PR/SET domain 16
PVDF	polyvinylidene fluoride
qPCR	quantitative polymerase chain reaction
RFU	relative fluorescence units
RHIM	RIP homotypic interaction motif
RIPK	receptor-interacting serine/threonine kinase
RNA	ribonucleic acid
ROS	reactive oxygen species
RT	room temperature
RT-PCR	reverse transcription polymerase chain reaction
Scd1	stearoyl-CoA desaturase-1
SD	standard deviation
SDS-PAGE	sodium-dodecyl-polyacrylamide gel electrophoresis
siRNA	small interfering RNA
SLD	steatotic liver disease
SPA	spontaneous physical activity
STAT	signal transducer and activator of transcription
TAG	triacylglycerol
TNF	tumor necrosis factor
TNFR1	tumor necrosis factor receptor 1
TLR	toll-like receptor
Traf	TNF receptor associated factor

TRADD	TNFR1-associated death domain
TSZ	TNF + Smac-Mimetic + zVAD
T2D	type-2-diabetes
UCP1	uncoupling protein 1
VLDL	very low-density lipoprotein
WAT	white adipose tissue
WD	western diet
WT	wild type
ZBP1	Z-DNA binding protein 1
zVAD	Z-Val-Ala-Asp(OMe)
4HB	4-helix bundle

Chapter 1

Introduction

1.1 Obesity

Over the past several decades, the prevalence of overweight and obesity has steadily increased, particularly in western countries. Driven by sedentary lifestyles and excessive caloric intake, obesity is now recognized as a global pandemic, affecting approximately 1 in 8 individuals worldwide. This poses significant challenges for society and global healthcare systems.[1,2] Obesity, defined by excessive fat accumulation and a body mass index (BMI) greater than 30, has profound negative effects on health.[1] It is closely associated with a wide range of comorbidities, including metabolic disorders such as type-2-diabetes (T2D), cardiovascular disease (CVD), metabolic dysfunction-associated steatoic liver disease (MASLD), and certain types of cancer, among others.[3]

Effective weight management is essential for combating obesity and its related health risks. Lifestyle interventions remain the cornerstone of obesity treatment, emphasizing dietary changes, increased physical activity, and behavioural modifications. Additionally, pharmacological therapies such as semaglutide have demonstrated significant efficacy in promoting weight loss.[4] To date, weight loss remains the most effective strategy for preventing and mitigating obesity-related diseases.

1.2 Metabolic function of adipose tissue in health and disease

Adipose tissue is primarily made from adipocytes, stem cells, vascular endothelial cells, fibroblasts as well as some immune cells.[5,6] Adipocytes and adipose tissue are pivotal in energy metabolism and thermoregulation and additionally have mechanical protective functions.[7,8] Furthermore, adipose tissue is a complex metabolic and the largest endocrine organ, regulating various processes including glucose and insulin response.

There are different types of adipose tissue, each with specialized tasks: brown adipose tissue (BAT) and white adipose tissue (WAT), the ladder of which can be further subdivided into inguinal/subcutaneous WAT (iWAT) and epididymal/visceral WAT (eWAT) (Figure 1). BAT is highly innervated and vascularized, has multilocular lipid droplets (LD), is rich in mitochondria, uncoupling protein 1 (UCP1)-positive and uses fatty acids (FA) to generate heat and maintain body temperature.[9] Adult mammals only have small amounts of BAT,

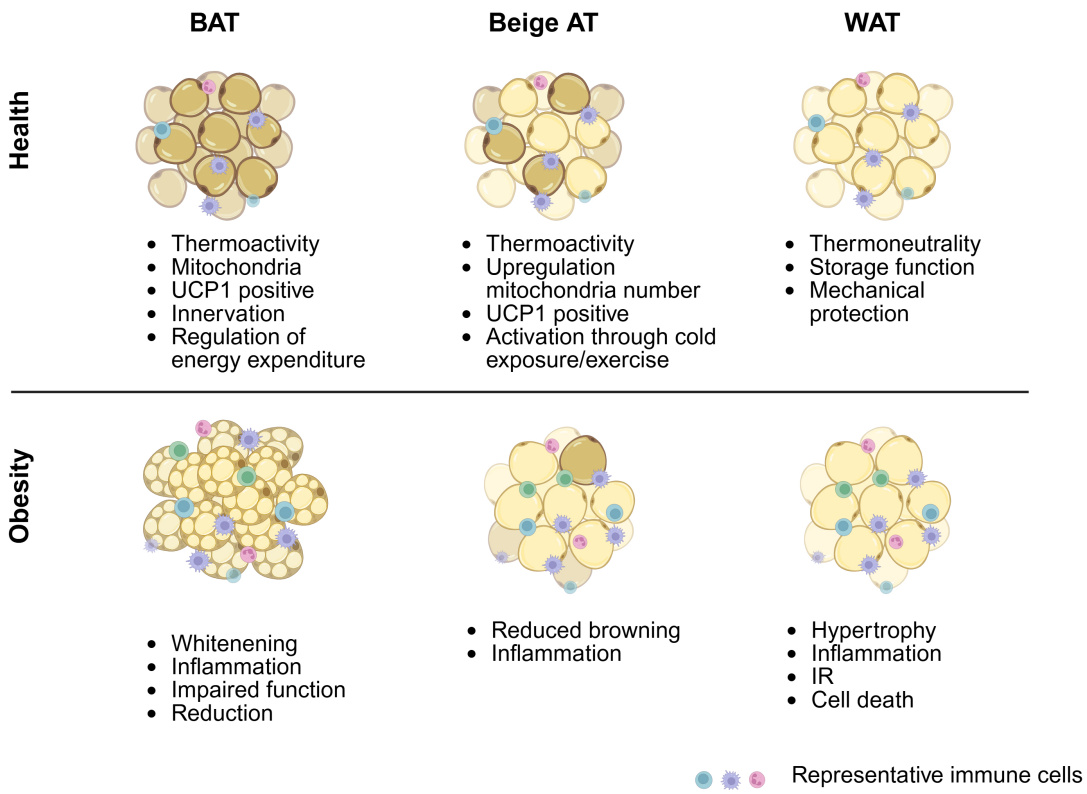

Figure 1: Schematic description of different adipose tissues with functions in healthy subjects as well as structural and functional changes induced during obesity. BAT is highly innervated, has multilocular LDs and a high amount of mitochondria. WAT on the other hand is mostly used for FA storage and is not thermoactive. Certain adipose tissue depots are able to induce browning, increasing its mitochondrial numbers and energy expenditure, further making it thermally active. During obesity, the increased amounts of FAs cause overload of fat tissues generally introducing inflammation, what further leads to impairment of their functions as well as IR or even cell death. Adapted from Scheja *et al.* and illustrated using Biorender.[12]

meanwhile infants have increased amounts.[10] Compared to BAT, adipocytes in WAT usually have only one large unilocular LD, a small number of mitochondria and their main task is to store energy (lipids) in the form of triacylglycerols (TAGs).[9] Under certain conditions such as cold stimuli, exercise or in response to specific diets, WAT has the potential to induce the process of browning, giving rise to a population of cells with characteristics intermediate between BAT and WAT, so-called beige adipose tissue, having increased energy expenditure, a higher number of mitochondria, and being UCP1-positive.[11]

After nutrient intake, pancreatic β-cells secrete insulin, primarily in response to elevated blood glucose levels. This response is further amplified by free fatty acids (FFAs). The insulin then stimulates different tissues, like skeletal muscle, liver and adipose tissue to directly regulate glucose uptake and indirectly influence lipid metabolism and overall energy homeostasis (Figure 2).[13,14] Notably, insulin secretion can also be influenced by hormonal and neuronal mechanisms. However, a detailed discussion of these processes is beyond the scope of this thesis and can be found in a study by Skelin Klemen *et al.*[15] Furthermore, immune cells are essential to maintain adipose tissue integrity as well as its metabolic function.[16] Healthy and lean adipose tissue is secreting various adipokines, chemokines, cytokines and other soluble metabolites regulating processes controlling satiety, metabolite storage and catabolism. Myeloid cells are the most abundant resident immune cells and contribute to

regulating these processes by secreting different interleukins (ILs), according to the energy state of the adipose tissue. Under healthy conditions this creates a mostly anti-inflammatory microenvironment positively affecting energy homeostasis.[17]

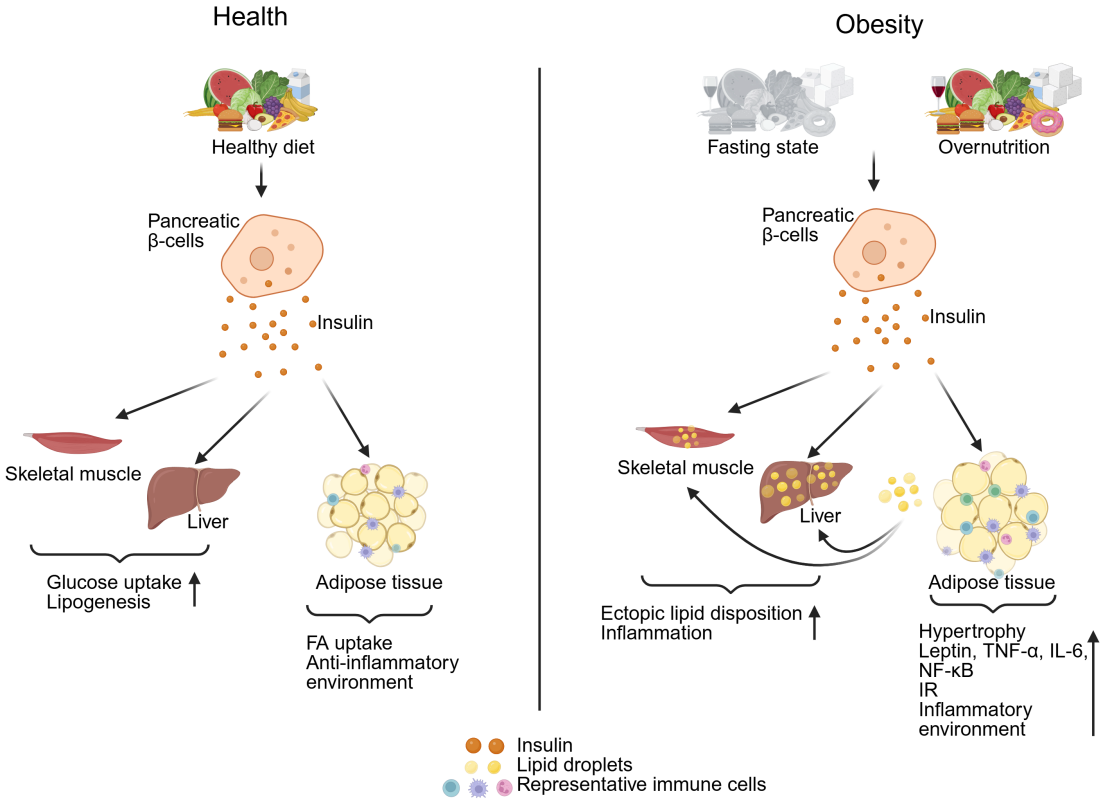

Figure 2: Overnutrition severely impacts glucose response, insulin signaling and inflammatory environment. Under healthy conditions insulin promotes fast glucose uptake to organs like skeletal muscle and liver. It further stimulates adipose tissue to uptake FA and maintain an anti-inflammatory environment. In obesity and overnutrition this sensitive balance is disturbed. Adipose tissue adapts to permanently increased nutrients by hypertrophy and altered cytokine and adipokine secretion creating an inflammatory environment. Persistant inflammation within the adipose tissue further drives IR development and ectopic lipid disposition. Adapted from Sakers *et al.* and illustrated using Biorender.[18]

In case of overnutrition adipose tissue is able to expand and resorb lipids from serum to protect from lipotoxic effects as well as ectopic lipid disposition in other organs like muscle and liver.[19,20] In general, excess of nutrients leads to increased secretion and circulation of insulin, even during fasting periods, thereby favoring anabolic processes like lipogenesis and fat storage.[21] In response to these signals, adult adipocytes enlarge (hypertrophy) and differentiation of pre-adipocytes (hyperplasia) is induced. Hypertrophy of adipocytes is one key characteristic of adipose dysfunction, inducing not only tissue remodeling but also altered secretion of a multitude of mostly pro-inflammatory adipokines and cytokines, that lead to insulin resistance (IR) as well as to induction of local inflammation.[22–25] In obesity two of the most abundant adipokines are differentially regulated in adipose tissue compared to healthy conditions: adiponectin and leptin. Adiponectin normally acts anti-inflammatory, by the downregulation of cytokines like tumor necrosis factor (TNF)-α and IL-6, maintains insulin sensitivity and helps to prevent excessive lipid accumulation in liver and skeletal muscle.[26,27] In obese subjects hypoxic and proinflammatory signaling within the WAT lead to inhibition of adiponectin secretion.[28] Leptin is produced proportionally to WAT mass and regulates under

physiological conditions a variety of processes such as energy expenditure via upregulation of lipolysis and downregulation of food intake, tissue remodeling via pre-adipocyte maturation and immune response via modulation of macrophage polarization and microenvironment. In obesity, high levels of leptin are observed in patients, yet the signaling is impaired due to commonly developed leptin resistance. Dysregulation of these adipokines shows to have severe impact on tissue and systemic homeostasis fueling inverse effects such as inflammation and fibrosis.[29–32]

Hypertrophy of adipocytes can further induce hypoxia, which through the expression of hypoxia inducible factor 1 (HIF1)-α should stimulate tissue remodeling and angiogenesis, which is impaired during obesity and further adds to the pro-inflammatory microenvironment.[33,34] The increased LD size in hypertrophic adipocytes also leads to endoplasmic reticulum (ER) stress that leads to increased activation of nuclear factor kappa-light-chain-enhancer of activated B-cells (NF-κB) signaling. NF-κB activates pro-survival as well as pro-inflammatory gene expression such asTNF-α and IL-6, which in turn recruit immune cells, especially macrophages adding to the local inflammation.[35] Maintaining that state of inflammation eventually can lead to lipotoxicity and systemic inflammation due to IR fueling development of metabolic syndrome.[25]

Taken together, these findings show how complex the development of adipose tissue dysfunction during obesity is. This also highlights how multifaceted this disease and its treatment can be, making the development of therapeutic approaches a challenging endeavor.

1.3 Metabolic function of the liver

As crucial as fat tissue is for maintaining and regulating energy, lipid and glucose metabolism, the liver plays an equally vital role. With 1.5 to 2.5% of the lean body weight it is responsible for a vast number of biochemical processes essential for surviving.[36]

One of them is the regulation of glucose homeostasis (Figure 3). Following ingestion and digestion, carbohydrates are absorbed from the small intestine and enter the bloodstream in the form of glucose. Glucose then can directly enter hepatocytes via glucose transporter 2 (GLUT2). Furthermore, in response to increased blood glucose and lipid levels, pancreatic β-cells secret insulin, which stimulates anabolic processes like glycogenesis within hepatocytes, transforming glucose into glycogen as an energy storage.[37,38] When the body enters a fasting state, and glucose and insulin levels decrease, glycogenolysis is activated in hepatocytes, breaking down glycogen into glucose, which can be transported to other tissues, where it is utilized for adenosine triphosphate (ATP) production.[39,40] During excessive fasting or exercise glycogen reserves in the liver can be depleted. In that case, liver activates gluconeogenesis, a process using glycerol, amino acids and lactate to generate glucose, that is released to stabilize blood glucose levels.[41,42]

Further, the liver plays an essential role in protein metabolism. Amino acids can either be derived from the break-down of dietary or cellular proteins. For once, the liver uses these amino acids for the synthesis of new proteins, since it is responsible for up to 90% of circulating protein, like hormones, growth factors and plasma proteins like Albumin. As earlier mentioned, the liver is able to utilize amino acids for glucose production. During this process

reactive nitrogenous molecules are formed, that can be detoxified and disposed through the urea cycle.[42,43]

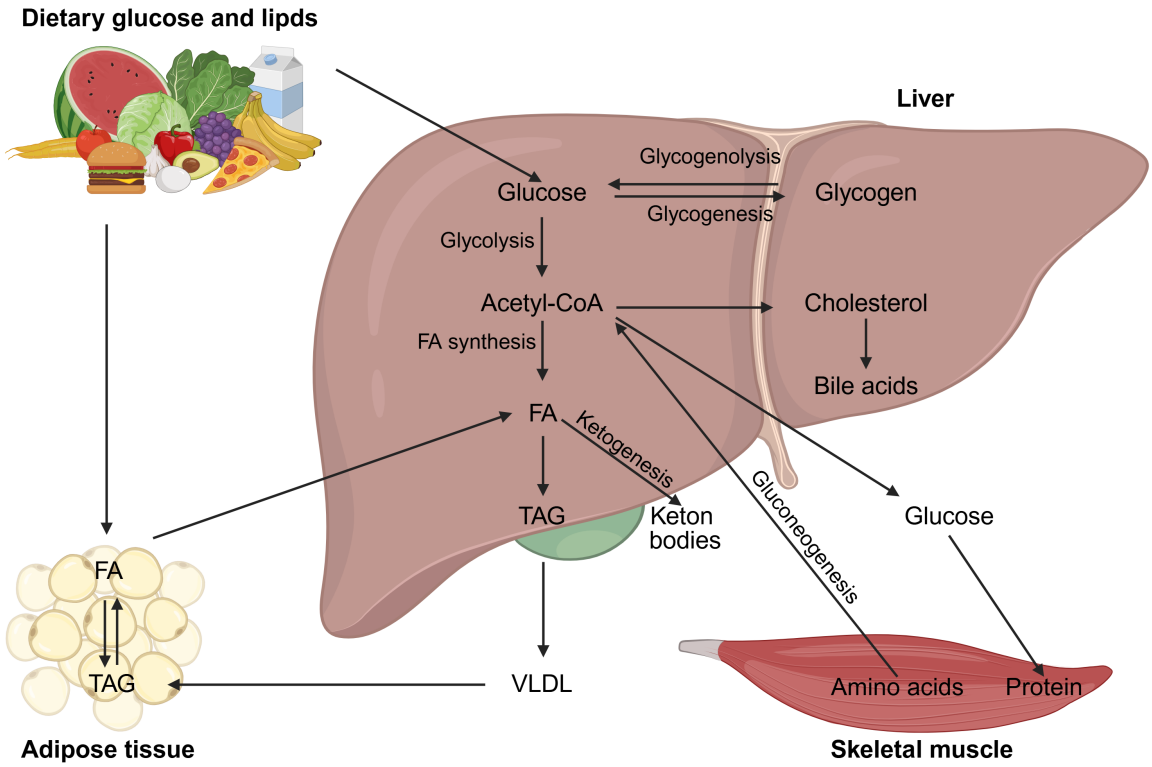

Figure 3: Overview of metabolic processes within a healthy liver. Metabolic processes in the liver are essential for keeping energy homeostasis and is closely linked with processes in other organs like adipose and muscle tissue. Dietary glucose is uptaken from the blood stream and can be used for glycogenesis for storage or for glycolysis. Adapted from Alamri *et al.* and illustrated using Biorender.[42]

Furthermore, the liver has a crucial role in lipid metabolism, owing to its profound reaction to increased lipid levels (Figure 3). Dietary lipids reach the liver either in the form of chylomicron remnants or as FFAs through the bloodstream, which can also be derived from adipose tissue. While chylomicrons enter the hepatocytes through endocytic uptake, FFAs are taken up by a variety of FA transporters, often controlled by signaling molecules like insulin.[44,45] Within the hepatocytes FAs can be utilized in multiple ways, depending on the metabolic state of the organism. While there is an excess of energy/glucose available, FAs are esterified, producing inert TAGs, as an energy storage. An excess of carbohydrates, glucose or amino acids also enables *de novo* lipogenesis, a biochemical process converting them to FAs and TAGs.[45] FAs can also be used for *de novo* cholesterol production, which is essential for generation of bile acids as well as for a functional membrane structure. TAGs can then either be stored in LDs or together with cholesterol packed into very low-density lipoproteins (VLDLs), which can be transported to *e.g.*, the adipose tissue for storage.[46] During fasting conditions on the other hand, FAs can be used for energy/ATP generation via mitochondrial β-oxidation. This process further produces acetyl-co-enzyme A (CoA), which is a substrate for *de novo* lipogenesis as well as production of ketone bodies, which can be used as alternative energy source during elongated fasting periods.[45,47,48]

Dysregulation of any of these processes from liver metabolism can have detrimental effects not only on liver, but on systemic levels. Increased or high levels of cholesterol, for example, are associated with cardiovascular disease, while a disbalance between lipolysis and lipogenesis is associated with the development of steatotic liver disease (SLD) and IR.[47]

1.4 Steatotic Liver Disease and Metabolic Dysfunction-Associated Steatoic Liver Disease

As previously seen in Chapter 1.3, dysregulated levels of circulating FFAs due to impaired adipose tissue can lead to ectopic lipid disposition in a variety of organs such as heart, liver, or muscle and have severe effects on health in general.[49,50]

SLD includes a variety of pathological conditions that all display an abnormal amount of lipid accumulation (>5%) in liver (Figure 4).[51,52] The incidences of MASLD, formerly known as nonalcoholic fatty liver disease (NAFLD), is steadily increasing worldwide and already affects more than 30% of the population, making it the most common chronic liver disease (CLD).[53–56] MASLD itself is a subcategory of SLD which at least meets one other cardiometabolic criteria additional to liver steatosis. These criteria are increased BMI (< 25), impaired glucose metabolism, high blood pressure, high triglyceride levels or low high-density cholesterol levels.[51] Moreover, meta-analyses showed that, MASLD is found in 75% of obese population and in up to 65% of diabetic population, making these major risk factors for driving the disease.[57,58]

About 20% of patients affected by MASLD further develop its progressive and inflammatory form metabolic dysfunction-associated steatohepatitis (MASH) characterized by additional hepatocellular injury such as increased immune cell infiltration and hepatocellular ballooning, making them even more prone to developing liver fibrosis, cirrhosis or even cancer (Figure 4).[52,59] Another important steatotic liver pathology is alcoholic liver disease (ALD), defined by excessive alcohol consumption (> 60 g of ethanol (EtOH) per day), accounting for 5.1% of all disease globally, also being one of the major risk factors for development of hepatocellular carcinoma (HCC).[60] For further improvement of diagnostic categorization, a new term was introduced, which is both metabolic dysfunction and alcohol associated liver disease (MetALD), describing a MASLD pathology which includes alcohol consumption and pathology, making diagnosis more precise and inclusive, overall benefiting patients.[3,61]

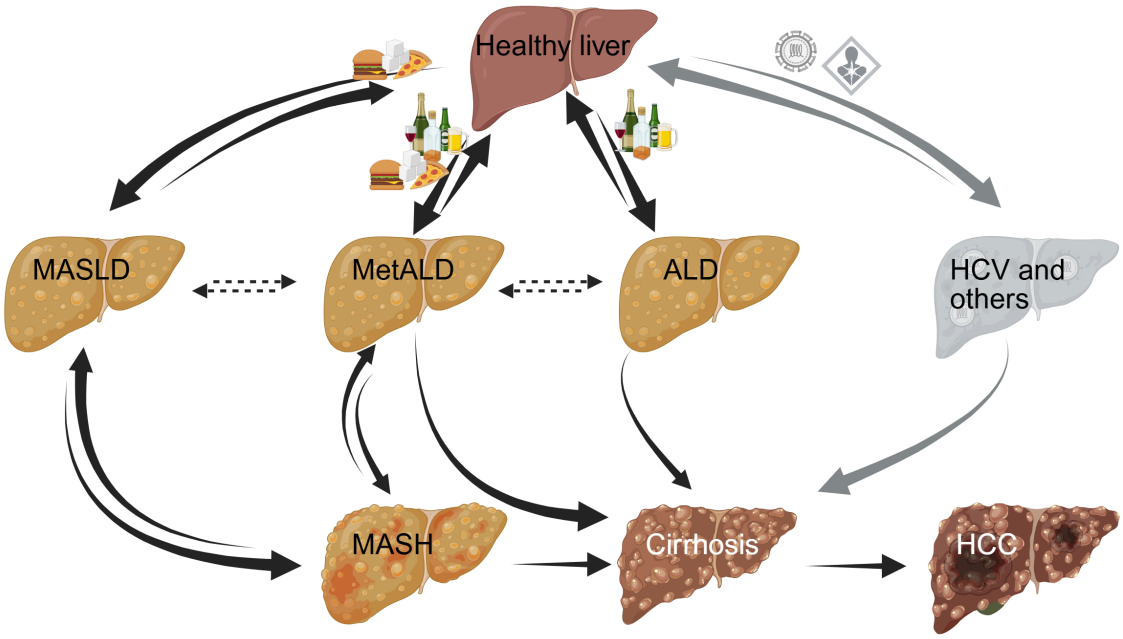

Figure 4: SLD and its various subforms. All forms of SLD are defined by the abnormal accumulation of LDs which can be triggered by stress factors such as high-caloric diets (MASLD), alcohol consumption (ALD), a mixture of both (MetALD) as well as other factors such as viral infections (e.g. hepatitis C virus (HCV)) or environmental stimuli. The solid arrows display in what way the different SLD forms can progress if untreated as well as depicting their reversibility further highlighting the complexity of CLDs. Once the state of cirrhosis is reached, liver damage is irreversible and chances for developing HCC increase drastically. The dotted arrows should highlight that the different subforms cannot always be clearly distinguished and commonly share certain pathological features. Adapted from Rinella *et al.* and Israelsen *et al.* and illustrated using Biorender.[51,52]

Risk factors as well as pathogenesis of MASLD, MASH and MetALD are complex and multifactorial. As mentioned above, obesity, T2D and alcohol consumption present the biggest risk factors for the development of MASLD and MASH. Per definition, the abnormal accumulation of lipids within hepatocytes is a central disease mechanism. In Section 1.2 the importance of adipose tissue inflammation in metabolic and liver disease was already highlighted. An ongoing state of excessive overnutrition eventually induces fat tissue inflammation and IR, followed by increased lipolysis and FFA production leading to high levels of circulating lipids. Surplus FFAs then can be dispositioned in ectopic organs like muscle, heart and liver, causing so called lipotoxicity (Figure 5).[58,62] Excessive levels of insulin as well as carbohydrates further drive intra-hepatic *de novo* lipogenesis, increasing LD formation.[63] Ultimately, the hepatocellular compensation mechanisms like β-oxidation or lipid export are exhausted, eventually increasing the production of reactive oxygen species (ROS).[64] ROS further can lead to ER stress, as well as mitochondrial damage ultimately triggering cell death and inflammatory signaling. The persistence of inflammation in the liver not only marks the progression from MASLD to MASH but is further highly associated with development of fibrosis, cirrhosis and even HCC.[57,64] For the development of a MetALD pathogenesis alcohol must be considered as an additional stressor and risk factor. Alcohol metabolism also primarily taking place in the liver can further fuel inflammatory processes, add to dysregulation of lipid metabolism and worsen insulin regulation and IR, to only name some of its effects.[65,66]

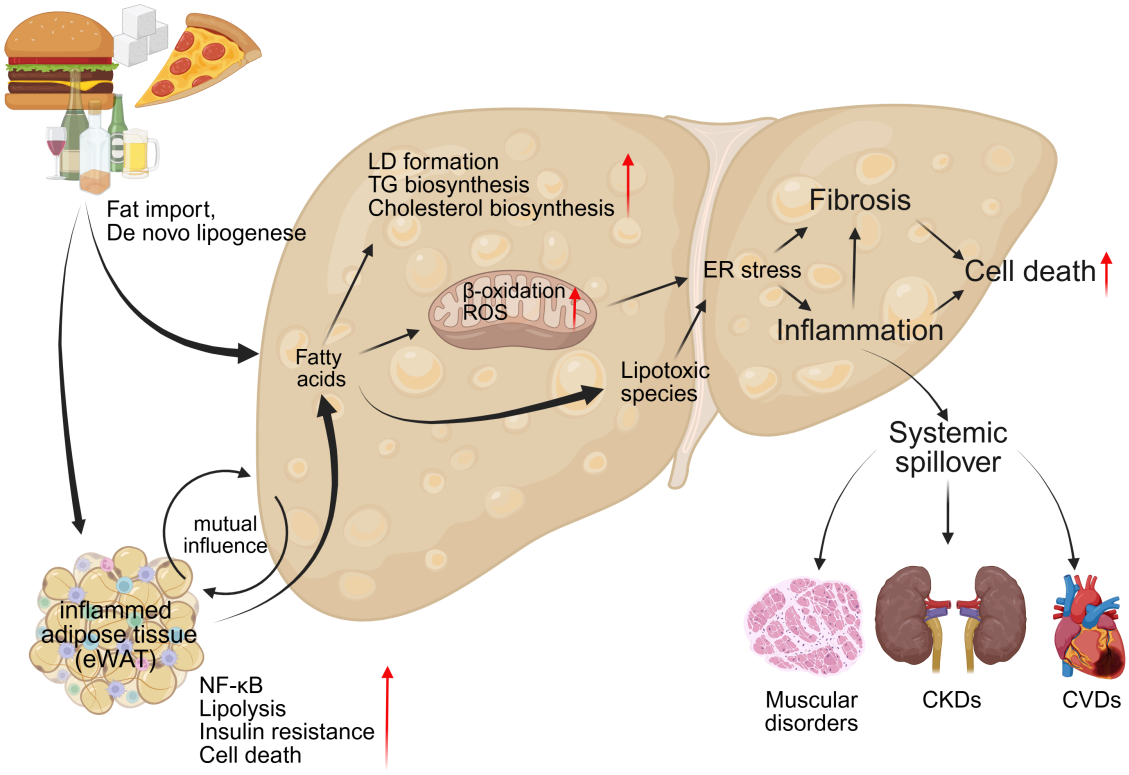

Figure 5: Diet induced changes in liver that drive MASLD and MASH pathology. Chronic caloric surplus high in fat and sugars can severely impact adipose tissue and liver homeostasis. The two organs influence each other. While increased inflammation, NF-κB signaling and cell death lead to upregulation of lipolysis, remodeling of immune cell populations and altered adipokine signaling in the adipose tissue. The increased levels of FAs released from adipose tissue can be ectopically dispositioned in the liver or other organs such as muscle or heart. Within the liver the abnormally high amount of FAs trigger processes like LD formation and high levels of β-oxidation further cause ROS production leading to ER stress, ultimately introducing severe chronic inflammation, fibrosis and cell death. Altered signaling in the liver can also lead to systemic spillovers, affecting the heart, kidneys or muscles. Adapted from Yanai *et al.* and illustrated using Biorender.[67]

Even though SLD and its subforms already affect around 30% of world's population, treatment options are still limited. First in line MASLD treatment still comes with changes in lifestyle or diets, weight management as well as the treatment of symptoms or comorbidities.[68,69] Yet these are often hard to maintain by patients, pointing out the urgent need to identify competent pharmacological targets. Currently there is still no licensed drug available that is targeting specifically a MASLD/MASH pathology, due to its heterogeneous nature, what makes current research on the topic indispensable.[70]

Given the recent change in terminology in 2023, aiming for a more inclusive and non-stigmatizing language, only limited literature is currently available under the new terms MASLD and MASH, which replace NAFLD and nonalcoholic steatohepatitis (NASH), respectively. Re-evaluations of NAFLD cohorts showed, that more than 98% of patients formerly diagnosed with NAFLD are also fulfilling criteria for MASLD.[71,72] For these reasons, references about NAFLD and NASH, will be used equally to MASLD and MASH references.

1.4.1 Programmed cell death in MASLD pathogenesis

As previously mentioned in Chapter 1.4, dysregulation of liver or fat tissue homeostasis can lead to lipotoxicity causing oxidative and ER stress, dysfunction of mitochondria, ultimately leading to hepatocellular injury as well as cellular death.[73] Programmed cell death (PCD), especially apoptosis, is long known to be associated with liver disease. But apoptosis is not the only PCD that was found to be activated in different stages of MASLD progression: pyroptosis, ferroptosis, necroptosis as well as autophagy can have pivotal effects on the severity and outcome of MASLD.[74,75] Multiple studies showed that markers of PCD, such as for apoptosis and necroptosis were upregulated in livers of patients with MASLD/ MASH, making them potential targets for new therapeutic approaches.[75,76]

Within the liver in general as well as in liver diseases like MASH, apoptosis represents the best studied form of PCD and is usually seen as non-immunogenic. Pyroptosis as well as necroptosis are both lytic cell death forms, leading to leakage and release of intracellular contents into the extracellular space, triggering immune response and inflammation.

Apoptotic cells display shrinkage, dense cytoplasm, condensation and fragmentation of chromatin as well as formation of apoptotic bodies.[77] Apoptosis can be triggered either ex- or intrinsically, leading to cysteine-dependent aspartate-directed protease (caspase) activity, resulting in nuclear fragmentation and cell death eventually (Figure 6).[75] Apoptotic cells further present so called “eat me” signals on their cell surface, allowing phagocytes fast and efficient clearance.[78,79]

Increased oxidative and ER stress within hepatocytes of MASLD and MASH patients specifically are able to trigger intrinsic apoptosis, which is characterized by mitochondrial outer membrane permeabilization (MOMP). Through the disrupted mitochondrial membrane, apoptotic mediators, such as cytochrome C (CytC) are released into the cytosol, binding apoptotic protease activating factor-1 (Apaf-1). Subsequent formation of the apoptosome complex recruits and activates caspase-9, as initiator caspase further cleaving and activating executioner caspases-3 and -7 leading to cell death.[75]

Extrinsic apoptosis can be triggered by changes in the extracellular microenvironment and is mostly activated through the binding of substrates to specific transmembrane death receptors (DRs). Fas ligand (FasL) and TNF-α are both ligands binding receptors of the TNF superfamily and can be expressed in response to pro-inflammatory cytokines and immune response in general. Binding of FasL to its receptor induces FS-7-associated cell surface antigen (Fas) receptor trimerization, leading to intracellular recruitment of Fas-associated protein with death-domain (FADD), which in turn recruits caspase-8 through a death effector domain (DED) interaction. The thereby formed complex is called death-inducing Signaling complex (DISC) and is able to cleave and thereby activate the initiator caspase-8, which in turn activates downstream caspase-3 and -7 to execute apoptosis.

Compared to Fas, tumor necrosis factor receptor 1 (TNFR1) has multiple modalities and is able to form three distinct complexes leading to either induction of NF-κB signaling (pro-inflammatory and pro-survival) or PCD (apoptosis or necroptosis). Upon TNF-α binding, complex I forms by recruitment of receptor-interacting serine/threonine kinase 1 (receptor-interacting serine/threonine kinase (RIPK)1), TNFR1-associated death domain (TRADD), TNF receptor associated factor (Traf) 2/5 and cellular inhibitor of apoptosis

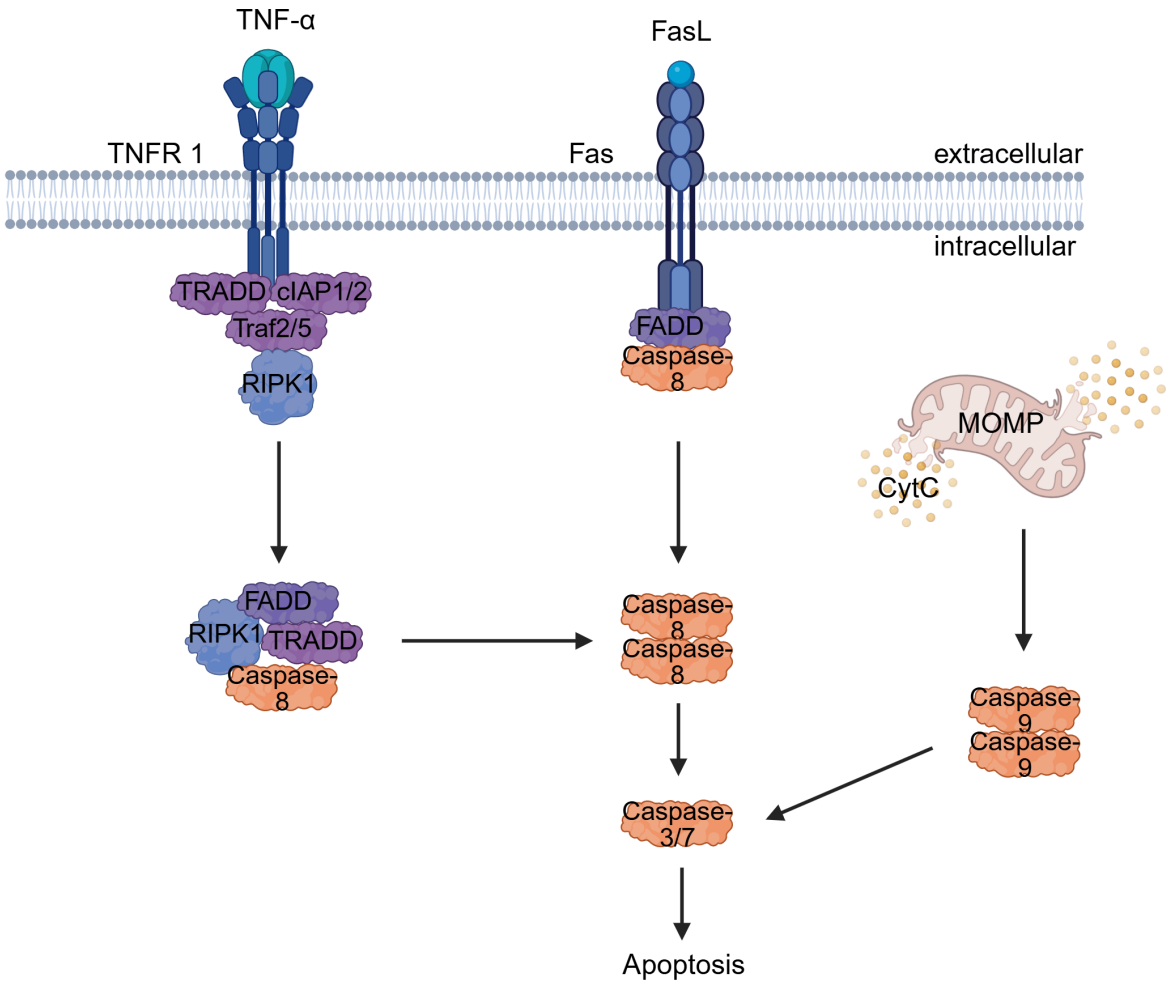

Figure 6: Extrinsic and intrinsic activation of apoptosis pathway. Excessive oxidative stress can cause mitochondrial damage, MOMP and CytC release leading to activation of intrinsic apoptosis through apoptosome complex formation and initiator caspase-9 activation. Extrinsic apoptosis activation can be either through TNF-α or Fas receptor. Both lead to caspase-8 dimerization, cleavage and thereby activation. Both intrinsic and extrinsic apoptotosis pathways lead to activation of executioner caspase-3/7 ultimately causing PCD. Adapted from Zhao *et al.* and illustrated using Biorender.[75]

protein (cIAP). After several ubiquitination steps by cIAP and linear ubiquitin chain (M1) assembly complex (LUBAC) and further activation and assembly of the NF-κB essential modulator (NEMO) and IκB kinase (IKK) complex, NF-κB is phosphorylated and translocated to the nucleus, activating pro-inflammatory gene expression (Figure 7).[80] Especially the post-translational modifications of RIPK1 are crucial for the switch between cell survival and cell death. Inhibition of NF-κB signaling and incomplete ubiquitination of RIPK1 can mediate the shift towards cytoplasmic complex IIa and IIb (apoptosis) or IIc (necroptosis), respectively. Complex IIa forms, when RIPK1 is deubiquitinated by cylindromatosis (CYLD), thereby dissociating from the TNFR1 receptor. It then assembles with TRADD, FADD, FLICE-like inhibitory protein (FLIP) and pro-caspase-8, transforming it to its active form, cleaved caspase-8. The complex IIb forms under the absence of cIAP, causing incomplete ubiquitination of RIPK1. After dissociation from the membrane RIPK1 associates with FADD, FLIP and pro-caspase-8, initiating its activation.[81]

During active apoptosis, caspases degrade cytosolic RIPK1/3 complexes, thereby inhibiting the formation of complex IIc and its cytotoxic effects. The inhibition or insufficiency

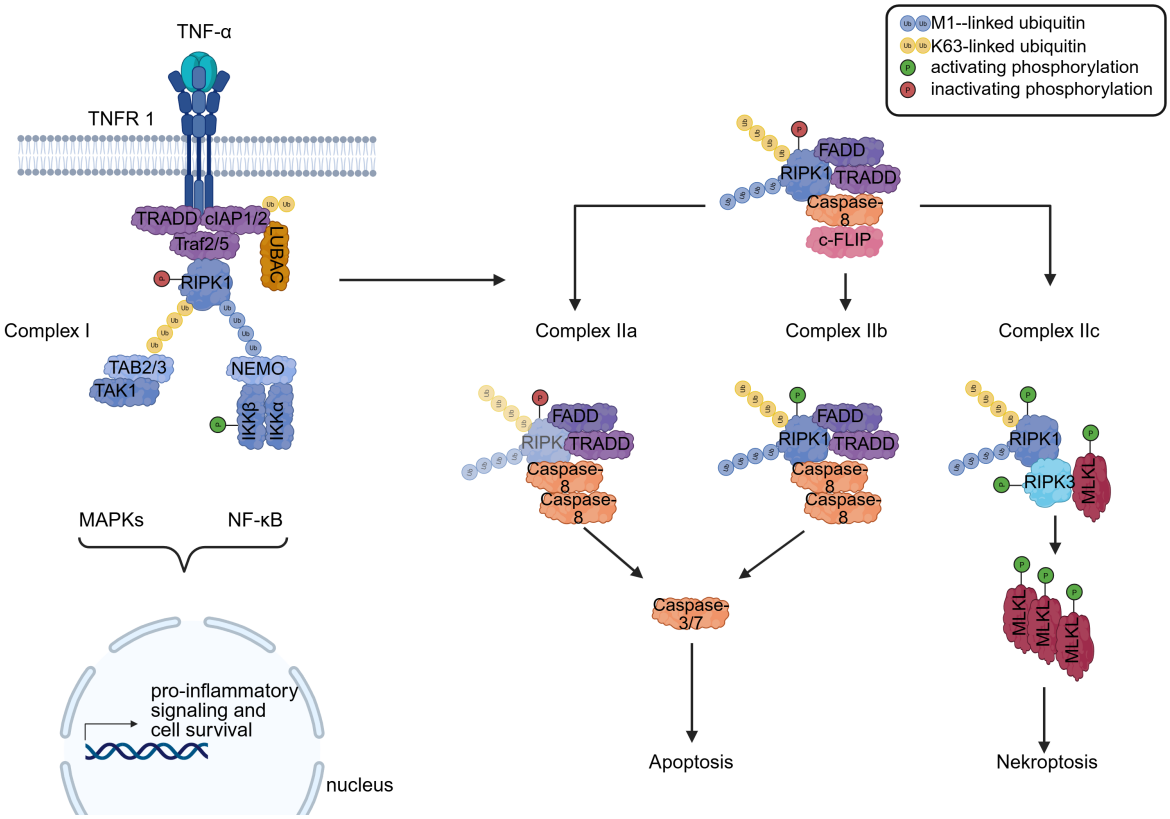

Figure 7: TNF-α signaling decision between life and death. Complex I forms upon TNF-α binding, consisting of TRADD, Traf2/5, cIAP1/2 and RIPK1. Downstream it activates pro-survival and pro-inflammatory mitogen-activated protein kinase (MAPK) and NF-κB signaling. Upon destabilization, complex I can transition into its cytosolic and cytotoxic form, complex II. Apoptosis can be activated either independent of RIPK1 (complex IIa) or dependent of RIPK1 (complex IIb). In absence of caspase-8 RIPK1 can form a complex with RIPK3 and mixed lineage kinase domaine like (MLKL) (complex IIc) and execute necroptosis. Adapted from Schwabe *et al.* and illustrated using Biorender[82]

of caspase leads to the stabilization of the RIPK1 and RIPK3 interaction through their RIP homotypic interaction motif (RHIM) domains, forming the necrosome. RIPK3 is then phosphorylated and activated, enabled to subsequently phosphorylate MLKL at Ser345 in mouse, inducing a conformational change. This conformational change is followed by ubiquitination with K63-linked ubiquitin chains at Lys219, allowing MLKL to optimally oligomerize and further translocate to the plasma membrane.[83–85] At the membrane, the N-terminal 4-helix bundle (4HB) of MLKL can incorporate into the cell membrane, leading to membrane rupture, cell leakage and ultimately lytic cell death.[85,86] Necroptosis can be further activated by other pathways, especially during viral or bacterial infections. Viruses, for example, are able to express cFLIP mimics, which are capable of blocking caspase activity enabeling necroptosis induction.[87] Hence, necroptosis can be seen as backup in case of apoptotic failure.[84] Intracellular viral double stranded ribonucleic acid (RNA) can be recognized and bound by Z-DNA binding protein 1 (ZBP1), which also contains RHIM domains enabling it to interact with and activate RIPK3, thereby inducing necroptosis. ZBP1 can also be activated through toll-like receptor (TLR) 3/4 also recognizing viral RNA and bacterial lipopolysaccharide (LPS) or through interferon receptor (IFNR) activation through Janus kinase (JAK) and signal transducer and activator of transcription (STAT) signaling.[88,89] After execution of necroptosis intracellular contents, like ATP and damage-associated

molecular patterns (DAMP), are released from the cell, creating a highly inflammatory microenvironment further driving inflammation and linked processes like fibrosis, cirrhosis or HCC formation. For its association with diseases including cancer, neurodegenerative diseases, acute kidney injury or liver pathologies, it makes necroptosis an interesting target for therapeutical approaches.[90]

1.5 Inhibition of necroptosis by MLKL^{K219R} mutation

As introduced in the previous section (section 1.4.1), MLKL is the protein primarily responsible and known for the execution of necroptosis. Among the studies addressing the role of MLKL in a metabolic context, the ones most relevant for comparison with this thesis relied on knock out (KO) models.[91–93] Although KO models are well-established in research, they come with certain limitations and pitfalls. For once, genetic ablation does not reflect clinical practice, as patient treatment mainly uses inhibitory and not deleterious approaches. Furthermore, the complete absence of a protein could not only effect the primary targeted pathways, but also impact off-target binding partners and thereby influence unexpected or even unknown pathways. In the case of MLKL, its deletion may primarily lead to inhibition of necroptosis, but further is impacting a variety of non-necroptotic functions, known or unknown, making analysis highly complex and challenging. The MLKL^{K219R} mouse model used in this study offers several advantages over commonly used KO models.

When TNF-α binds to its receptor TNFR1 ① (Figure 8) but NF-κB is defective or caspases are absent, a RIPK1/3 complex can form ② and subsequently phosphorylate MLKL in RIPK3-dependent manner at Ser345 ③. This phosphorylation induces a conformational change activating MLKL ④. The Lys219 of endogenous MLKL is then conjugated with K63-linked ubiquitin-signaling chains ⑤ enabling optimal oligomerization at cellular membranes ⑥, introducing membrane rupture and DAMP release ⑦. Functionally, the exchange of amino acids from lysine to arginine at position 219 preserves the hydrogen bond to Glu343 during the unphosphorylated and inactive state, such as within the endogenous MLKL. However, Arg219 cannot be ubiquitinylated. This has detrimental effects on MLKL oligomerization and membrane association, as well as on the overall execution of necroptosis.[85]

Furthermore, MLKL is only altered by one amino acid and thereby still expressed in full-length. This way processes that involve MLKL in unphosphorylated states as scaffold or for structural functions/purposes should not be disturbed. Additional phosphorylation at S345 is not impaired. Only subsequent oligomerization is affected, which should not impact p-S345-dependent pathways. In the MLKL^{K219R} model, primarily the execution of lytic cell death should be inhibited. This should also block the negatively associated DAMP release following necroptosis.

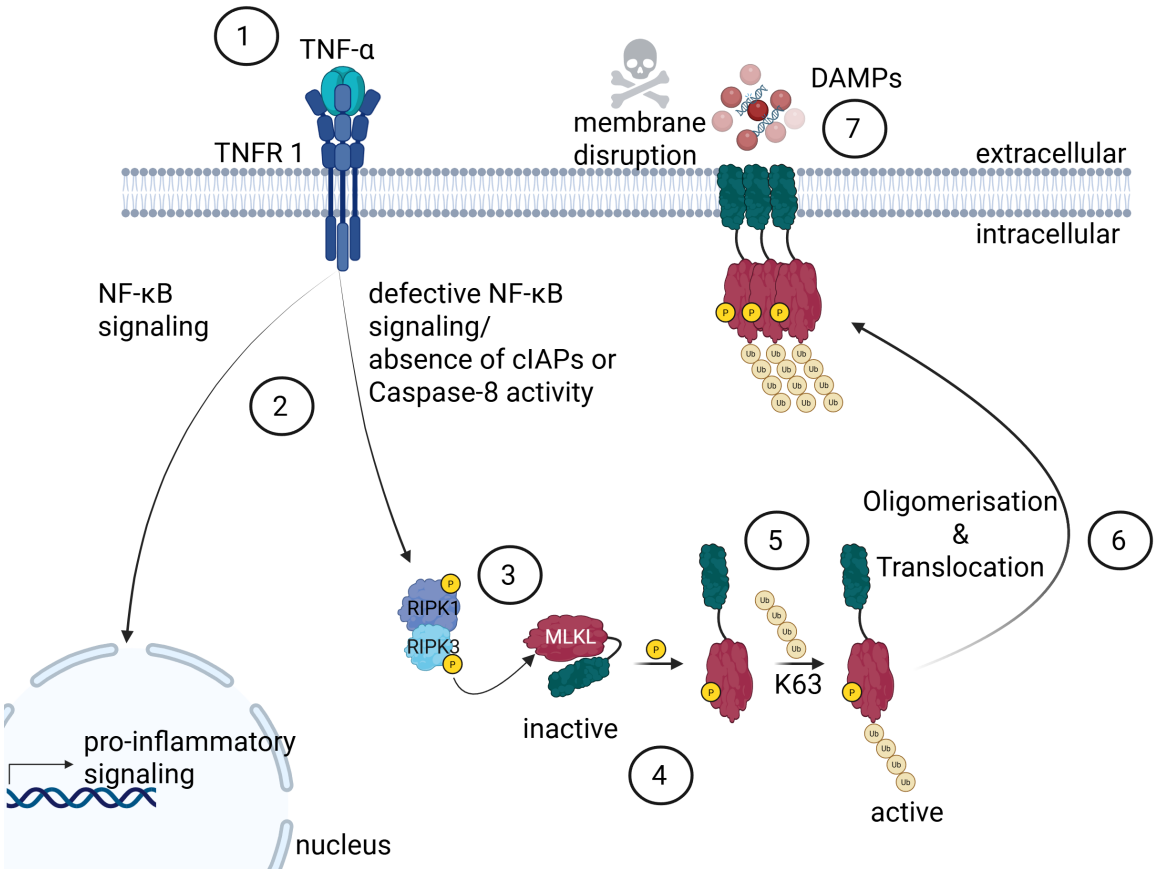

Figure 8: MLKL activation and necroptosis execution. When NF-κB signaling is defective and apoptosis is not active, RIPK1 and 3 can interact through their RHIM-domains further phosphorylating and activating MLKL. Additional ubiquitylation and conformational changes form MLKL oligomers, which in turn are able to be inserted into the cell membrane, causing membrane disruption and ultimately cell death. Adapted from Garcia *et al.* and illustrated using Biorender.[85]

1.5.1 MLKL – functions beyond necroptosis execution

For many years MLKL was only known for its function as executioner of necroptosis. However, the number of studies, showing necroptosis-independent functions of MLKL, is consistently increasing. Many mechanisms around MLKL are still not fully understood. Most prominent example for this is the mechanism, on how MLKL actually does lead to membrane disruption. Some studies suggest the formation of unspecific pores, disrupting the lipid layer, others the formation of ion channels, causing the release of DAMPs or ions like Mg^{2+} or Ca^{2+}.[94–96] Lastly, a study suggest MLKL to form amyloid-like fibers, directly affecting membrane integrity.[97] Considering that much remains unknown about the widely accepted functions of MLKL, this highlights the potential for discovering yet unknown roles of MLKL that are independent of necroptosis execution. Certain modifications like ubiquitination, for instance, can redirect MLKL to other cellular compartments like endosomes instead of the cell membrane. There it enhances endosomal trafficking of intracellular bacteria, controlling infection by fusion with lysosomes independent of RIPK3.[98] By the activation of MLKL through RIPK3 endosomal trafficking is not only increased, but further the association with endosomal sorting complexes required for transport (ESCRT) proteins, crucial for the production of extracellular vesicles (EVs). This process enables the cell, for example, to internalize and degrade ligands and

receptors like TNF/TNFR1 faster as well as to restrict or delaying cell death by exporting phosphorylated mixed lineage kinase domain-Like (pMLKL) within EVs.[99] Another study could show, that MLKL is able to translocate into the nucleus and is able to influence gene expression as well increase messenger RNA (mRNA) stability indirectly through the interaction with other proteins.[100] MLKL is not only able to influence gene expression but further can impact the immune response on many levels. Activated MLKL can induce NOD-like receptor protein 3 (NLRP3) inflammasome assembly, what in turn leads to IL-1β activation and secretion.[101] IL-1β is highly pro-inflammatory, stimulating the activation and recruitment of immune cells.

Even though the number of necroptosis-independent functions continuously rises, many of them are associated with disturbance of the cellular membrane under sublethal conditions of necroptosis. In addition, its effects on the immune response receive more and more attention. Furthermore, it is important to know that MLKL is widely expressed in most cell types, but that there are tissue specific differences. Its highest expression levels are displayed in immune and hematopoietic tissues, highlighting its importance in inflammation and immune response. Other tissues like the brain and the central nervous system have only very low levels of basal MLKL, yet under certain stress or inflammatory conditions, it can be induced or upregulated in most tissues.[102]

This brief introduction of MLKL functions that go beyond the execution of necroptosis has merely served to illustrate its many facets as well as its importance as a highly interesting target for therapeutic approaches.

1.6 Aim of this study

Emerging evidence highlights the therapeutic potential of targeting PCD pathways in metabolic contexts. Among these, necroptosis, a regulated form of inflammatory cell death, has garnered attention. Studies have demonstrated that markers of necroptosis, such as RIPK3 and (phosphorylated) MLKL, are upregulated in patients with MASLD and MASH specifically, contributing to disease pathogenesis.[76] While some studies indicate that the knockout of MLKL, the key executioner of necroptosis, confers protection against diet-induced weight gain and MASLD development, other reports contradict these findings, showing no protective effects of MLKL deficiency. Thus, the role of MLKL in metabolic disease remains highly debated.

To address this controversy, we employed a novel MLKL mutant (K219R) model incapable of oligomerizing and associating with the cell membrane, thereby blocking necroptosis. By subjecting these animals to a high-caloric western diet (WD) ± additional alcohol, we aimed to induce obesity and MASLD/MASH further investigating the resulting metabolic alterations compared to wild-type controls. The tissues of these experimental animals, different adipose tissues as well as the liver are the main focus of analysis. The embedded tissues will then be subjected to immunohistochemistry stainings to evaluate the inflammatory state as well as pathological changes within the tissues as well between the different experimental cohorts and genotypes. For in-depth examination of changes induced by the WD, tissues will then be used for protein and gene expression analysis, primarily focusing on lipid metabolism, cell death and inflammation, particularly in liver and adipose

tissue.

Additionally, *in vitro* assays using different primary cells were performed to uncover the molecular mechanisms potentially underlying the observed phenotypic differences observed in liver and fat tissue. This study aims to elucidate the contribution of MLKL to the metabolic disturbances associated with obesity and offers insights into therapeutic strategies for metabolic disorders.

Chapter 2

Material and Methods

The following chapter lists all the experimental methods and materials used in this study.

2.1 Material

2.1.1 Laboratory devices

Table 1: Laboratory devices and their manufacturer.

Device	Manufacturer
Autostainer XL	Leica
Balance	Mettler
Bead Ruptor	Omni International
Benchtop Centrifuge 5424R	Eppendorf
Blood glucose meter NEXT ONE	Contour
Blotting chamber	Scie-PLAS
BOND RX	Leica
Camera (SLR) + lens	Canon
Centrifuge Rotina 420R	Hettich
Clinical chemistry analyzer Pentra 4000	Acsonlab Horiba Medical
CO_2 chamber	Medres
Cooling plate	PFM Medical
Dehydration device	Leica
Dissecting utensils	Hammacher-Solingen
Electrophoresis chamber	Biometra, Amersham
ELISA Reader	Tecan
Fine balance	Sartorius
Gel manager ChemiDoc MP	Biorad
Gel station (Western-Blot)	Amersham
ImageQuant 800	Cytiva
Incubator (stainings)	Fisher Scientific
Incubator Heracell (cell culture)	Thermo Fisher
Magnetic stirrer	Heidolph

Device	Manufacturer
Microscope Axioscope 5 (histology)	Zeiss
Microscope AxioVert A1 (cell culture)	Zeiss
Microtome	Leica
Microwave	Bosch
Mouse-E-Motion universal mobile data logger	Infra-E-Motion GmbH
Nanodrop	Implen
Neubauer counting chamber	Nano Entek
Paraffin embedding station	Leica
Perfusion pump	Abimed Gilson, CellMedia
pH meter	Toledo
Pipettes/pipetting aid	Eppendorf
Powersupply	Biometra
Printer (slides/histology cassette)	Primera
Rocker	Heidolph
Slide scanner Aperio AT2	Leica
Staining automat	Leica
Staining chamber (wet)	Simport
Staining row	Biosystems
Sterile bench	Labogene
Suction pump (cell culture)	CellMedia
Thermoblock	Eppendorf
Thermocycler	Applied Biosystems
ViiA7 (RT-qPCR)	Applied Biosystems
Vortexer	Ika
Water bath (perfusions)	Julabo
Water bath (stainings)	Leica

2.1.2 Consumables

Table 2: Consumables and their manufacturer.

Material	Manufacturer
96-well plate (Nunc)	Thermo Scientific
Absorbent compress	Meditrade
Blood glucose test stripes	Contour
Cell culture plates (6-, 12-, 96-well)	Greiner/TPP
Cell filter	Falcon
Cell filters (70 µm, 100 µm)	Greiner/Falcon
Cell scratcher	Kisker
Ceramic beads	Omni International
Cover glas	VWR
Cryo tubes + colour coded caps	Thermo Scientific

Material	Manufacturer
ELISA tub	VWR
Embedding cassette	Cell Path
Eppendorf tubes (1.5 ml, 2 ml)	Eppendorf
Falcon tubes (15 ml, 50 ml)	Greiner
Filter wells	Greiner
Gloves	Dermagrip
Indwelling venous catheter	Braun
Needles (20 g)	Braun
NuncleonSphera 96U Bottom Plate, 96-Well-Plate (ultralowinfinity-round bottom)	Thermo Scientific
PCR tubes	Thermo Scientific, Sarstedt
Petri dishes (4 cm, 10 cm)	Greiner/TPP
Pipette tips (with/without filter)	Biozym
PVDF transfer membran	Merck
RT-qPCR plates + adhesive film	4titude
Screw cap tubes	Sarstedt
Screw tubes	Sarstedt
Serological pipettes	Greiner
Serum tubes	Sarstedt
Slides	Klinipath
Sterile filter	Falcon
Stripettes (5 ml, 10 ml, 25 ml, 50 ml)	Costar/Greiner
Syringes (1 ml, 2 ml, 5 ml, 10 ml, 50 ml)	Braun
Vacuum filtration bottles	TPP
Whatman paper	GE Healthcare

2.1.3 Chemicals and kits

Table 3: Chemicals and their manufacturers.

Chemical	Manufacturer
Asparagine	Sigma
AdipoRed	Lonza
3-Isobutyl-1-methylxanthine (IMBX)	Sigma
Acetic acid	Sigma
Acrylamide	Bio-Rad
Agarose	Invitrogen
Amphotericin B	Sigma
Antibody diluent (stainings)	Immunologic
Ammoniumpersulfate (APS)	Sigma
Bromphenol blue	Sigma
Bovine serum albumin (BSA)	Roth

Chemical	Manufacturer
Calcium chloride ($CaCl_2$)	Sigma
BSA, fatty acid free	Roth
Chloroform	VWR
Collagenase D	Roche
Collagenase Type II	Worthington
Complete Mini tablet	Roche
3,3'-Diaminobenzidine (DAB)	Epredia
Dexamethasone	Roth
Dexamethasone	Sigma
Dispase II	Roche
DMEM (div.)	PAN-Biotech, GIBCO
DMEM/GlutaMAX	Gibco
Dimethylsulfoxide (DMSO)	Sigma
DNA Ladder	Thermo Fisher
Dithiothreitol (DTT)	Roth
Earle's Balanced Salt Solution (EBBS)	GIBCO
Enhanced chemiluminescence solutions	Advansta
EDTA (0.5 M)	Applichem
EGTA	Roth
Eosin	Sigma
Ethanol (70%, 99.5%)	VWR
Percoll	Cytiva
Fetal Bovine Serum (FBS), Good	PAN Biotech
Gentamicine	Invitrogen
Glucose	Roth
Glucossteril 40%	Fresenius Kabi
Glycerin	Merck
Glycine	Sigma
Grease pencil (stainings)	Dako
HDGreen	Instas
Hematoxylin	Dako
Hoechst 34580	Invitrogen
HEPES	Sigma
Histofix (4% Formaldehyde)	Roth
HistoZym	Sigma
Hydrochloric acid (HCl)	Merck
HBSS (10×, w/o $NaHCO_3$)	GIBCO
Hydrogen peroxide (H_2O_2)	Merck
ImmPress serum + secondary antibody	Vector
Isoflurane	Piramal
Isopropanol	Merck
Lämmli buffer	Bio-Rad

Chemical	Manufacturer
L-Glutamine	Invitrogen
Magnesium chloride ($MgCl_2$)	Sigma
Magnesium sulfate ($MgSO_4$)	Roth
Methanol	VWR
Sodium chloride (NaCl, 0.9%, isotonic)	Fresenius
Sodium chloride (NaCl)	VWR
NeoClear	Sigma
Nonidet-P40 (NP-40) alternative	Merck
Oleic acid	Sigma
Palmitic acid	Sigma
Paraffin	Vogel
Pefablock	Roche
Penicillin/Streptomycin	Sigma
Phosphate buffered saline (PBS)	Sigma
PhosSTOP	Roche
Ponceau S Solution	Serva
Potassium chloride (KCl)	Sigma
Propidium iodide	Sigma
Protein standard (Marker)	Novex
Proteinase K	Roche
Rosiglitazone	Sigma
RWT Buffer	Qiagen
SDS running buffer (10×)	Roth
Skimmed milk powder	Roth
SDS	Sigma
Sodium hydroxide (NaOH)	Sigma
Sulfuric acid (H_2SO_4)	Merck
TAE buffer	Applichem
TEMED	Sigma
Triiodothyronine	Sigma
Tris	Roth
Triton X-100	Fluka
Trizol	Qiagen
Trypan blue	Sigma
Trypsin	Invitrogen
Trypsin inhibitor	Invitrogen
Tween-20	Serva
Vitroclud	Langenbrinck
WesternBright Quantum/Sirius HRP substrate	Advansta
William's E Medium	Sigma
Xylol	Sigma
β-Mercaptoethanol	Roth

Table 4: Used kits and their manufacturer.

Kit	Manufacturer
RNeasy Mini Kit	Qiagen
RevertAid RT Kit (cDNA synthesis)	Thermo Scientific
Protein Assay Dye (Bradford)	Bio-Rad
NucleoSpin RNA plus	Macherey-Nagel
Mouse Insulin ELISA Kit	Mercodia
GoTaq G2 Flexi DNA Kit	Promega
GoTaq qPCR Master Mix	Promega

Table 5: Diets and supplies used for the experimental animal feeding.

Animal experiment supplies	Manufacturer
Western diet, D16022301i	Research diets
Normal chow diet	Research diets
Banana flavor drops	MyProtein
EtOH, 99.5%	VWR

2.1.4 Buffers

If not mentioned otherwise, all buffers and stock solutions were prepared with distilled Water (dH2O).

Table 6: Buffers for mouse genotyping.

Buffer	Components
Tail lysis buffer	50 mM KCl 10 mM Tris HCl (pH = 8.3) 2 mM $MgCl_2$ 0.1 mg/ml Gelatine 0.45 % NP-40 (v/v)
TAE buffer (1×)	2 % TAE buffer (50×, v/v)

Table 7: Buffers and stock solutions for immunochemistry.

Buffer/solution	Components
EDTA buffer	10 mM Tris
	1 mM EDTA
	0.05 % Tween-20 (v/v)
Citrate buffer (pH = 6)	1.8 % stock solution A (0.1 mM citric acid) (v/v)
	8.2 % stock solution B (0.1 mM Sodium citrate) (v/v)
TBST wash buffer	20 mM Tris
	150 mM NaCl
	0.05 % Tween-20 (v/v)
Peroxidase blocking solution	3 % H_2O_2 (v/v)

Table 8: Buffers and stock solutions for western blot analysis.

Buffer/solution	Components
NP-40 lysis buffer	50 mM Tris-HCl (pH = 7.5)
	150 mM NaCl
	PhosphoSTOP tablet
	Mini Complete tablet
	1 mM DTT
	1 mM Pefablock
Lämmli buffer (2×)	Lämmli buffer (2×)
	5 % β-Mercaptoethanol (v/v)
SDS loading buffer (5×)	250 mM Tris-HCl (pH = 6.8)
	30 % Glycerine (v/v)
	10 % SDS (m/v)
	5 % β-Mercaptoethanol (v/v)
	Bromphenol blue
SDS running buffer	10 % SDS running buffer (10×, v/v)
Towin transfer buffer	25 mM Tris
	190 mM Glycine
	20 % Methanol (v/v)
TBS washing buffer (10×)	200 mM Tris-HCl (pH = 7.6)
	1.5 M NaCl
TBST washing buffer (1×)	10 % TBS washing buffer (10×, v/v)
	0.1 % Tween-20 (v/v)
Blocking solution	5 % skim milk powder (m/v) in TBST washing buffer
Stripping buffer (pH = 2.2)	199 mM Glycine
	0.1 % SDS (m/v)
	1 % Tween-20 (v/v)

Table 9: Gels for western blot analysis.

Gel	Components
SDS collection gel	28 % Tris HCl (1.5 M, pH = 8.6, v/v) 7 % Acrylamide (v/v) 0.1 % SDS (m/v) 0.1 % APS (m/v) 0.2 % TEMED (v/v)
SDS separation gel (10 %, 12.5 %, 15 %)	25 % Tris HCl (1.5 M, pH 8.8, v/v) 10 % / 12.5 % / 15 % Acrylamide (v/v) 0.1 % SDS (m/v) 0.1 % APS (m/v) 0.15 % TEMED (v/v)

Table 10: Buffers and stem solutions for adipocyte isolation.

Buffer	Components
Digestion medium	10 mM $CaCl_2$ 2.4 U/ml Dispase II 1.5 U/ml Collagenase D DMEM/1x GlutaMAX
Growth medium 1	DMEM/1x GlutaMAX
Growth medium 2	20 % FBS
Induction medium	DMEM/1x GlutaMAX 20 % FBS 1 % P/S 5 µg/ml Amphotericin B
Differentiation medium	DMEM/1x GlutaMAX 20 % FBS 1 % P/S 5 µg/ml human insulin 0.5 mM IBMX 1 µM Dexamethasone 4 µg/ml Rosiglitazone

Table 11: Buffers for isolation of primary hepatocytes.

Buffer	Components
Solution 1	EBSS without Ca^{2+} and Mg^{2+} 0.5 mM EDTA
Solution 2 (pH = 7.4)	EBSS with Ca^{2+} and Mg^{2+} 10 mM HEPES 0.02 % Collagenase II 0.004 % Trypsin inhibitor
Maintenance medium	William's E medium 10 % FBS 1 % P/S 1 % L-Glutamine
Stimulation medium	William's E medium 1 % P/S 1 % L-Glutamine

2.1.5 Antibodies

Table 12: Primary antibodies for Western blotting. All antibodies were diluted in TBS-T containing 5 % BSA.

Antibody	Host species	Dilution	Manufacturer, Cat. No.
GAPDH	Mouse-anti-mouse	1:2000	AbD-Serotec, #MCA 4739
UCP1	Rabbit-anti-mouse	1:1000	Abcam, #ab10983
MLKL	Rabbit-anti-mouse	1:2000	Biorypt, #orb32399
Phospho-MLKL	Rabbit-anti-mouse	1:1000	Abcam, #ab196436
RIP3 (D4G2A)	Rabbit-anti-mouse	1:2000	Cell Signaling, #95702
Phospho-RIP3	Rabbit-anti-mouse	1:1000	Cell Signaling, #91702
caspase 3	Rabbit-anti-mouse	1:2000	Cell Signaling, #9662
Cleaved caspase 3	Rabbit-anti-mouse	1:1000	Cell Signaling, #9661
Beta-Actin	Rabbit-anti-mouse	1:2000	Sigma, #A2066

Table 13: Secondary antibodies for Western blot analysis.

Antibody	Host species	Dilution	Manufacturer, Cat. No.
Rabbit-HRP	Donkey-anti-rabbit	1:5000	GE Healthcare, GENA934
Mouse-HRP	Sheep-anti-mouse	1:5000	Amersham, NA931V

2.1.6 Oligonucleotides

The oligonucleotides were designed using Primer blast (NCBI). They were purchased from Eurofins Genomics and reconstituted to 10 nmol in water. When used for reverse transcription polymerase chain reaction (RT-PCR) 1:10 dilutions of these stocks were used.

Table 14: Oligonucleotides used for RT-PCR analysis.

Target	Forward 5' → 3'	Reverse 5' → 3'
UCP1	GAGGTCGTGAAGGTCAGAATG	AAGCTTTCTGTGGTGGCTATAA
FGF-21	CTCAGAAGGACTCCCCAAAC	AGGAATCCTGCTTGGTCTTG
HPRT	CTGGTGAAAAGGACCTCTCGAAG	CCAGTTTCACTAATGACACAAACG
Cidea	TGACATTCATGGGATTGCAGAC	GGCCAGTTGTGATGACTAAGAC
Prdm16	CAGCACGGTGAAGCCATTC	GCGTGCATCCGCTTGTG
Adiponectin	GTTCCCAATGTACCCATTCGC	TGTTGCAGTAGAACTTGCCAG
Fasn	TTGCTGGCACTACAGAATGC	AACAGCCTCAGAGCGACAAT
Cpt1a	CTCAGTGGGAGCGACTCTTCA	GGCCTCTGTGGTACACGACAA
Dgat1	CGTGGGCGACGGCTACT	TGAGCTGAACAAAGAATCTTGCA
PPARα	ACGATGCTGTCCTCCTTGATG	GCGTCTGACTCGGTCTTCTTG
TNFα	ACCACGCTCTTCTGTCTACTGA	TCCACTTGGTGGTTTGCTACG
IL-6	GCTACCAAACTGGATATAATCAGGA	CCAGGTAGCTATGGTACTCCAGAA
GM-CSF	GGCCTTGGAAGCATGTAGAGG	GGAGAACTCGTTAGAGACGACTT
CCl2	GTGTTGGCTCAGCCAGATGC	GACACCTGCTGCTGGTGATCC
IL-1β	GCAACTGTTCCTGAACTCAACT	ATCTTTTGGGGTCCGTCAACT
IL-1α	GCACCTTACACCTACCAGAGT	AAACTTCTGCCTGACGAGCTT
Leptin	CTCCATCTGCTGGCCTTCTC	CATCCAGGCTCTCTGGCTTCT
Cidea	TGACATTCATGGGATTGCAGAC	GGCCAGTTGTGATGACTAAGAC
Scd-1	CTTCAAGGGCAGTTCTGAGG	CAATGGTTTTCATGGCAGTG

Table 15: Primers used for sequencing for mouse genotyping.

Target	Forward 5' → 3'	Reverse 5' → 3'
$MLKL^{K219R}$	CCGTGGAGGAAACTGAAGAC	TACCTTTCTCTTTGGGAAGTTG

2.1.7 Software

Table 16: Software and their versions that were used for data analysis and the drafting of this thesis.

Software	Version	Function
GraphPad Prism	9.3.1	Statistical analysis and graph generation
Mendeley	2.129	Reference management
ImageJ	1.4.3.67	Analysis of immunohistochemistry images
Overleaf/LaTeX editor	–	Text and formatting of the manuscript
QuantStudio	6	RT-PCR data acquisition and analysis
Aperio ImageScope	12.4.0.5043	Acquisition of histological images
BioRender	–	Scientific illustration and schematic generation
Primer-BLAST (NCBI)	–	Design of oligonucleotides for RT-PCR
ChatGPT	GPT-4o	Language editing and clarity improvement: Used during the preparation of this work to enhance grammar and conciseness. All content was subsequently reviewed and approved by the author, who takes full responsibility for the final version.

2.2 Methods

2.2.1 Experimental animals and generation of mouse data

2.2.1.1 MLKL^{K219R} mice and genotyping

The mouse line of MLKL^{K219R} was kindly provided by Pascal Meier (The Breast Cancer Now Toby Robins Research Centre, The Institute of Cancer Research, London, UK) and bred under standard conditions (20 ±2 °C, 12 h light/dark cycle in the “Zentrale Einrichtung für Tierforschung” (ZETT)). In short, mice were generated by the microinjection of pro-nuclei of fertilised oocytes of C57BL/6 mice using Cas9 mRNA together with ssDNA repair oligo and sgRNA targeting the region surrounding K219 of the murine MLKL gene.[85] Mice were provided with *ad libitum* normal chow diet (NCD) and water (pH = 3.0). Furthermore, the mice have a C57BL/6J background. All animal protocols were approved by the ”Landesamt für Natur, Umwelt und Verbraucherschutz (LANUV)” of North Rhine-Westphalia and carried out accordingly with EU directive 86/609/EEC.

For initial genotyping of mice, ear punches were used, while for regenotyping after sacrificing animals tail tips were used. deoxyribonucleic acid (DNA) was isolated from tissues using the GoTaq G2 Flexi DNA kit following manufacturer’s instructions. DNA was then used for sequencing to determine the K219R mutation in the genome.

2.2.1.2 Experimental animals

For the feeding experiments, male animals aged 6-8 weeks were used. Due to the breeding strategy MLKL^{K219R} and wild type (WT) animals were held separately in cages of 2-4 animals each. Each animal received 25 g of WD (40 kcal % fat, 20 kcal % fructose and 2 % Cholesterole) per week. Animals of NCD and MASH cohort were provided with water *ad libitum*, while animals from the MetALD cohort were provided with 10% (v/v) of EtOH diluted in water, containing 10 drops of banana flavor per liter. Animals were fed for 20 weeks. In week 16 animals underwent a glucose tolerance test (GTT).

Figure 9: Scheme for experimental animals. Experimental animals started with their different diets (WD alone or WD + 10 % alcohol) with 6 weeks of age, for 20 weeks in total. 16 weeks after starting the diet a GTT was performed to determine glucose uptake and fasting insulin levels. With 26 weeks of age animals were sacrificed and tissues and blood were exracted.

2.2.1.3 Scoring, body weight and food intake

Experimental animals were scored once a week. Scores were determined by using a score sheet, that scores animals according to body weight loss, overall appearance, spontaneous behaviour and clinical findings. Unless they showed any abnormalities concerning their behaviour, injuries or weight loss they were scored with 0, meaning that they are not burdened

by the experimental procedure. The WD was exchanged every week, while also determining the amount consumed by animals. For the MetALD cohort, 10 % (v/v) EtOH solution was also changed once a week.

2.2.1.4 Glucose tolerance test

Since diabetes is commonly associated with obesity and poor eating habits, a glucose tolerance test was performed on animals, 16 weeks after the start of feeding experiments. Therefore, animals were fasted for 6 hours prior taking initial blood sample (0 min) from an incision in the tail to determine fasted glucose and insulin levels. After the mice were injected *intra peritoneal* with 2 g/kg body weight of glucose solution, subsequently glucose levels were determined 15, 30, 60, 120, 150 and 180 mins past injection using the NEXT ONE glucometer. During fasting and GTT itself, animals were housed in fresh cages and provided with water.

The area under the curve (AUC) (Equation 1) was further calculated to make the glucose response better comparable.

$$\mathrm{AUC}_{\mathrm{total}} = \sum_{i=1}^{n-1} \frac{(t_{i+1} - t_i)(G_i - G_{i+1})}{2} \tag{1}$$

2.2.2 Tracking of mouse movements

To determine the spontaneous physical activity (SPA) of untreated mice on NCD, the mouse-e-motion tracker was used. Therefore, mice aged between 7 and 20 weeks were put individually in cages in a mouse housing cabinet for at least 24 hours for acclimatisation to their new environment. Movements then were tracked for another 48 hours. The motion tracker detects an event/movement, whenever its infrared light sensor is interrupted. These events then were summarized and used for graphical representation.

2.2.3 Analyses of murine blood serum

After mice were fasted for 4 hours and sacrificed by carbon dioxide (CO_2) asphyxiation, blood was collected from vena cava with a 20G syringe. After transferring the blood into a serum tube, samples were centrifuged for 5 min at 10.000 xg. The serum was then transferred to an Eppendorf tube and stored at -80°C until further analysis.

For the analysis of general liver-associated serum markers (aspartate transferase (AST), alanine transaminase (ALT), glutamate dehydrogenase (GLDH), alkaline phosphatase (AP) and Bilirubin), samples were diluted 1:10 with a 0.9 % natrium chloride (NaCl) solution and subsequently measured with according kits in the Pentra C400 clinical chemistry analyzer.

Additionally, markers for the lipid metabolism (non-esterified fatty acid (NEFA), Triglycerides, high density lipoprotein (HDL), low density lipoprotein (LDL) and total Cholesterol) were measured in a 1:5 dilution with 0.9 % NaCl solution.

2.2.4 Embedding of organs in paraffin and further processing

After dissection, organs were stored in a 4 % formaldehyde solution and were allowed to fixate for 24 hours before changing to phosphate buffered saline (PBS) and storing organs at 4 °C until embedding.

For the generation of the tissue sections, livers were cut with a thickness of 2 µm, whilst fat tissues were cut with 4 µm by using a Microtome. After placing the tissue sections on a slide they were dried overnight at 37 °C and high humidity. Tissue was then ready for histological stainings and analysis.

2.2.5 Hematoxylin and Eosin staining

As a first instance for tissue analysis hematoxilin & eosin (H&E) staining was performed, revealing pathological changes between the different animals and tissues by staining of the cell nucleus (Hematoxylin) and cytoplasm and collagen (Eosin). Using the Leica Autostainer XL (ST5010) tissue sections were stained with tissue specific in-lab established protocols.

2.2.6 Determination of lipid droplet and adipocyte size from H&E stainings

To further evaluate steatosis in liver as well as expansion of adipocytes the “MRI Adipocyte Tool” plugin for ImageJ was used.[102] Default settings of the source code were kept unchanged. Automated preprocessing and segmentation steps aim to minimize false positive fat accumulations by setting the threshold of a minimum size at 30 px^2.

2.2.6.1 Determination of lipid droplet size in liver from H&E stainings

After evaluation and initial testing, the Adipocyte Tool was used for liver sections as described in the following. For the determination of the LD size in liver sections pictures of H&E stainings were used in a 10× magnification. For each animal/liver five individual pictures were used for analysis. After running the plugin on each picture, results of each animal were combined, pixels were converted into µm ($px^2 \times 0.25 = \mu m^2$) and then binned according to their size (20-50, 50-100 and > 100 μm^2). LDs smaller than 20 μm^2 were excluded from the further analysis and graphical representation. Lastly, the mean area of all included LDs was calculated.

2.2.6.2 Determination of adipocyte size

Due to partially poor quality of fat tissue sections, pictures of H&E sections of iWAT and eWAT in 5× magnifications were used for adipocyte size determination. For each cohort, three animals were analysed. After running the plugin on each picture, pixels were converted into µm ($px^2 \times 4 = \mu m^2$) and then binned according to their size (250-750, 750-1250 up to > 7000 μm^2). Adipocytes or artefacts smaller than 250 μm^2 were excluded from analysis and graphical representation.

2.2.7 Sirius red staining

Sirius red is used to stain collagen networks and extracellular matrix, which play a crucial role in fibrosis. As for the H&E staining the Leica Autostainer XL was used to stain tissue sections with in-lab established protocols.

2.2.8 Immunohistochemical staining

Immunohistochemical (IHC) stainings of tissue sections were done using the automated BOND RX system. Sections were deparaffinised, stained and coverslipped automatically according to in-lab established protocols. Antibodies used and their dilutions as well as their incubation times are stated in Table 17.

Table 17: Antibodies used for IHC stainings of tissue sections with dilution.

Antibody	Dilution	Incubation time	Manufacturer Cat. No
F4/80	1:300	60 sec	Abcam, #ab6640
CD3	1:1000	60 sec	Cell Signaling, #78588
B220	1:1000	60 sec	BD Biosciences, #553084

2.2.8.1 Evaluation of immunohistochemical stainings

After staining the tissues, they were scanned by using the Leica slide scanner Aperio AT2 for further processing. Scans were used to take ten pictures in a 200× magnification of each tissue section with the help of ImageScope. For B220 and CD3 stainings all positive cells were counted in each picture using ImageJ. Positive cells are displayed in total numbers per mm^2. For the F4/80 stainings ten pictures were used to determine the percentage of positive area by using ImageJ and a compatible macro. Positive area was displayed in percent. For the evaluation of crown-like structures (CLS) ten pictures were taken in a 50× magnification of eWAT tissue sections and adipocytes surrounded by F4/80+ macrophages were counted in each picture using ImageJ. CLS are displayed in total numbers per mm^2.

2.2.9 Isolation of pre-adipocytes

Isolation of primary pre-adipocytes was adapted to previously published protocols.[103]

For the isolation of primary pre-adipocytes from subcutaneous adipose tissue, male mice aged 8-12 weeks were used. After they were sacrificed by CO_2 asphyxiation, fat pads from flanks were excised (avoid lymph nodes) and put into ice cold 1x PBS containing 5 µg/ml Amphotericin B and 1% P/S until further processing. Then, the adipose tissue was finely minced with scissors until it formed a homogeneous pulp. For each mouse (two fat pads) 5 ml of digestion medium, containing 2.4 U/ml Dispase II, 1.5 U/ml Collagenase D and 10 mM calcium chloride ($CaCl_2$) was used. Pulp then was digested for 30 mins at 37 °C, shaken every 5 mins vigorously. Then the digested tissue was diluted in a 1:2 ratio with DMEM/1xGlutaMAX containing 20 % fetal bovine serum (FBS), 1% P/S and 5 µg/ml Amphotericin B and strained through a 100 µm cell strainer. The cell strainer was flushed

with an additional 10 ml of DMEM/1xGlutaMax before centrifuging for 5 min at 500 xg and 4 °C. The fat layer and supernatant was then carefully discarded and the cell pellet was resuspended in 8 ml of DMEM/1xGlutaMAX containing 20 % FBS and 1% P/S before seeding the cells in a 25 cm^2 flask. After 24 hours cells were washed three times with 1x PBS and medium changed to DMEM/1xGlutaMAX containing 20 % FBS (culture medium). Cells then were grown to 80-90 % confluency before trypsinising them for 5 mins at 37 °C and seeding them on a 75 cm^2 flask. Medium was changed every two to three days until 75 cm^2 plate was confluent.

For differentiation, cells were seeded on 6- or 12-well plates (300/100 k cells per well) and cultured until they reached confluency again. Cells then were treated with induction medium made from culture medium containing 5 µg/ml human insulin, 4 µg/ml Rosiglitazone, 0.5 mM 3-isobutyl-1-methylxanthine (IBMX) and 1 µM Dexamethasone for 72 hours. After three days cells were washed three times with PBS before changing to culture medium supplemented with 5 µg/ml insulin. Pre-adipocytes then differentiate into beige-like adipocytes, forming lipid droplets and were considered fully differentiated seven days after induction.

2.2.10 Isolation of primary fibroblasts

Primary fibroblasts were isolated from mice aged 8-12 weeks as previously described.[104] For this, mice were sacrificed by CO_2 asphyxiation and tails were amputated and put into 70 % EtOH for 5 mins. Tails were then air-dried in 10 cm dishes under the sterile hood, before they were cut into pieces with a size of maximum 3 mm. The cut tissues then were transferred into a 50 ml tube with 5 ml of Trypsin/ethylenediaminetetraacetic acid (EDTA) solution per tail. Tubes then were put in a rotator at 37 °C for 1.5 to 2 hours or until solution appears cloudy. After digestion, 10 ml of RPMI 1640 medium supplemented with 10 % FBS, 50 µM β-Mercaptoethanol, 100 µM Asparagine, 1x L-Glutamine, 1% P/S and 250 ng/ml Amphotericin B were added into a 10 cm dish. Next a 70 µm cells trainer was put in the dish, to which the digested tissue and Trypsin solution was added. Using a syringe stamp the tissue was grinded through the strainer for about 5 mins to release cells. The cell suspension then was transferred to a 15 ml tube and centrifuged for 7 mins at 580 xg and 4 °C. Cells were washed at least one more time or until supernatant was clear, before platting them in a 25 cm^2 dish and allowing them to adhere for 24 hours. Cells were washed thoroughly with 1x PBS before applying fresh medium. Medium was changed every two to three days until cells were 90 % confluent. Cells then were sub-cultured by trypsination of 5 mins at 37 °C and subsequently adding medium and centrifuging them for 5 min at 450 xg at 4 °C. Cells were then seeded on 25 cm^2 flask. Sub-culturing has to be repeated two to three until culture only contains fibroblasts and no other contaminative cell populations. After expansion fibroblast were ready to be used for experiments or freezing.

2.2.11 Isolation of primary hepatocytes

Primary hepatocytes were isolated from mice aged 8-12 weeks via adapted two-step perfusion as previously described.[105] Prior to isolation, appropriate cell culture dishes were coated with in-house made collagen from rat tails. Therefore, collagen was incubated on dishes for

30 mins before aspirating and air-drying them at room temperature (RT).

For the isolation itself, mice were sacrificed with CO_2 asphyxiation and peritoneal cavity was opened. Venous catheter was inserted into *vena cava* and liver was perfused with Earle's balanced salt solution (EBSS) without Ca^{2+} and Mg^{2+} containing 0.5 mM EDTA for 5 mins with a flow rate of 4 ml/min. Immediately after starting perfusion, portal vein was cut to release pressure and perfusion buffer. After the liver is free of blood, medium is changed to EBSS with Ca^{2+} and Mg^{2+} containing 10 mM 4-(2-hydroxyethyl)-1-piperazineethanesulfonic acid (HEPES) and freshly added Collagenase II (0.02 % m/v) and Trypsin inhibitor (0.004 % m/v). Liver then was digested for 10 mins or until it turned soft. Afterwards liver was dissected and transferred to 10 cm dish containing Williams E medium under the sterile bench. Cells then were released by carefully scraping the liver with a cell lifter, before passing the cell suspension through a 70 µm cell strainer. The dish used for releasing the cells as well as the cell strainer was washed with another 15 ml of Williams E medium. For better separation of viable and dead cells, a Percoll gradient was used by adding 25 ml of 9:1 Percoll/Hank's balanced salt solution (HBSS) solution and centrifugation for 7 mins at 440 rpm and 4 °C. After aspiration of supernatant, pellet was washed by resuspending it with 25 ml of Williams E by carefully inverting the tube four to five times before the cell suspension was centrifuged again for 3 mins at 440 rpm and 4 °C. Wash step was repeated one more time. Depending on pellet size, cells were resuspended in 5-10 ml of Williams E culture medium supplemented with 10 % FCS, 1x L-glutamine and 1% P/S. Hepatocytes were then diluted 1:10 in trypan blue to evaluate overall viability and cell number by using a Neubauer counting chamber. Primary hepatocytes were seeded with densities of 2.5×10^6 cells/10 cm dish or 300.000 cells/6-well and cultured in supplemented Williams E medium over night at 37 °C and 5 % CO_2. In case four hours after isolation a large number of cells were not attached to the plates, the medium was changed before overnight incubation.

2.2.11.1 Fatty acid uptake assay

To investigate, if the $MLKL^{K219R}$ mutation does have any effect on the FA uptake of hepatocytes, cells were seeded in 12 well plates at 100.000 cells/well. After overnight incubation, medium was changed to culture medium containing 200 or 500 µM of either palmitic or oleatic acid coupled to FA free bovine serum albumin (BSA). Hepatocytes then were incubated for 24 hours. To measure the uptake of FAs, cells were washed with 1x PBS and stained with 1 µg/ml Hoechst (1:5000) for 10 mins at 37 °C. After Hoechst was washed off, cells were stained with Adipored according to manufacturer´s instructions. By using the Fluorimeter, fluorescence of Hoechst at 380/460 nm and subsequently of AdipoRed at 485/535 nm was measured.

2.2.12 Protein isolation from tissue and cell pellets

Whole protein was isolated from animal tissue and cell pellets and all steps were performed on ice. NP-40 lysis buffer is adapted to either size of tissue piece or pellet size. For liver tissue 200 µl of lysis buffer, while for fat tissues or cell pellets 50-100 µl were used. Animal tissues were homogenized by using ceramic beads and the BeadRuptor for 25 sec at medium

intensity. Cell pellets were only resuspended manually.

Afterwards all samples were centrifuged for 10 mins at 14.000 xg and 4 °C. Without disturbing fat layer on top, supernatant was transferred to a fresh tube. For determination of protein concentration, samples were diluted 1:50 with water for tissue and 1:10 for cell pellets. Dilutions then were used for Bradford assay following manufacturers instructions in a 96-well plate format. By using a calibration curve, protein concentration was determined, and samples were set to needed concentration by further addition of NP-40 lysis buffer and 2x or 5x Lämmli buffer. After cooking samples for 5 mins at 95 °C, they were stored at -80 °C until further use.

2.2.13 Western blot analysis

Isolated proteins (Section 2.2.12) were thawn on ice before loading 20-60 µg of protein on a denaturing polyacrylamide gel for sodium-dodecyl-polyacrylamide gel electrophoresis (SDS-PAGE) (Table 9). The percentage of separating gels were chosen depending on the molecular weights of the investigated protein. In the beginning, gels were run with a voltage of 80 V and a current of 80 mA per gel in the electrophoresis chamber. After 20 mins, voltage was increased to 120 V until samples reached the bottom of the gel.

After SDS-PAGE, separated proteins were transferred to a polyvinylidene fluoride (PVDF) membrane by using semi-dry blotting. PVDF membranes were activated in methanol for 15 sec and stored in Towin transfer buffer (Table 8) until needed. Membranes and polyacrylamide gels were layered between two Towin buffer-soaked Whatman papers in the blotting chambers. Proteins were blotted for 70 mins with a voltage of 20 V and a current of 80 mA per gel.

After successful blotting membranes were blocked with 5 % skim milk in TBS-T buffer (Table 8) for 60 mins. Membranes then were incubated over night at 4°C with primary antibody with the concentrations stated in Table 12. On the next day, membranes were incubated with horse radish peroxidase (HRP)-coupled secondary antibody for 60 mins at RT (Table 13).

Detection of the blots was then done by using the enhanced chemoluminescence (ECL) and ChemiDoc MP gel analyzer according to manufacturer's instructions.

2.2.14 Real-time polymerase chain reaction

Total RNA from tissues and cell pellets was isolated using the NucleoSpin RNA plus kit according to manufacturer's instructions. Concentration of RNA samples was determined using the NanoDrop followed by synthesis of complementary deoxyribonucleic acid (cDNA) templates. Therefore, 1 µg of total RNA was reversly transcribed by using the RevertAid kit following manufacturer's instructions and finally diluted 1:10 with water.

RT-PCR was then performed using the Promega GoTaq quantitative polymerase chain reaction (qPCR) system in a 96-well format. Samples were measured in duplicates with a total reaction volume of 15 µl containing 0.02 nmol of forward and reversed primer (Table 14), 1 $\times$ GoTaq master mix and 4 µl of cDNA template. After centrifuging 96-well plates for 1 min at 1200 xg, samples were measured using the ViiA7 Real-Time polymerase chain reaction (PCR)

system with the following program:

Table 18: Program for RT-PCR.

Temperature	Time	Step	Cycles
50 °C	2 min	–	
95 °C	10 min	Initial denaturation	
95 °C	15 sec	Denaturation	40×
60 °C	1 min	Annealing, elongation	
95 °C	15 sec	–	
60 °C	1 min	Generation of melting curve	
95 °C	15 sec	–	

Generated cycle threshold (Ct) values were further used for expression analysis, which was then done with the ΔΔ-Ct method, normalising samples in a first step to the hypoxanthine guanine phosphoribosyltransferase (HPRT) housekeeping gene and then to untreated WTs as follows (2-4):

$$\Delta\text{Ct} = \text{Ct}(\text{Gene of Interest}) - \text{Ct}(\text{Housekeeper}) \quad (2)$$

$$\Delta\Delta\text{Ct} = {}^{\Delta\text{Ct}}/_{\text{mean } \Delta\text{Ct}(\text{WT}_{\text{untreated}})} \quad (3)$$

$$\text{x-fold change} = 2^{-\Delta\Delta\text{Ct}} \quad (4)$$

To graphically represent the generated data, the calculated x-fold change was used to further calculate a Z-score (Equation 5), which then was used to create heatmaps.[106]

$$Z - \text{Score} = {}^{(\text{x-fold change}) - (\text{mean x-fold change})}/_{\text{mean SD}} \quad (5)$$

Chapter 3

Results

3.1 MLKL^{K219R} completely abolishes necroptosis execution

MLKL is essential for the execution of necroptosis, since its activation leads to disruption of the cell membrane, causing leakage and ultimately, cell death.[107] For the verification of K219R mutations´ functionality, primary fibroblasts from mouse tails of WT and MLKL^{K219R} mice were used for live cell imaging and western blot analysis (Figure 10). The live cell imaging of WT cells clearly shows increased signal of propidium iodide (PI), which can permeate leaky membranes of dead cells, four hours after TNF + LCL161 (smac-mimetic) and Z-Val-Ala-Asp(OMe) (zVAD) (TSZ) stimulation, a well-established inhibitor cocktail used for necroptosis induction.[107] Cells isolated from MLKL^{K219R} mice are protected from cell death and do not show any PI-positive signals.

For analysis via Western blotting, primary fibroblasts were treated with different combinations of inhibitors. Treatment with TSZ induces phosphorylation at S345 of MLKL in WT as well as in MLKL^{K219R} cells. Yet, this phosphorylation alone in MLKL^{K219R} mice is not sufficient to execute necroptosis. Additional treatment with necrostatin-1s (Nec1s) rescues cells from necroptosis by inhibition of RIPK1 (pictures not shown) and thereby repressing the phosphorylation of RIPK3 and MLKL. Results were further confirmed by using primary bone-marrow-derived macrophages from WT and MLKL^{K219R} mice treated in the same manner as the fibroblasts (data not shown).

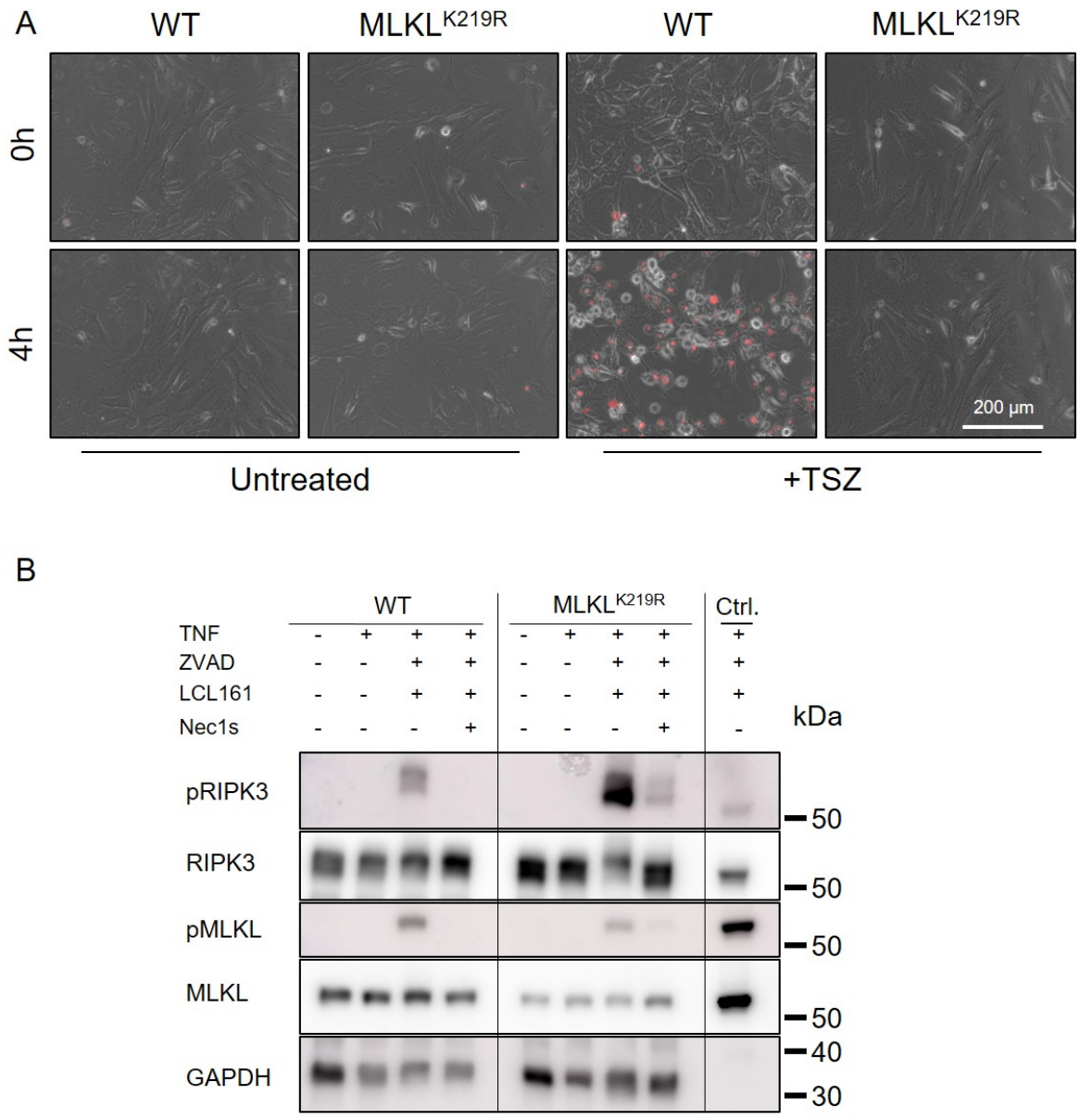

Figure 10: Live cell imaging of primary fibroblasts from MLKL^{K219R} mice show complete blockage of necroptosis execution. (A) Exemplary pictures of live cell imaging of primary fibroblasts at 0 h and 4 h. While WT cells undergo cell death and display strong PI signal, MLKL^{K219R} cells are completely protected. (B) Western blot analysis of stimulated cells (3 h) clearly show induction of phosphorylated RIPK3 and MLKL which is blocked by additional treatment with RIPK1 inhibitor Nec1s. L292 cells were used as positive control (Ctrl.) and treated similar to primary fibroblasts. Cells are untreated or treated with 25µM zVAD, 10 µM N-[(1S)-1-cyclohexyl-2-[(2S)-2-[4-(4-fluorobenzoyl)-2-thiazolyl]-1-pyrrolidinyl]-2-oxoethyl]-2S-(methylamino)-propanamide (LCL)161, 2 ng/ml TNF and 10 µM Nec1s. PI was measured at 305/617 nm.

3.2 MLKL^{K219R} mutation reduces weight gain, improves glucose response and leads to age-dependent increase in activity

To further investigate the role of the MLKL^{K219R} mutation in the context of metabolic dysregulation, 6-8-week-old mice were fed a WD alone (MASH cohort from here on) (Figure 11A) or with additional alcohol (MetALD cohort from here on) (Figure 11B) for 20 weeks. Their body weight as well as their food intake was measured weekly. In both models mutant mice show reduced body weight gain over the investigated time period. For the MASH cohort mutant mice are significantly leaner from week 8 on of feeding. The cumulative food intake is equal over all models and genotypes, but compared to the MASH cohort, MetALD animals consumed slightly less food (405 g vs. 380 g).

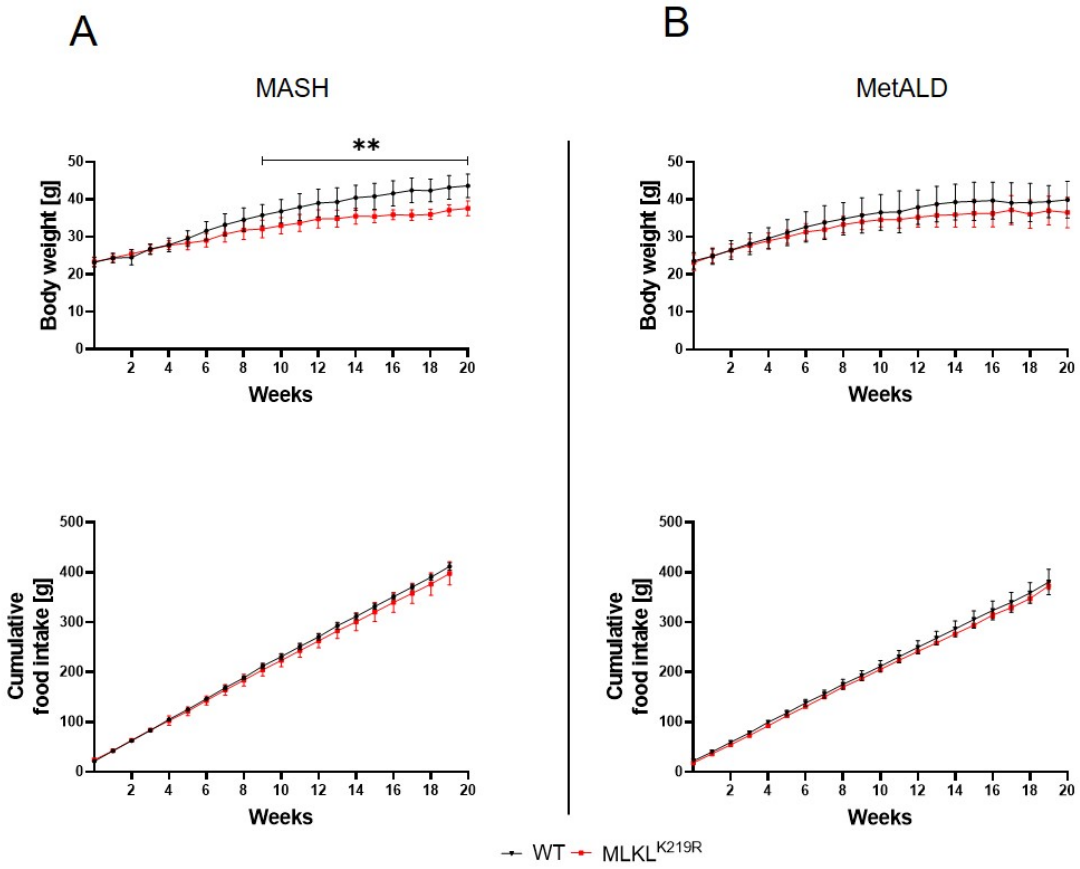

Figure 11: Even though WT and MLKL^{K219R} animals consume the same amount of food, MLKL^{K219R} animals showed significantly reduced body weight. (A) WT and MLKL^{K219R} mice receiving a WD for 20 weeks and (B) WT and MLKL^{K219R} mice receiving a WD with 10% (v/v) alcohol for 20 weeks. Significantly different body weights between experimental groups were ** or higher. Values are mean ± standard deviation (SD). Statistical analyses were done by ordinary two-way ANOVA with an uncorrected Fisher's least significant difference (LSD); *p<0.05; **p<0.01

In order to gain further insights into the metabolic consequences of the dietary intervention, glucose metabolism was examined by performing an *i.p.* GTT in week 16 of feeding the mice with WD (± alcohol). MLKL^{K219R} mice exhibit a markedly reduced glucose profile in both models (Figure 12A), accompanied by a significantly enhanced overall glucose clearance in the both models (Figure 12B). Fasting insulin levels are significantly decreased

in the mutant mice of the MASH cohort compared to WT control animals (Figure 12C). For the MetALD cohort there is no difference between the genotypes detectable.

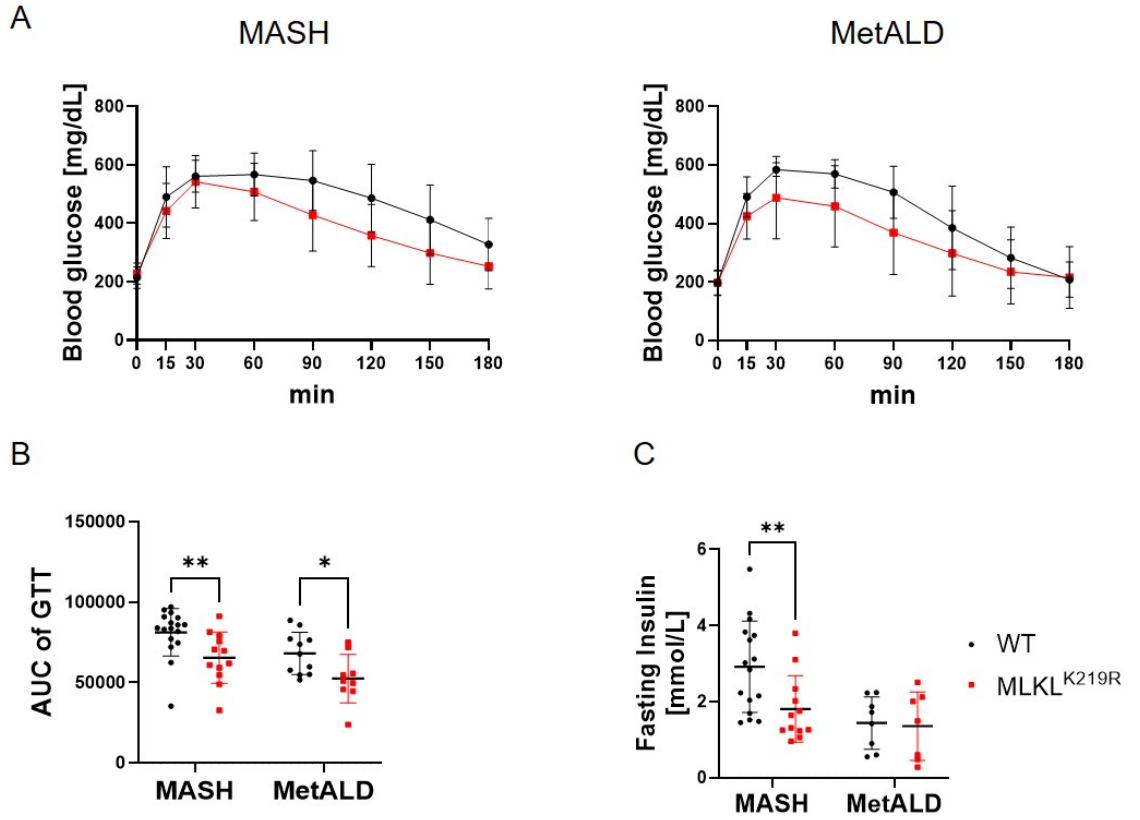

Figure 12: MLKL^{K219R} mice show improved GTT results than WT control animals in both dietary models. (A) Blood glucose levels in [mg/dL], determined every 15-30 mins of WT (MASH: 17 animals; MetALD: 11 animals) and MLKL^{K219R} (MASH: 12 animals; MetALD: 10 animals) mice 16 weeks on WD and WD + 10% (vol/vol) alcohol (B) AUC of GTT curves. (C) Fasting insulin levels in [mmol/l] of blood taken before injecting glucose. Values are mean ± SD. Statistical analyses were done by unpaired multiple t-test using Benjamini, Krieger and Yekutieli for two-staged step up analysis (GTT curves) and ordinary two-way ANOVA with an uncorrected Fisher´s LSD; *p<0.05; **p<0.01; (AUC and fasting insulin).

After 20 weeks of diet, mice were fasted for four hours before sacrificing them and isolating livers, fat tissues and muscle. Animals of same age (26-28 weeks old), maintained on an NCD for the same duration, served as the untreated control group. On macroscopic level (Figure 13A), livers of fed MLKL^{K219R} mice are smaller than that of control animals in both feeding models, however the liver/body weight ratios do not show differences between genotypes. Neither do the absolute weights of livers differ greatly within the groups, but the MLKL^{K219R} mice display overall smaller livers in both diet models (Figure 13B).

H&E stainings of livers clearly show steatosis in both feeding models, but for both models the MLKL^{K219R} mice have lower grades of steatosis compared to control animals. Furthermore, this is confirmed by the NAFLD activity score (NAS) of livers, that shows significant reduction of steatosis and ballooning of hepatocytes in MLKL^{K219R} mice. On the other hand, inflammation is increased in MLKL^{K219R} animals in both models (Figure 13C). In summary, the majority of mice receiving WD ± alcohol have a NAS score of five or higher rendering them diagnostically as MASH.[108] For further analysis of liver steatosis, LDs were

analyzed, and size was determined (Figure 13D). For both diet models the MLKL^{K219R} mice show higher number of small LDs in the range of 20-50 µm^2 and lower number of big LDs in the range above 100 µm^2, even significantly lower within the MASH cohort. Furthermore, the additional feeding of alcohol displays a slight shift towards bigger LDs compared to WD feeding alone.

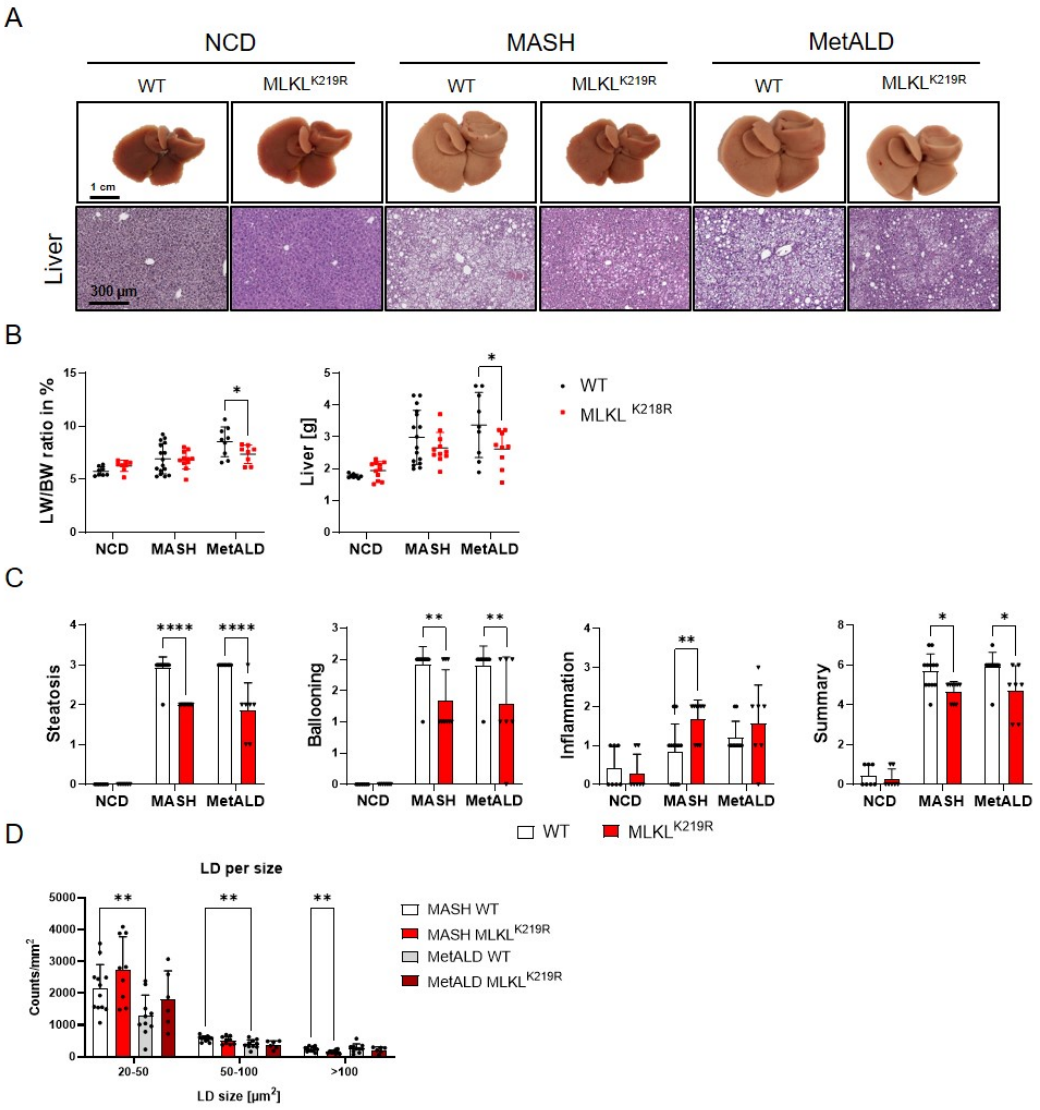

Figure 13: MLKL^{K219R} mutation ameliorates diet induced liver steatosis and macrosteatosis in MASH model. (A) Exemplary macroscopic pictures of livers of 26-28 week-old animals with corresponding H&E staining liver (B) Organ to body weight ratios as well as (C) Single parameters and summary of NAS score from livers (D) Quantification of Lipid droplet size distribution from liver H&E stained livers. Values are mean ± SD. Statistical analyses were done using an ordinary two-way ANOVA with an uncorrected Fisher´s LSD; *p<0.05; **p<0.01; ***p<0.001; ****p<0.0001

In order to further evaluate chronic liver damage, livers were stained with Sirius red, which is commonly used to determine fibrosis (Figure 14). Compared to MASH animals, MetALD animals exhibit interstitial positive areas beyond blood vessels, but still to a minor extend. Due to the overall low signal and minor differences of Sirius red staining, it was not possible to perform evaluation on the tissue sections.

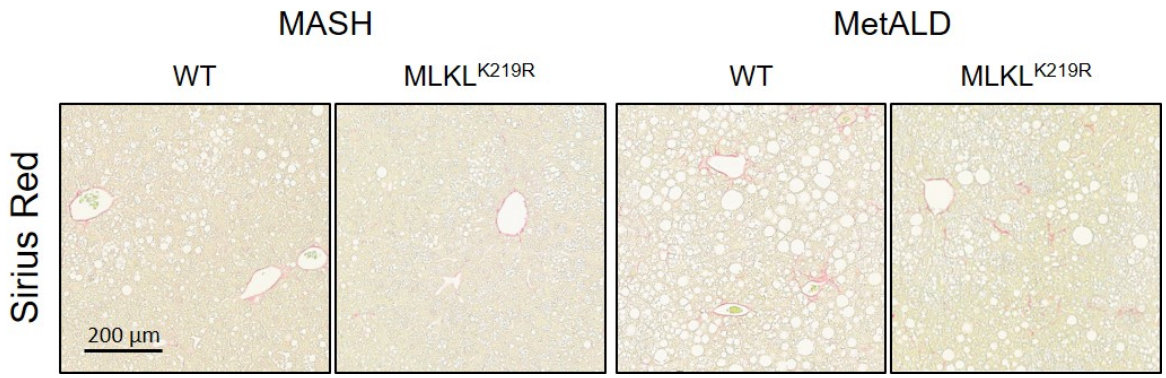

Figure 14: 20 weeks on WD or WD + alcohol is not sufficient to induce liver fibrosis. Graph shows representative pictures of Sirius Red staining from experimental animals aged 26-28 weeks.

To further analyze metabolically important tissues, different fat depots were investigated more in-depth. The H&E stainings of iWAT and eWAT clearly display adipose hypertrophy upon receiving WD ± alcohol independent of the genotype (Figure 15A).

Furthermore, both dietary models show that organ to body weight ratios of iWAT and eWAT are increased in both genotypes. But in the MASH model iWAT is significantly reduced in MLKL^{K219R} mice compared to control mice. These results are also reflected in the graphs for absolute organ weight where iWAT is significantly reduced in MASH mutant mice compared to WT (Figure 15B). For the MetALD group both genotypes show reduced tissue weights in iWAT when compared to the MASH WT, which overall showed the biggest increase. For the eWAT this decrease is not as big, but tendencies can be clearly seen, that additional alcohol does influence diet induced fat tissue expansion. For in-depth analysis of fat tissue and its expansion, adipocyte size was further determined. Size distribution of iWAT (Figure 15D) shows that adipocytes of WT animals in the MASH cohort significantly expand, compared to MLKL^{K219R} as well as NCD animals. Especially the number of big adipocytes above 2500 µm^2 are increased in MASH WT animals. Compared to MASH WT, size of adipocytes in iWAT of MetALD cohort is not increased very much, yet MLKL^{K219R} animals have significantly bigger mean size. Also mutant mice in this cohort display less small (500-1000 µm^2) and more bigger (>1500 µm^2) adipocytes. For the visceral fat deposit, eWAT, size distribution differs to that of the iWAT. Compared to the NCD cohort, adipocyte size increases in both diet models to a similar extent (Figure 15E). But in both diet models mutant mice tend to have less smaller and more bigger adipocytes, while in the NCD cohort the mutants generally show to have smaller ones.

In summary, analysis of fat tissues revealed that mostly iWAT in the MASH cohort is protected from expansion by MLKL^{K219R} mutation. eWAT on the other hand does not show any protective effects on adipocyte expansion, even though MLKL^{K219R} animals on NCD tend to have smaller adipocytes than WT controls.

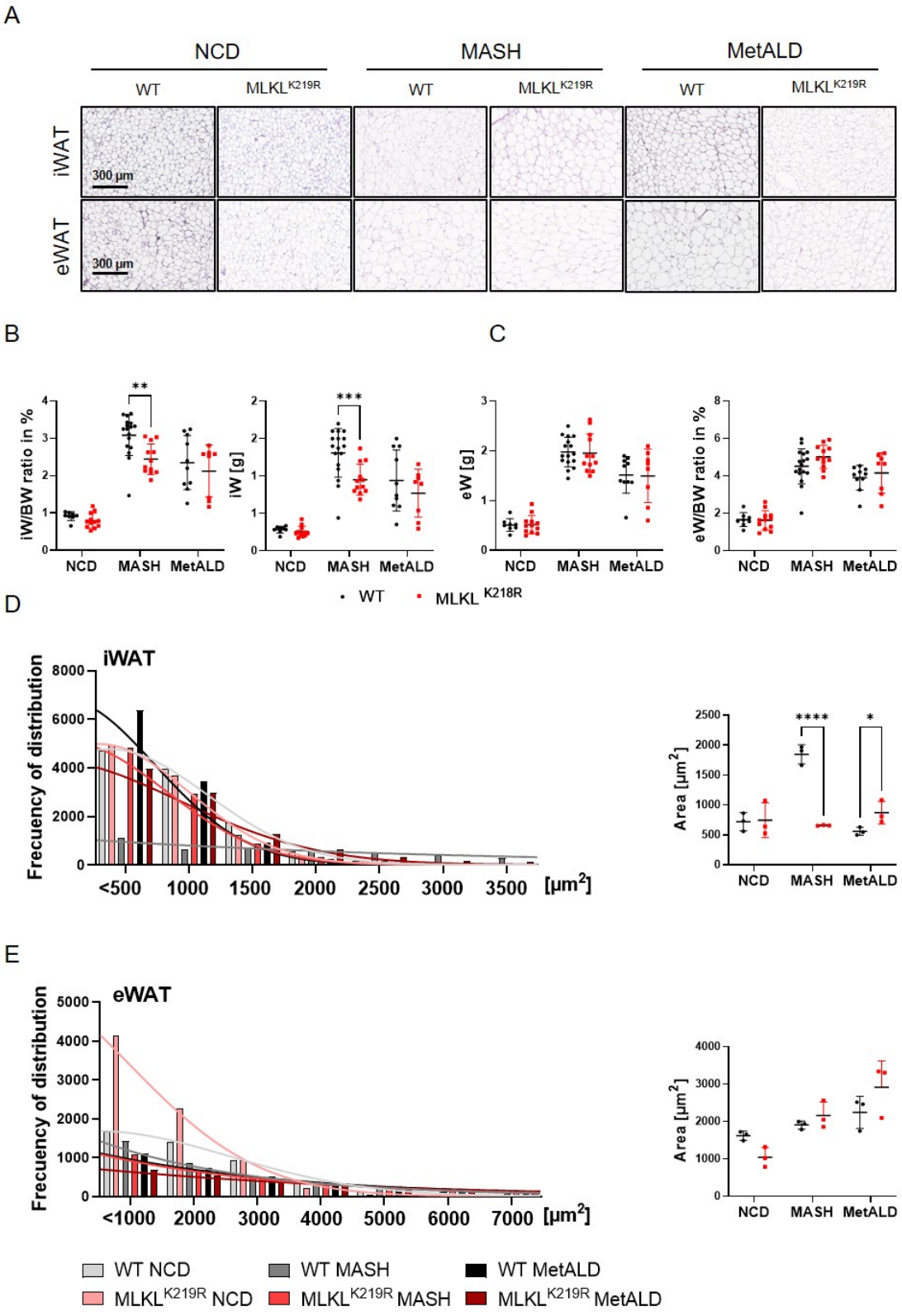

Figure 15: Analysis of fat tissues show significant reduction of iWAT in MLKL^{K219R} MASH animals. (A) Exemplary macroscopic pictures of iWAT and eWAT of 26-28 year-old animals with corresponding H&E stained liver (B) iWAT to body weight ratios as well as absolute organ weights (C) eWAT to body weight ratios as well as absolute organ weights. Frequency of distribution of adipocytes in (D) iWAT and (E) eWAT tissue as well as corresponding average adipocyte size determined from pictures H&E stainings (three animals per group). Values are median (B,C) or mean ± SD (D). Statistical analyses were done using an ordinary two-way ANOVA with an uncorrected Fisher´s LSD; *p<0.05; **p<0.01; ***p<0.001; ****p<0.0001

Since lifestyle adaptation and an increase in physical activity are still essential for treating obesity as well as related co-morbidities, SPA was investigated in untreated animals on NCD.

SPA was measured in untreated individual animals of various ages over a 48-hour period, following a 24-hour habituation phase. An event was detected whenever the light barrier was interrupted. For the investigations, animals aged 7 to 20 weeks were tracked and subsequently analyzed in two age groups: up to 15 weeks and over 15 weeks (Figure 16). The analysis of the movement data shows that untreated animals aged up to 15 weeks, regardless of genotype, exhibit similar levels of movement/activity (Figure 16A), which is also clearly reflected in the representation of average SPA (Figure 16C). However, in the older group (>15 weeks), a clear increase in events is observed in MLKL^{K219R} animals, which not only generate more events during the dark phases but also show significantly increased activity during both light phases (Figure 16B). This is also evident in the graph depicting average SPA (Figure 16D). This age-specific effect is consistent with the observed body weight data (Figure 11A). Here, the weight curves clearly diverge after nine weeks of feeding, at which point the animals are 15 to 16 weeks old.

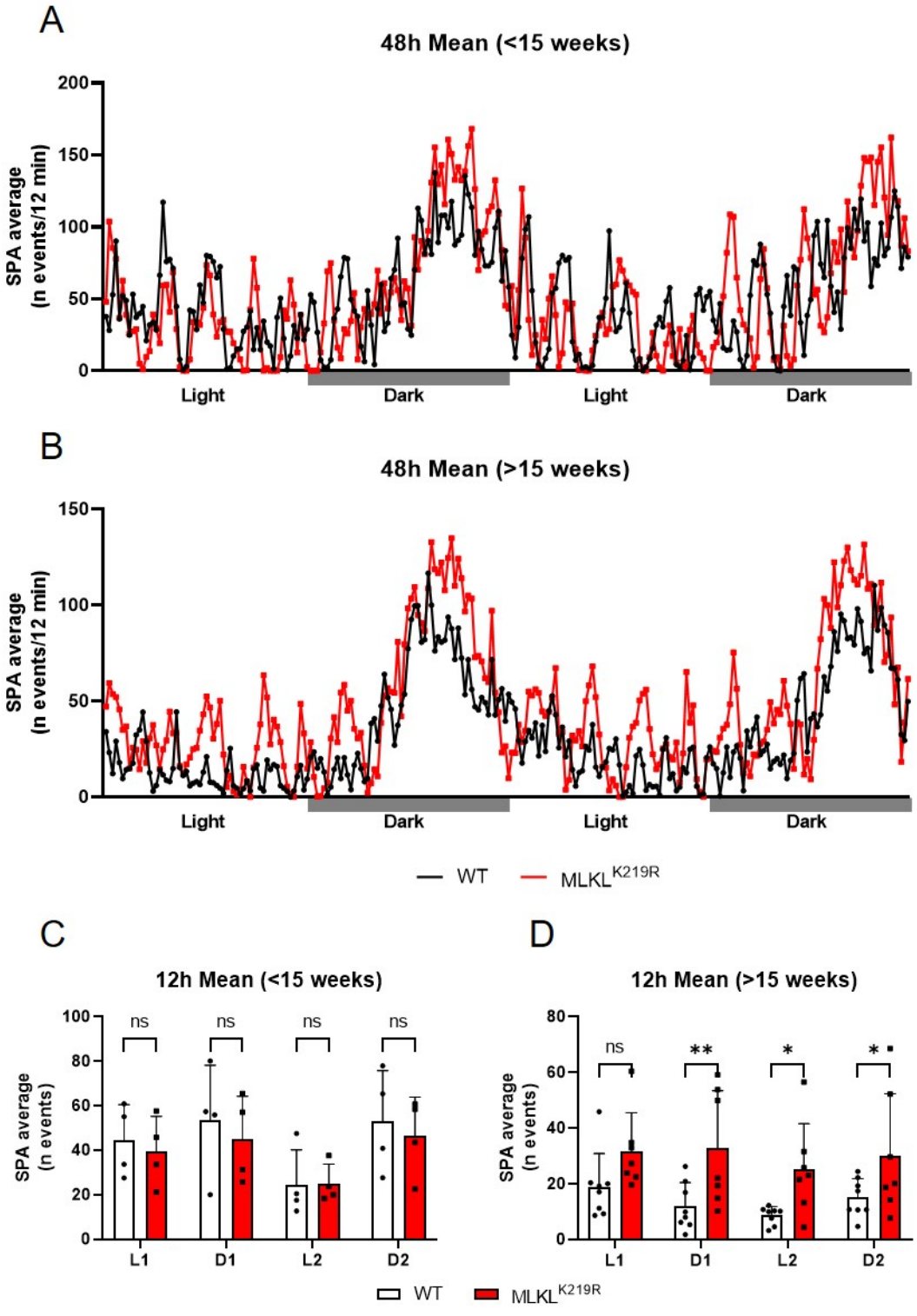

Figure 16: SPA profiles of MLKL^{K219R} and WT animals reveals that untreated mutant mice show overall higher activity. (A) 7–14-week-old (WT n = 4, MLKL^{K219R} n = 4) and (B) 15–20-week-old (WT n = 8, MLKL^{K219R} n = 7) mice were analyzed for 48 hours (two full light (L)/dark (D) phases). Each data point represents the average number of movements detected in a time interval of 12 minutes. (C, D) Summarized averaged SPA of 12-hour period from (A) and (B) respectively. Values are mean ± SD. Statistical analyses were done by an ordinary two-way ANOVA test with an uncorrected Fisher´s LSD. *p<0.05; **p<0.01

3.3 MLKL^{K219R} mutation confers protection from adipose tissue inflammation

To further determine the health condition of mice, markers associated with liver damage and lipid metabolism were analysed in the blood serum. The standardized liver marker panel (Figure 17A) shows that all serum markers increase upon diet.

Within the NCD group there are no differences between the two genotypes observed concerning the liver damage markers. For the dietary models there is an evident increase in AST, ALT, GLDH and AP in all WT control animals when comparing to the NCD group. The MetALD group displays big variances in the WTs, suggesting a heterogeneous liver damage phenotype. Compared to each their controls, MLKL^{K219R} show significant reduction in damage markers across both models.

Interestingly, even though mutant mice displayed lower body weight, markers for the fat metabolism (Figure 17B) over all did not reveal major differences. Cholesterols (LDL, HDL and total cholesterol) are all increased to similar extend in both diets compared to the NCD group. But for LDL and total cholesterol MLKL^{K219R} display partially significant lower levels in both dietary models even though they are still higher than the values for the NCD animals. NEFAs display a decrease in MLKL^{K219R} mice of the NCD as well of the MetALD cohort, surprisingly not in the MASH cohort. Lastly, the serum triglyceride concentration, mostly produced in the liver, is the highest in NCD MLKL^{K219R} animals, even noticeably higher than these of WT animals. Otherwise, triglycerides are slightly lower in MetALD animals, compared to MASH animals but do not show any genotype specific differences.

These serum analyses suggest, that MLKL^{K219R} mutation does confer a protective effect on diet-induced liver damage but has only mild effects on cholesterol and none on triglyceride levels in blood serum.

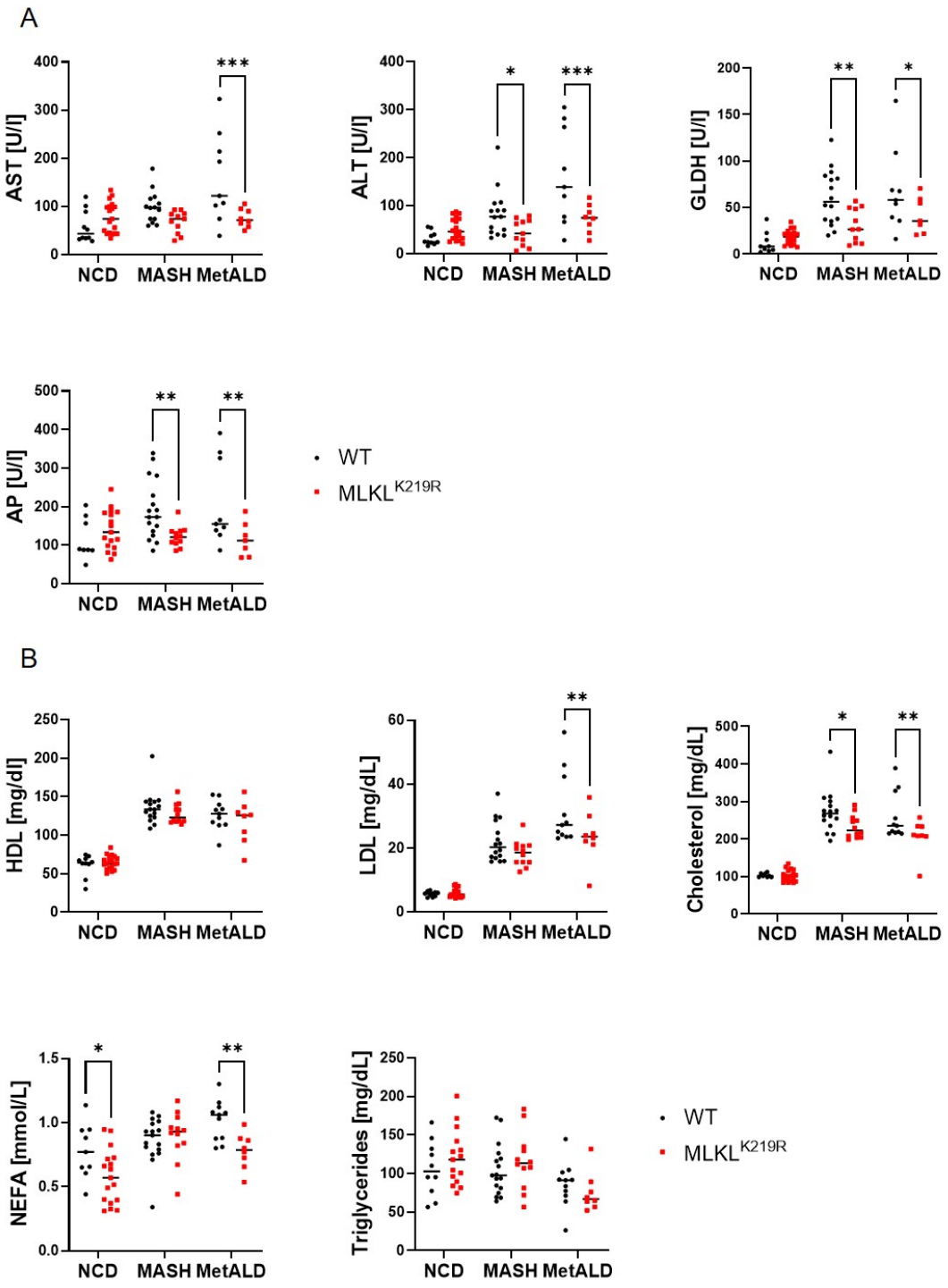

Figure 17: MLKL^{K219R} mutation confers protective effect on induction of diet-induced liver damage. (A) liver damage markers AST, ALT, GLDH and AP in U/l measured in blood serum (B) analysis of metabolic/lipid metabolism markers HDL, LDL, Cholesterol, Triglycerides in mg/dL and NEFA in mmol/L in blood serum. Blood samples of 26-28 week old mice fed a NCD or WD diet ± 10% (vol/vol) alcohol. Values are mean ± SD. Statistical analyses was done by an ordinary two-way ANOVA test with an uncorrected Fisher´s LSD. *p<0.05; **p<0.01; ***p<0.001

Inflammation is a key driver of MASH, thus liver sections were analysed by immunohistochemistry for inflammatory markers such as F4/80 (macrophages), B220 (B-cells), and CD3 (T-cells). Both dietary models led to increased infiltration of macrophages and T-cells, with a stronger effect observed in the MetALD cohort. Notably, $MLKL^{K219R}$ animals exhibited a higher degree of immune cell infiltration compared to WT controls, whereas no differences were found between genotypes in the NCD group for any of the immune cell populations investigated (Figure 18). B220+ cells, on the other hand, were reduced in both MASH and MetALD groups compared to NCD animals. However, this reduction was partially ameliorated in $MLKL^{K219R}$ animals under both dietary models.

These stainings show that $MLKL^{K219R}$ mutation does affect liver infiltrating immune cell populations.

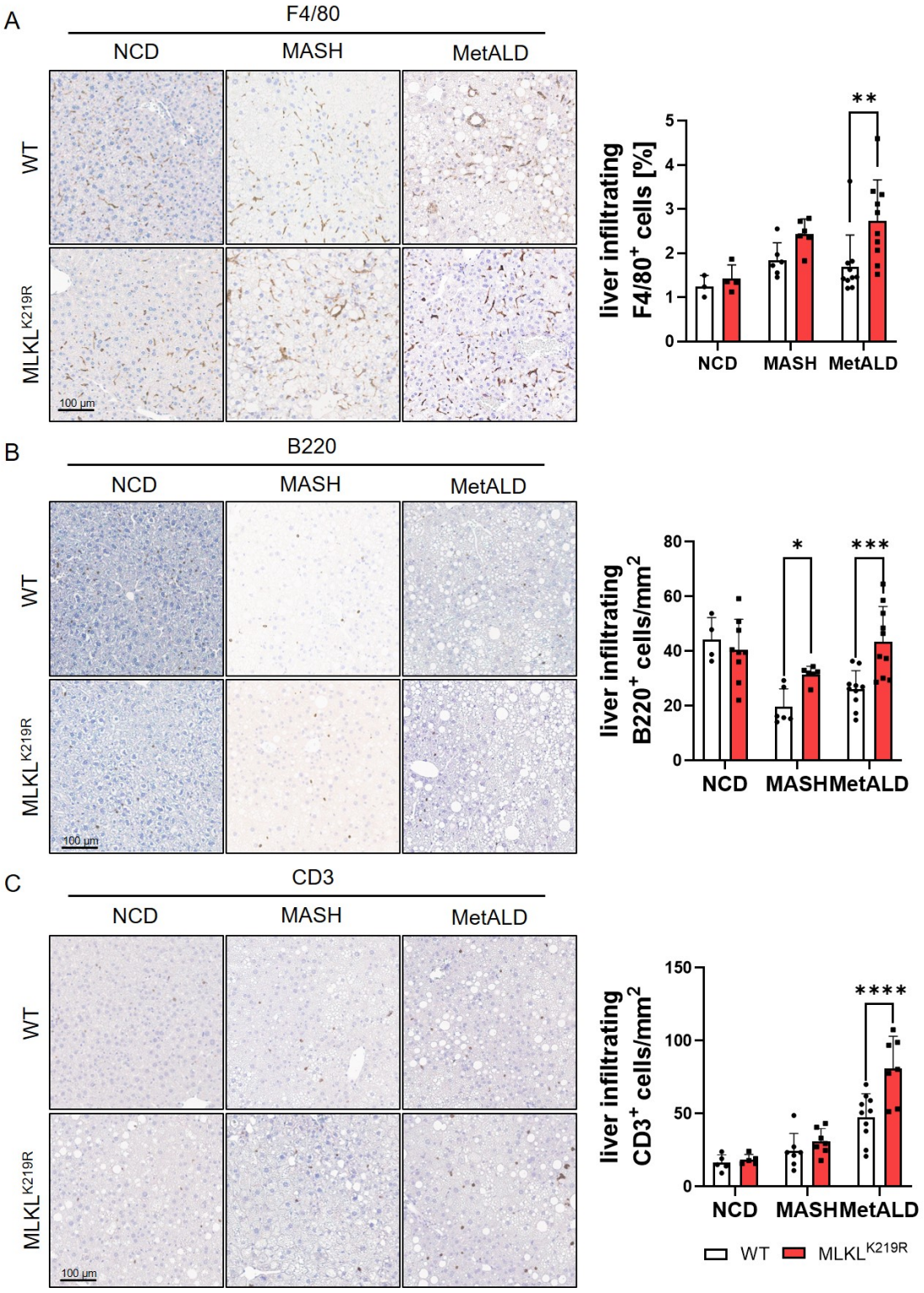

Figure 18: MLKL^{K219R} mice show increased immune cell infiltration in livers compared to WTs. Exemplary pictures of IHC stainings of (A) F4/80, (B) B220 and (B) CD3+ immune cells in liver sections with corresponding evaluation of stainings. Values are mean ± SD. Statistical analyses were done by an ordinary two-way ANOVA test with an uncorrected Fisher´s LSD. *p<0.05; **p<0.01; ***p<0.001; ****p<0.0001

In obesity and metabolic disease, inflammation in adipose tissue and adipocyte death has a crucial role in the disease's pathology, therefore sections of eWAT were stained for F4/80+ macrophages and CLS were counted.[109] CLS are formed by macrophages surrounding dying adipocytes/cells and thereby can be used for an indicator of adipocyte death and adipose

tissue inflammation. Animals on NCD only displayed CLS occasionally to a minor extent, meanwhile both dietary models clearly increased the numbers of CLS. Compared to the results of the livers above, MASH MLKL^{K219R} mice do have significantly less F4/80+ CLS than WT animals in both dietary models. Compared to the MASH, the MetALD cohort shows a reduced number of CLS in eWAT (Figure 19).

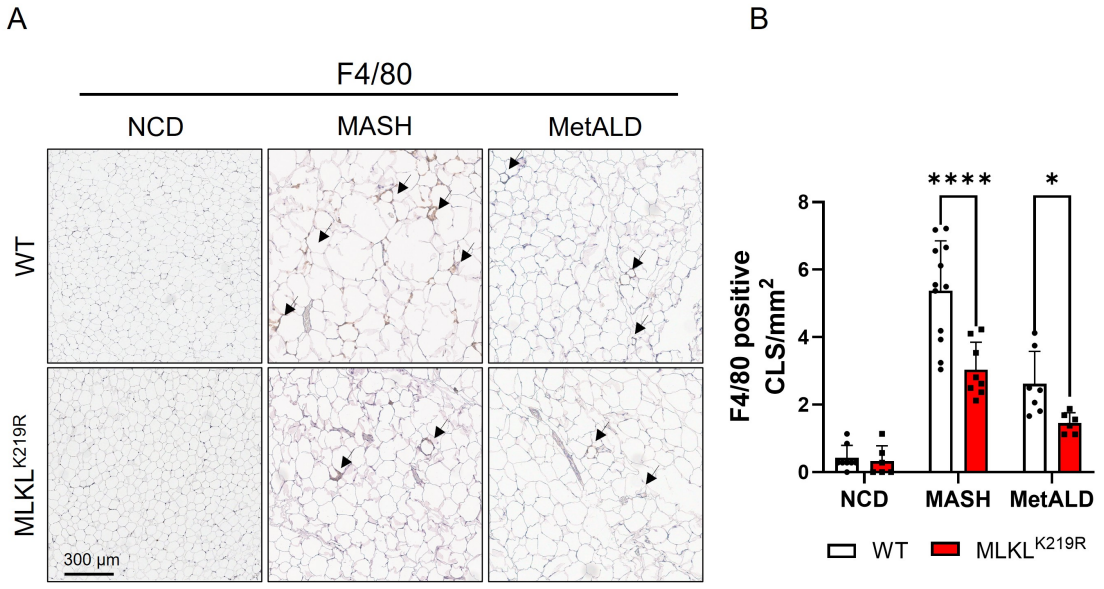

Figure 19: CLS are significantly decreased in eWAT of MLKL^{K219R} animals. (A) Exemplary pictures of F4/80 staining of eWAT tissue sections of untreated and experimental animals aged 26-28 weeks. (B) Evaluation of CLS/mm^2. Values are mean ± SD. Statistical analyses were done by an ordinary two-way ANOVA test with an uncorrected Fisher´s LSD. *p<0.05; **p<0.01; ***p<0.001; ****p<0.0001

Lastly, mRNA expression analyses of inflammatory genes were performed in liver, iWAT and eWAT.

In liver, MetALD cohort shows the overall highest upregulation of inflammatory genes while the expression of IL-1α is significanrly decreased in MLKL^{K219R} animals. The MASH cohort displays only a slight increase of chemokine C-C-motif ligand 2 (CCL2) in both genotypes, compared to NCD animals. All other genes show only a small upregulation compared to NCD group (Figure 20). These findings are in line with the results of the histological analysis of immune cells (Figure 18), that there is upregulation but not as much as in the MetALD group.

Looking into adipose tissue, specifically iWAT and eWAT, it is evident that pro-inflammatory genes are significantly upregulated, particularly in the MASH group (Figure 20). Within each feeding group, gene regulation between MLKL^{K219R} and WT animals shows no significant differences. Differences are only observed between the different feeding groups. Compared to the results from the liver, the investigated genes in the MetALD group are only slightly induced, whilst the MASH cohort shows strong induction of proinflammatory genes. This is likely due to the fact that the animals in this group have smaller fat depots (Figure 12).

In summary, both feeding models increase inflammation in all examined tissues. However, genotype does only play a minor role in this context.

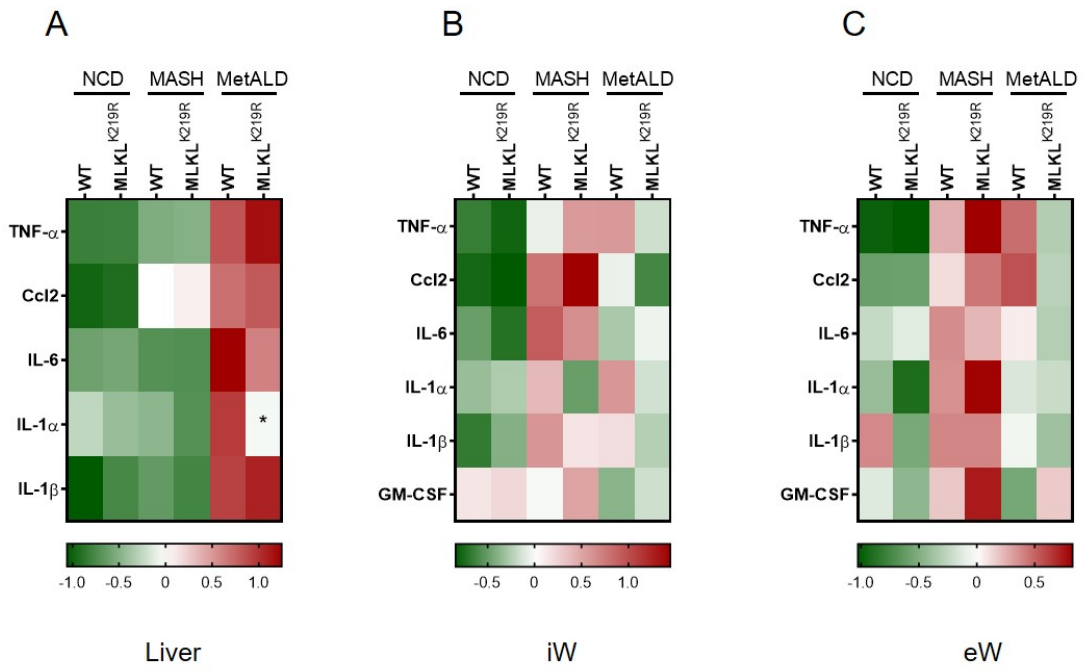

Figure 20: qPCR analysis of pro-inflammatory genes in different tissues does rather show tissue then genotype specific effects. qPCR analysis of (A) liver, (B) iWAT and (C) eWAT tissue from 26-28 week old experimental animals. Graphs illustrate the Z-scores, which were calculated from the x-fold change of mRNA expression, normalized to NCD WT and HPRT as housekeeper gene. Between four and ten animals from each genotype and diet group were examined for every gene. Analysis was done with a 2-way ANOVA using a Tukey test for multiple comparisons. *p<0.05

Western blot analysis of different tissues was not able to show increased or any levels of programmed cell death (Figure 21). Neither markers for apoptosis (cl.-Casp 3) nor for necroptosis (p-MLKL) show activation in the investigated tissues (liver, iWAT, eWAT). Only appropriate positive controls show signal for each of the activated cell death pathways.

These data suggests , that neither WD alone, nor the combination with additional alcohol induces detectable levels of executioner proteins of necroptosis or apoptosis.

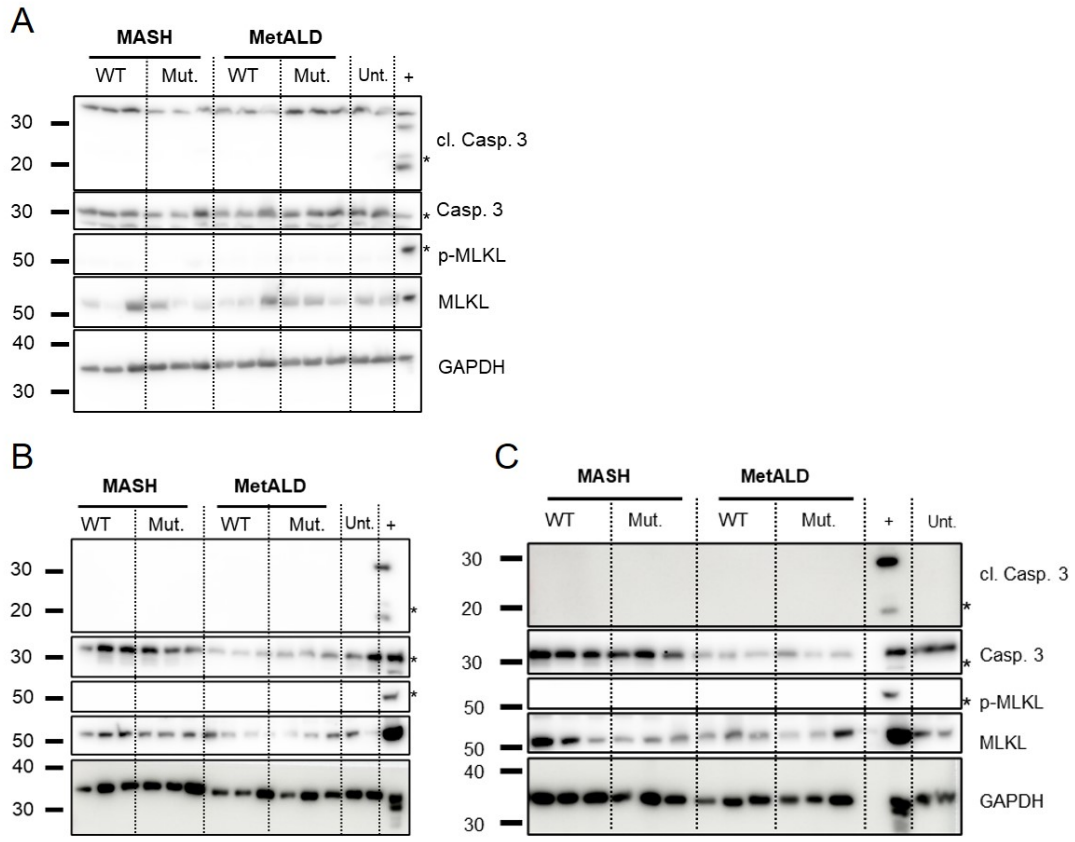

Figure 21: Western blot analysis did not reveal apoptosis nor necroptosis induction in any of the investigated tissues or dietary cohorts. Western blots from 26-28-week-old experimental animals of (A) liver, (B) iWAT and (C) eWAT tissue analyzing (cleaved-) caspase 3, (phospho-) MLKL and glyceraldehyde-3-phosphate dehydrogenase (GAPDH) as loading control. Each lane was loaded with 60 µg of protein. WT, wild-type; Mut., MLKL^{K219R} mutation; unt., untreated; cl., cleaved; p, phospho; size on the left in kDa.

3.4 MLKL^{K219R} mutation leads to alterations in overall lipid metabolism on cellular level

Even though adipose tissue plays a major role in storing and absorbing energy in the form of lipids, it also has a variety of other functions, such as regulating FFAs in the serum and maintaining insulin sensitivity. Furthermore, thermogenesis is of significant importance for maintaining body temperature.[8] Therefore, the expression of the UCP1, a central enzyme in thermogenesis, was investigated in adipose tissue. Gene expression of UCP1 does show downregulation in iWAT and a mild upregulation in eWAT in both dietary models compared to the control WT on NCD (Figure 22). Even though the MLKL^{K219R} mice of the MetALD cohort in iWAT do show UCP1 upregulation, genotype does not seem to have a major effect on expression levels. PR/SET domain 16 (PRDM16), playing key role in adipogenesis, differentiation and beiging of iWAT, on the other hand shows upregulation in the MASH cohort. Further, adiponectin, involved in insulin signaling, is downregulated and leptin, the saturation hormone, is upregulated compared to NCD animals again in both fat tissues.[110] Fibroblast growth factor 21 (FGF21), involved in glucose and lipid metabolism, is also upregulated in both dietary models and genotypes.[111] Carnitin-palmitoyltransferase

1 (Cpt1)A and stearoyl-CoA desaturase-1 (Scd1) show upregulation, especially in the MetALD cohort, suggesting increased fat oxidation and lipogenesis.

Overall MLKL^{K219R} does only show mild genotype- but strong diet-specific effects on the investigated metabolic genes in iWAT and eWAT.

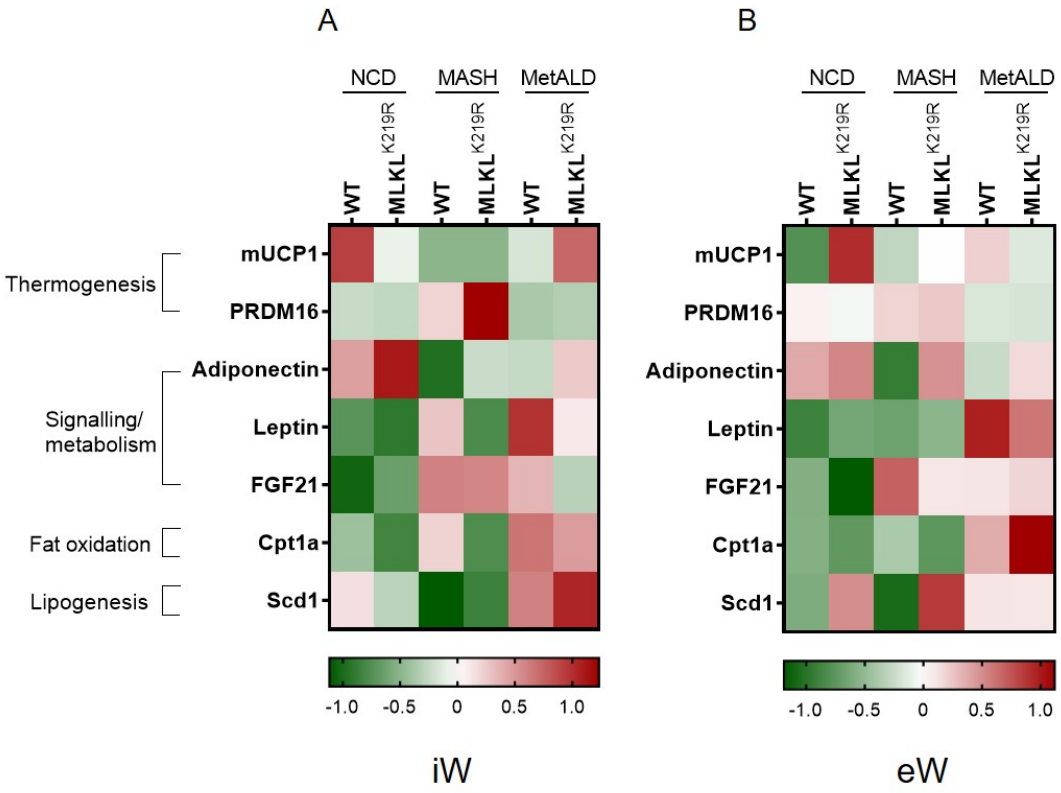

Figure 22: mRNA expression analysis of lipid metabolism shows especially diet-dependent but only mild genotype-specific changes. qPCR analysis of (A) iWAT and (B) eWAT tissue from 26-28 week old experimental animals. Graphs illustrate the Z-scores, which were calculated from the x-fold change of mRNA expression, normalized to NCD WT and HPRT as housekeeper gene. Between four and ten animals from each genotype and diet group were examined for every gene. Analysis was done with a 2-way ANOVA using a Tukey test for multiple comparisons

Investigation of UCP1 upregulation on protein levels through western blot analysis does not show any positive signal of UCP1 in either iWAT or eWAT (Figure 23).

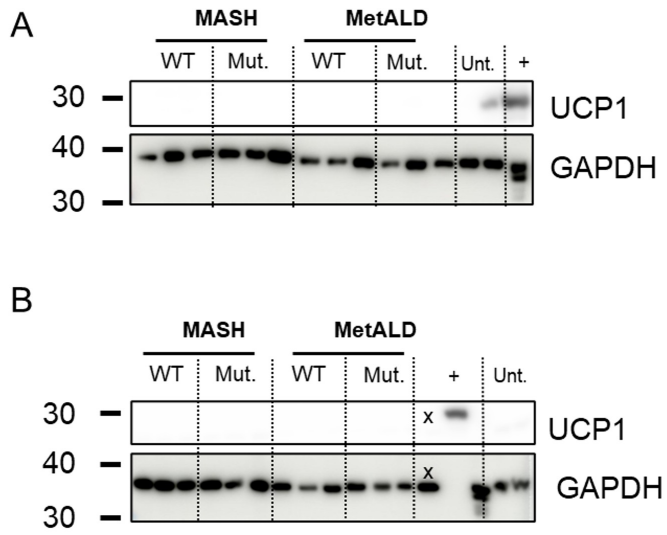

Figure 23: Western Blot analysis did not show signal for UCP1 in adipose tissue. Western blots from 26-28 week old experimental animals of (A) iWAT and (B) eWAT tissue analyzing UCP1 and GAPDH as loading control and BAT from untreated animals as positive control. Each lane was loaded with 60 µg of protein. WT, wild-type; Mut., MLKL^{K219R} mutation; unt., untreated; size on the left in kDa. X marks falsely loaded samples.

Histological analysis revealed not only reduced steatosis in MLKL^{K219R} animals but also increased infiltration of immune cells. To further investigate these findings, liver metabolism was analyzed with qPCR, focusing on energy metabolism (peroxisome proliferator-activated receptor α (PPARα)) as well as lipid metabolism due to the liver's critical role in lipid synthesis (fatty acid synthesis (Fasn), Scd1), storage (cell death-inducing DFFA-like effector A (Cidea)), transport (fatty acid binding protein 4 (Fabp4)), and oxidation (Cpt1, diacylglycerol-O-acyltransferase 1 (Dgat1)). Fasn is upregulated in all groups compared to untreated WT animals, with the most pronounced increase in MASH MLKL^{K219R} animals. Genes involved in lipogenesis (Scd1), fat transport (Fabp4), fat storage (Cidea), and energy metabolism (PPARα) were upregulated in response to high-caloric diets. Highest Cidea upregulation seen in the MetALD cohort is in line with results from Figure 13 where this cohort shows a trend towards macrosteatosis. Further analysis of β-oxidation revealed inverse regulation of Cpt1A and Dgat1, with Cpt1A being upregulated while Dgat1 was downregulated upon receiving WD. However, no significant differences between genotypes within the respective dietary models were observed for any of the investigated genes.

In summary, the data indicate an upregulation of anabolic pathways, while catabolic pathways are downregulated.

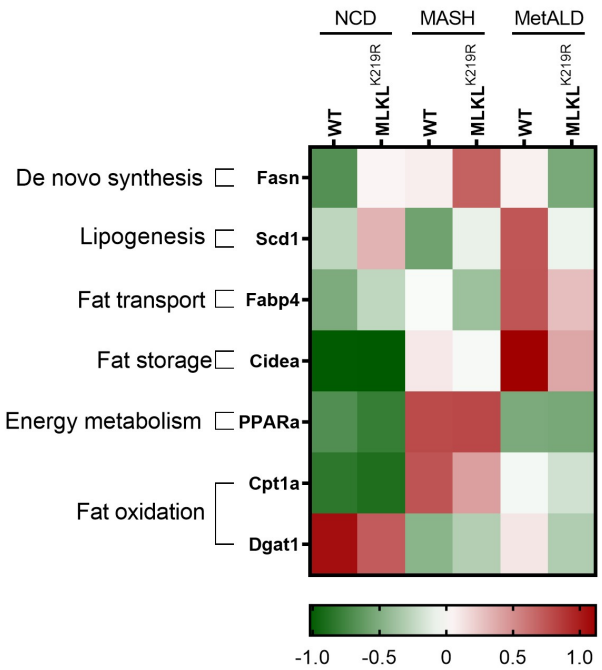

Figure 24: Changes in lipid metabolism within the liver only show mild variation between genotypes. qPCR analysis of liver tissue. Graphs illustrate the Z-scores, which were calculated from the x-fold change of mRNA expression, normalized to NCD WT and HPRT as housekeeper gene. Analysis was done with a 2-way ANOVA using a Tukey test for multiple comparisons

.

When consuming an excess amount of calories, in the form of sugars and fats, lipid uptake and storage can be overloaded, meaning that the lipids circulating in the blood cannot be properly stored in adipose tissues. In this case, the liver, which has also a major role in lipid metabolism, is able to further store these excessive lipids and thereby regulate lipid levels of the serum. The uptake of these lipids to the hepatocytes hereby is essential. To further investigate, if MLKL^{K219R} does have an impact on lipid uptake, primary hepatocytes were treated with either BSA (negative control) or BSA-coupled palmitate (saturated) and oleate (unsaturated) in different concentrations. Treatment with FAs clearly increased intracellular lipids and AdipoRed signal (relative fluorescence units (RFU)) in a concentration dependent manner (Figure 25A/B). Further 500 µM of palmitate represents a very harsh stimulus, killing some of the hepatocytes within the 24 hours of treatment (rounded cells in the brightfield picture). The evaluation of the AdipoRed signal/RFU further reveals strong batch effects especially in the hepatocytes treated with the high concentration of FAs. The western blot analysis of primary hepatocytes treated with with FAs (Figure 25C) did not show any signal for (phospho-) RIPK3 nor phospho-MLKL in WT and MLKL^{K219R} cells. Therefore, FAs did not induce necroptotic signaling.

However, in sum the experiments show, that the genotype does not have a significant effect on the uptake of FAs.

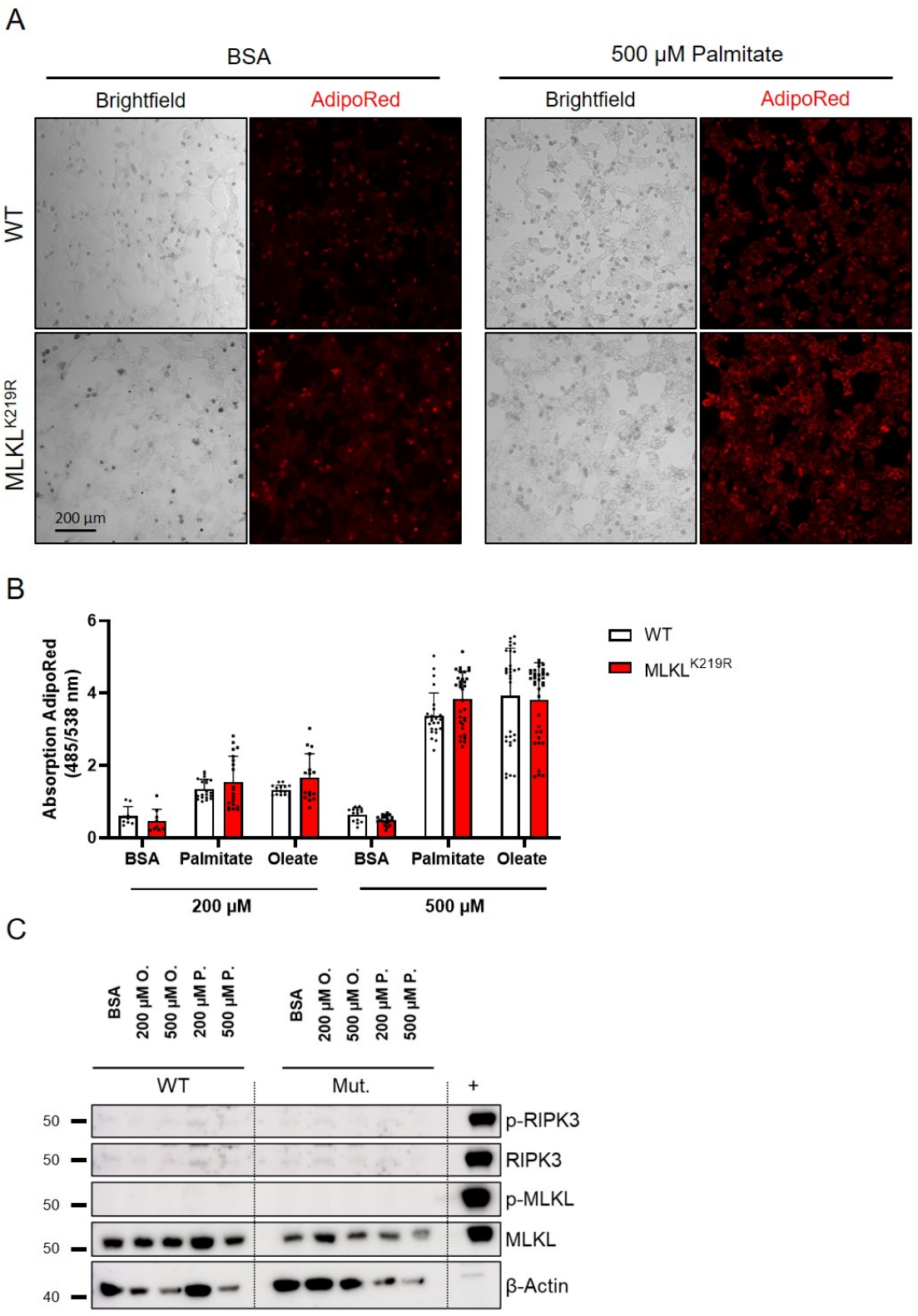

Figure 25: MLKL^{K219R} mutation does not affect fatty acid uptake in primary hepatocytes. (A) exemplary pictures primary hepatocytes cultured for 48 hrs and 24 hrs of treatment with BSA or FA and staining with AdipoRed imaged in brightfield and at 485/538 nm. (B) Evaluation of AdipoRed signal of n=3 independent experiments. (C) Western blot analysis of primary hepatocytes treated with fatty acids did not show induction of necroptotic pathway. Primary hepatocytes were isolated from 8-12 old animals and then treated with oleatic (O) or palmitatic (P) acid with the stated concentrations for 24 for hours. Tissue samples were analyzed for (phospho-) RIPK3, (phospho-) MLKL and β-Actin as loading control. Positive control (+) were L929 cells treated zVAD, sMAC-mimetic and TNF-α. Each lane was loaded with 30 µg of protein. Size on the left in kDa. Values are mean ± SD. Statistical analyses were done by a two-way ANOVA test using a Šídák correction for multiple comparisons. WT, wild-type; Mut., MLKL^{K219R} mutation; p, phospho.

Since the weight data of the experimental animals showed a clear reduction in iWAT in MLKL^{K219R} animals (Figure 13), primary preadipocytes from iWAT were isolated and examined. After isolation, preadipocytes were differentiated into mature adipocytes over 7 days and then stained with AdipoRed to visualize intracellular lipids (Figure 26A). Analysis of the AdipoRed signal showed that cells from MLKL^{K219R} animals had a significantly lower signal compared to WT controls thus accumulated less intracellular lipids. These results are in line with animal data, that showed overall reduced iWAT.

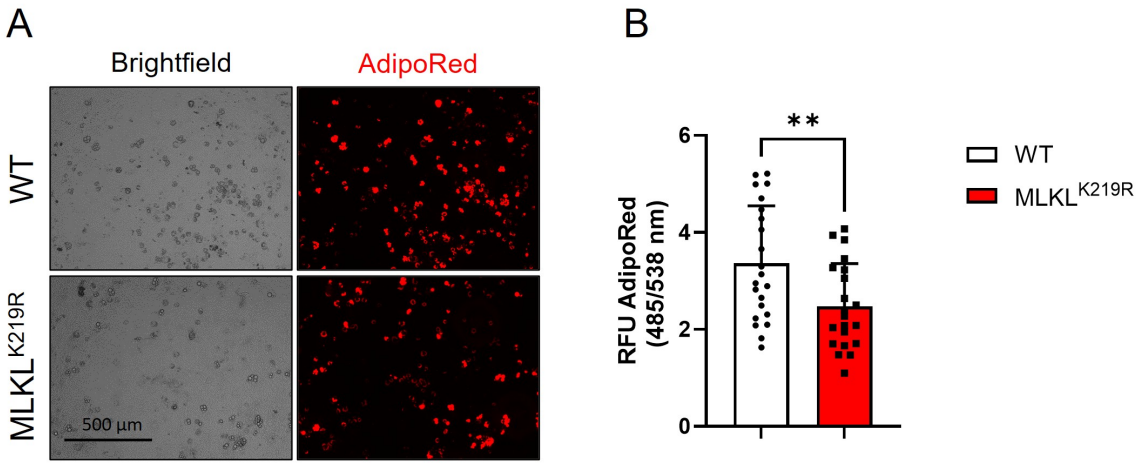

Figure 26: Primary adipocytes from subcutaneous fat tissue of MLKL^{K219R} mice accumulate less intracellular lipids than those of WT animals. (A) Exemplary pictures of 7d differentiated primary adipocytes stained with AdipoRed imaged in brightfield and at 485/538 nm. (B) Evaluation of AdipoRed signal of n=6 independent experiments. Values are mean ± SD. Statistical analysis was done using unpaired two-tailed t-test. *p < 0.05, **p < 0.01

Chapter 4

Discussion

The role of MLKL in metabolic contexts remains highly debated in literature. While some studies have demonstrated protective effects of MLKL deletion, such as reduced body weight, steatosis, and fibrosis following high-fat diet (HFD), others have reported no significant differences when compared to control animals at all.[91,92,112] Unlike previous studies, this work used an MLKL mutant that expresses a full-length protein incapable of high-degree oligomerization, thereby preventing necroptosis execution. Additionally, a WD, more representative of typical diets in industrialized nations, was used instead of the traditionally employed HFD. Furthermore, in our study, we investigated the additional metabolic impact of alcohol in combination with a WD using the MetALD cohort, which currently is a highly underrepresented model.

In summary, this study demonstrated that impairing the function of MLKL in a MASH model led to significant metabolic improvements. These included lower body weight, reduced steatosis, decreased subcutaneous fat expansion, reduced inflammation in visceral adipose tissue, improved liver damage markers, and improved glucose response compared to WT animals. However, these effects were partially mitigated by alcohol administration. The protective effects mediated by the $MLKL^{K219R}$ mutation in the MASH cohort were diminished with alcohol, as evidenced by increased liver damage markers, exacerbated fibrosis, and elevated hepatic immune cell infiltration. Lastly, untreated $MLKL^{K219R}$ animals exhibited age-dependent increases in SPA.

4.1 $MLKL^{K219R}$ mutation positively affects metabolic health in mice

This study aimed to address several challenges commonly encountered in the investigation of metabolic contexts. Over the years, high-fat diets (HFDs; 60 % kcal fat, 20 % kcal protein, 20 % kcal carbohydrates) have been widely utilized in murine studies to induce obesity and associated conditions such as T2D, CVD, and MASLD or MASH. However, these experimental diets often fail to represent the nutritional patterns observed in overweight patients, as their high-fat composition does not reflect realistic dietary habits.

In contrast, the WD used in this study comprising of 40 % kcal from fat (primarily non-trans-fat Primex, which has known adverse effects on liver health), 20 % kcal from

fructose, 2 % from cholesterol, and 20 % from other carbohydrates, is more reflective of the actual dietary intake of overweight individuals.[113,114] Moreover, both macronutrients and micronutrients play critical roles in physiological processes, which are often overlooked in experimental diets due to the standardization and refinement of ingredients.[115]

Another advantage of this study lies in the inclusion of alcohol as an additional dietary factor. In the context of liver disease or MASLD specifically, alcohol has traditionally been excluded from, or intentionally omitted in, experimental designs.[51] Given, that in western countries, more than 50 % of the population regularly consumes alcohol, it is crucial to include it as a co-factor in studies investigating diet-induced liver injury.[116] This study design sought to incorporate the heterogeneity of real-world conditions into a controlled laboratory setting, with the goal of positively contributing to the current understanding of MLKL in metabolic contexts and metabolic diseases in general.

Analysis of the experimental animals highlighted pronounced variability in individual responses to treatments. This was especially evident in the MetALD cohort, which received a WD supplemented with 10 % vol/vol alcohol through drinking water. This high percentage was used, because it is known, that mice have a natural aversion to alcohol and that models with *ad libitum* application in general tend to big experimental scattering especially in regards of liver damage.[117] Further, the measurements of serum parameters and tissue weights revealed significant individual differences, underscoring the challenge of interpreting complex biological processes in the presence of such heterogeneity.[118]

Another advantage of this study , increasing its translatability to clinical practice as well as human studies, is the usage of a point mutation instead of a full body knockout of MLKL. The impairment of MLKL in this case mimics much more a spontaneous genetic mutation or a pharmaceutical inhibition than a complete genetic deletion.

Despite these challenges, this study successfully generated consistent and meaningful data that contribute to a deeper understanding of metabolic changes following MLKL impairment.

Analysis of general parameters to define overall metabolic health of the mice revealed that mice with $MLKL^{K219R}$ mutation displayed several improvements compared to control animals. Evaluation of body weight showed significant reduction in total body weight after receiving WD for 20 weeks (Figure 11). This finding aligns with multiple other studies that suggest MLKL deletion confers a protective effect on body weight.[91,92,119] Furthermore, analysis of blood serum revealed that markers of liver damage like AST and ALT only increased mildly in $MLKL^{K219R}$ animals in the MASH and MetALD cohort, while control animals of each cohort displayed significantly increased damage (Figure 17). Additionally, levels of total cholesterol as well as levels of fasting insulin were also significantly reduced, especially in the MASH cohort. Overall, glucose response was also improved in $MLKL^{K219R}$ animals within the MASH cohort.

Analyses of glucose response using an *i.p.* GTT showed that MLKL animals exhibited significant improvements within both cohorts compared to the controls (Figure 12). In the MetALD cohort, the protective effects of the MLKL mutation were diminished, similar to what was observed regarding the body weight data. During the fasting period and the GTT procedure, the animals in the MetALD cohort had continuous access to alcohol-containing

water, which could have influenced the outcome of the measurements.

Acute alcohol consumption can affect hepatic glucose production and lead to hypoglycemia, while chronic consumption often contributes to the development of IR and can directly damage the pancreas, thus reducing insulin secretion.[120,121] Whilst performing GTTs on animals of the MetALD cohort, some showed critically low glucose levels towards the end of the three-hour measurements, thereby aligning with literature concerning hypoglycemia.

Another diagnostic parameter associated with a disturbed glucose response as well as IR is the fasting insulin level. However, these levels were significantly lower in both genotypes of the MetALD cohort compared to the MASH cohort, which would argue against a severe IR, where increased levels of insulin during fasting periods would be expected. Since blood glucose levels also decreased, neither severe IR nor pancreatic impairment seem likely. Unfortunately, the pancreas was not excised during tissue isolation, preventing further histological or advanced analyses. Furthermore, in order to reduce the number of animals used for experimental procedures, no GTTs were carried out on control animals on NCD alone. As a result, there are no data points for determining the baseline values concerning glucose uptake and fasting insulin levels. This means that we cannot say whether there are differences between the two genotypes without treatment and to what extent the respective treatments influence glucose uptake and resting insulin levels.

The present data suggest that the administered alcohol has a regulating effect on glucose and insulin response. Interestingly, a study by Diao *et al.* demonstrated similar findings. The chronic administration of a low dose of alcohol (3.5 %) in combination with an HFD had positive effects on various metabolic parameters, including GTT results, insulin sensitivity, and physical activity. They claim that these effects were mainly mediated by enhanced AMP-activated protein kinase (AMPK) activation and the subsequent synthesis of long-lived proteins that improve insulin sensitivity.[122] Even though the GTT data of the MetALD cohort in our study seem to be positively impacted by alcohol consumption, it has to be kept in mind that the overall metabolic state in regards of inflammation, steatosis and body weight is much worse than the one of untreated control animals. Furthermore, a vast majority of studies clearly showed the overall negative impact of heavy chronic alcohol consumption on the metabolism in general as well as the glucose/insulin signaling.[120,123]

Another study, by Babuta *et al.*, showed that the sole chronic administration of 10 % alcohol is not sufficient to cause significant liver damage. However, they observed that combining alcohol with a high-fat, high-cholesterol diet, comparable to a WD, had an additive detrimental effect.[123] As a side note, in a third cohort, WT and $MLKL^{K219R}$ mice were fed a NCD supplemented with 10 % alcohol in drinking water. Basal metabolic analysis revealed no significant differences in body weight, glucose response, or liver damage associated markers, between genotypes or compared to animals on NCD alone (data not shown). These findings are consistent with results shown in Babuta *et al.*'s study.

The administration of alcohol in combination with specific diets rich in dietary saturated fat can lead to increased adiponectin concentrations in the serum further protecting from ALD in mice.[124] Adiponectin is considered an insulin-sensitizing hormone and may therefore contribute to an improved glucose tolerance (GTT outcome).[125] It is well established that alcohol consumption in animal models influences adiponectin levels in serum and can inhibit

both its expression and secretion.[126,127] In the MetALD cohort, adiponectin expression in adipose tissue was slightly elevated compared to the MASH cohort, particularly in MLKL^{K219R} animals (Figure 22). However, actual serum levels of adiponectin were not quantified in this study using enzyme-linked immunosorbent assay (ELISA) or other methods, which limits the conclusiveness of the actual expression of functional adiponectin.

Another relevant factor is the regulation of leptin. In the MetALD cohort, leptin was most strongly upregulated in gene expression analysis. Under physiological conditions, leptin reduces hunger, whereas chronic elevation, a sign of leptin resistance, can lead to impaired satiety and energy regulation. Additionally, under pathological conditions, the pro-inflammatory effects of leptin contribute to sustain the state of chronic inflammation during obesity.[128] Impairment of leptin signaling could lead to increased food intake, yet in the MetALD cohort, animals tend to even consume less food than in the MASH cohort (Figure 11 and Figure 20).[129] The slightly reduced food intake is most likely caused by the alcohol itself, which also contains almost the same amount of calories as pure fat does.[130] Thereby caloric intake between the MASH and the MetALD cohort are most likely very similar even though less food is consumed.

When analyzing metabolic health and obesity related phenotypes, adipose tissue is of great importance. Inflammation of adipose tissue is strongly associated with obesity and adipose tissue dysfunction.[131] On one side the histological analysis revealed that MLKL^{K219R} animals of both dietary cohorts showed a reduced number of CLS in eWAT (Figure 19) while on the other side pro-inflammatory genes partially showed higher activation in mutant mice (Figure 20). Considering histologically determined CLS, data suggest reduced inflammation and reduced adipocyte cell death in the eWAT depot. This would further align with overall improved glucose response and lower fasting insulin levels determined by GTT especially in the MASH cohort. Yet in-depth analysis of pro-inflammatory gene expression showed higher levels of TNF-α, IL-1α and granulocyte-macrophage colony-stimulating factor (GM-CSF) expression in eWAT, not aligning with histological analyses. To further add to this, Leptin is known to have pro-inflammatory effects and to upregulate IL-6 and TNF-α gene expression. With the increased leptin levels especially in the MetALD cohort, one could assume, that increased signaling is caused by that.[128] Yet these results are ambiguous and further investigation of the inflammatory signaling in all tissues, especially adipose and liver tissue is needed in order to shed light on the complex interactions with MLKL.

Development of liver steatosis is the abnormal accumulation of lipid droplets within the liver. This can be caused by intrahepatic processes like increased lipogenesis driven by alcohol consumption or due to impairment or inflammation of adipose tissue what in turn causes elevated systemic FAs being displaced ectopically to the liver. Once more the reduced levels of steatosis seen in MLKL^{K219R} animals could be associated with a reduced number of CLS and overall improved adipose tissue health. However, despite the lower inflammatory markers observed, liver steatosis remains comparably high in both dietary cohorts, with only a mild reduction in MLKL^{K219R} animals. This suggests that factors beyond systemic adipose tissue inflammation contribute to hepatic lipid accumulation.

A study performed by Xu *et al.* claim that MLKL has direct impact on hepatic insulin sensitivity independent of inflammation.[92] Their study shows metabolic improvements similar

to ours, but our detailed results do not align with theirs. Neither did we see clear upregulation of MLKL in either liver nor adipose tissue, nor could we detect any phosphorylated and thereby activated MLKL in either of these tissues (Figure 21). Furthermore, they claim that the inhibition of any of the key-regulators of necroptosis have positive impact on hepatic insulin sensitivity is not conform with current literature, nor with our own results, which will be discussed in more detail later on (Section 4.5). Furthermore, it is still up for debate whether hepatocytes can undergo necroptosis. Even though patients with MASH show the increased levels of RIPK1/3 and MLKL in liver, a recent study revealed, that RIPK3 is epigenetically silenced in hepatocytes, making them unable to activate MLKL in RIPK3-dependent manner and execute necroptosis.[76,112] At this point of research the role of necroptosis and MLKL especially have to still be seen critically and the focus should be brought to necroptosis independent function of these proteins.

Finally, the most notable genotypic difference in this study is the weight disparity under both dietary models. While animals on NCD showed no difference in weight between $MLKL^{K219R}$ and control groups at 26–28 weeks of age, WD and WD combined with alcohol consumption demonstrated significant protection of $MLKL^{K219R}$ mice against diet-induced weight gain. Similar studies on the function of MLKL in a metabolic context from Tye *et al.* and Xu *et al.* also were able to show a reduction of total body and adipose tissue weight (reduction in iWAT and eWAT) and were further able to show a reduction in CLS in eWAT.[91–93] Whilst Xu *et al.* focused on the involvement of MLKL in hepatic insulin response, they further hypothesized that MLKL is involved in energy metabolism. Tye *et al.* were further suggesting MLKL involvement in lipid metabolism.

In this study, the lower body weight of $MLKL^{K219R}$ animals, is primarily attributed to a reduction in subcutaneous adipose tissue (iWAT), most pronounced in the MASH cohort. This reduction is reflected in adipocyte distribution and size. $MLKL^{K219R}$ animals exhibit a higher number of small adipocytes and fewer large adipocytes, whereas WT animals have fewer small adipocytes and significantly more large adipocytes (≥2000 µm²) in iWAT. In contrast, the visceral fat depot (eWAT) showed no reduction in absolute nor relative tissue mass in $MLKL^{K219R}$ animals. Adipocyte size in eWAT was also unaffected by genotype but increased with a high-caloric diet across genotypes. In health and disease, fat tissue has important regulatory functions to maintain systemic lipid and glucose homeostasis. Its metabolism can rapidly shift between FA uptake and lipogenesis during nutrient surplus and FA release and lipolysis in times of energy demand. In obesity its plasticity through hyperplasia as well as hypertrophy of adipocytes plays a critical compensatory role in protecting other tissues from lipotoxic effects.[132] Particularly the expansion and inflammation of eWAT, is strongly associated with lipotoxicity and IR. Despite no differences in eWAT mass, immunohistochemistry revealed a significantly lower number of F4/80+ CLS in $MLKL^{K219R}$ animals, a marker of adipocyte cell death and adipose tissue inflammation as well as a hallmark of obesity. Gene expression analysis of pro-inflammatory cytokines and chemokines (TNF-α, CCL2, IL-6, IL-1α, IL-1β and GM-CSF) in eWAT showed upregulation upon diet independent of genotype. This will be discussed in detail later (4.2).

In summary, based on published literature as well as on our own results, it seems evident that both MLKL deletion and MLKL impairment, both of which inhibit necroptosis execution,

can positively impact overall metabolic health of experimental animals on high-caloric diets. Although MLKL is primarily known as the executioner of necroptosis, our results suggest necroptosis-independent functions. Studies suggest that MLKL could be involved in lipid and energy metabolism, although exact mechanism is unknown. In part, our research aligns with these findings. Concluding from our results, we were able to exclude impairment of lipid uptake in hepatocytes. Furthermore, due to the increased activity of untreated mutant animals we propose that MLKL^{K219R} animals have an increased metabolic rate, which could lead to an upregulation of lipid turnover and ultimately have a positive effect on total body adipose tissue mass and steatosis. Moreover, MLKL appears to play a significant role in adipose tissue. The reduction of adipose tissue inflammation as well as improved insulin sensitivity/glucose response could be considered direct effects of the inhibition of necroptosis execution. However, impairment of adipocyte differentiation and reduced lipid accumulation within adipocytes suggest necroptosis-independent processes, where the role of MLKL is uncertain for now. Taken together, these results further highlight the complexity of metabolic studies and their indispensable nature.

4.2 MLKL does affect adipocyte differentiation and adipose tissue distribution

In the preceding chapters, it was shown that MLKL plays a crucial role in the execution of necroptosis and how it can further impact inflammatory and immune cell signaling. While the functions and mechanisms of MLKL in cell death are quite well-characterized, its metabolic as well as tissue-specific effects are still poorly understood.

In this study, we show, that the total fat mass is clearly reduced in MLKL^{K219R} animals receiving WD, along with reduced inflammatory signaling within the eWAT depot. This prompted towards a closer investigation of the adipose tissue as well as primary adipocytes. *In vitro* differentiation experiments showed that primary adipocytes isolated from MLKL^{K219R} animals accumulated significantly less lipids than those of control animals (Figure 26).

In an earlier study Magusto *et al.* stated, that a MLKL-KO in the pre-adipocyte cell line 3T3-L1 does not only abolish TNF-induced cell death, but also impairs lipid droplet formation and white adipocyte differentiation compared to controls. This effect was linked to enhanced Wnt-signaling and was not observed in beige adipocyte differentiation.[133] Interestingly, the deletion of RIPK3, also inhibits necroptosis execution, yet lipid droplet formation and white adipocyte differentiation is not impaired. These results further highlight the necroptosis-independent functions of MLKL specifically. They further partially align with our results. Yet differentiation method used in our approach, contains Rosiglitazone, a PPARγ agonist, that is known to favor beige adipocyte differentiation. This could account for the less severe impairment in lipid droplet formation observed in the MLKL^{K219R} model compared to the work of Magusto *et al.*

As mentioned previously, analysis of adipose tissue from experimental animals showed that expansion and hypertrophy of adipocytes in iWAT was most severely affected by MLKL^{K219R}. WT animals of the MASH cohort do show the biggest increase in adipocyte size (Figure 15) together with upregulation of pro-inflammatory gene expression (IL-6, IL-1α,

-1β)(Figure 20). Adipocyte hypertrophy as well as IL-6 and IL-1 are known markers for adipose tissue inflammation, obesity and are associated with IR, further explaining increased fasting insulin levels and worsened glucose uptake.[134] Meanwhile expression profiles of MLKL^{K219R} animals are more ambiguous and show strong upregulation of CCL2 while IL-1α and -β are not upregulated in iWAT. For eWAT, MLKL^{K219R} animals in the MASH cohort tend to have the highest upregulation of inflammatory genes, which would contradict the overall better metabolic state the animals were found to have compared to WT animals. Adipocyte sizes between the different dietary cohorts and genotypes do not differ significantly in eWAT. A variety of studies claim that expansion of eWAT generally is more often associated with increased risk for CVD than iWAT expansion.[135] To put tissue inflammation further into perspective, neither of the adipose tissue depots show any significant level of cell death on protein level, suggesting rather mild forms of inflammation (Figure 21). Furthermore, the analysis of genes associated with lipid metabolism cannot provide a clear and conclusive explanation of the metabolic changes or positively impacted phenotype of adipose tissue of MLKL^{K219R} animals. In comparison to our results, Tye *et al.* were able to show reduced adipose tissue mass and adipocyte size of eWAT together with a reduction of CLS in MLKL-KO animals.[91] But the pro-inflammatory signaling and immune cell infiltration was only modestly impaired, suggesting that MLKL plays a tissue-specific role in development of adiposity and MASLD reflecting our findings.

Concerning markers of the lipid metabolism from serum such as cholesterols, NEFA and TAG only showed little differences (Figure 17), but MLKL^{K219R} animals tend to have lower levels of LDL, total cholesterol and NEFA. LDL is also known as bad cholesterol and increased levels are associated with higher likelihood of CVD. Also elevated NEFA levels are also associated with impaired adipose tissue and IR.[136]

Even though results are ambiguous, MLKL seems to play an important role in immune cell regulation within the adipose tissue. Local macrophages and their polarization state are crucial for maintaining adipose tissue homeostasis.[137] They influence not only adipocyte differentiation but also intracellular metabolic processes such as lipolysis via secretion of cytokines. Thus, MLKL may impact adipose tissue function through both direct and indirect mechanisms.

Furthermore, consistent with a study of Saeed *et al.*, untreated MLKL^{K219R} mice showed increased SPA when compared to controls (Figure 16).[138] Enhanced activity in general may contribute to increased energy expenditure and fat loss, potentially explaining the leaner phenotype of MLKL^{K219R} animals. Important to mention is that it is unknown, if animals receiving treatment with high caloric diets still show this increased levels of physical activity, because SPA of experimental animals were not measured. However, how the increased activity is caused and to which extent it accounts for the observed reductions in body and adipose tissue weight remains unclear. Therefore, metabolic cages are indispensable in order to clearly evaluate energy expenditure and to enlighten potential underlying signal pathways.

Lastly, the reduction of adipose tissue took place especially in iWAT, an adipose tissue depot which can give rise to an in-between cell population of beige adipose tissue with increased energy expenditure. Therefore markers for browning (UCP1) were analyzed. Browning can counteract adiposity up to a certain point, thereby offering interesting therapeutic

approaches.[139] Even though gene expression analysis showed certain differences between genotypes and dietary cohorts (Figure 22) we were not able to detect any signal for UCP1 on protein level (Figure 23). If the presence of beige adipose tissue in MLKL^{K219R} does play a role and contributes to the observed phenotype can only be speculated. The analysis of different and earlier time points therefore could bring light to this, since browning and beige adipose tissue might play a role in younger animals, yet the effect or signals are lost after 20 weeks of diet.

4.3 MLKL impairment positively influences liver damage-associated damage markers and hepatic lipid metabolism

MASLD counts as one form of SLD. Key characteristic of SLD is the abnormal accumulation of lipid droplets in at least 5 % of hepatocytes in the liver. Depending on the subtype of SLD, the underlying mechanisms in causing the lipid accumulation differ. In short, main drivers of lipid accumulation in MASLD are often a combination of chronic caloric surplus, dysfunctional and inflamed adipose tissue, local and systemic IR, causing increased circulating FAs and uptake of lipids and *de novo* lipogenesis in the liver. In the definition of MetALD on the other hand, alcohol is not excluded as it is for the most part in the MASLD definition, thereby contributing to disease development and progression. Alcohol detoxification mainly takes place in the liver, making it its primary target. Chronic consumption can cause increased inflammation and lipogenesis as well as mitochondrial dysfunction and reduced β-oxidation.[140] Even though the mechanisms are similar, the distinct differences between the models must not be forgotten whilst comparing and interpreting their results individually.

For initial determination of liver damage, blood serum analysis depicts a minimally invasive and simple method of monitoring biomarkers in clinics. To assess liver damage, initial serum markers such as AST and ALT were analysed, as they indicate hepatocellular damage, while AP can indicate damage to the biliary system.

In this model, animals with the MLKL^{K219R} mutation in both diet groups were shown to have significantly lower levels than the respective control animals. In addition, GLDH, a marker indicating mitochondrial damage when elevated, is significantly lower in MLKL^{K219R} animals (Figure 17). Comparable studies have shown ambiguous results. Preston *et al.* and Ohene-Marfo *et al.* observed no or only a very slight reduction in ALT levels in MLKL-KO animals, whereas Tye *et al.* reported a clear reduction in ALT levels.[91,112,119]

The diet used in the Ohene-Marfo *et al.* study (40 % kcal fat (palm oil, 50 % saturated and 50 % unsaturated fatty acids), 20 % fructose, 2 % cholesterol) and the feeding duration of six months are the most comparable to our study.[119] However, the reported ALT levels were already above 200 U/l in control animals on an NCD and almost 1000 U/l in animals on the HFD, which is more than five times higher than in the WT animals receiving diet in our study. The exact genetic background of the mice was not specified, only that they were C57BL/6. In the context of metabolic studies, the genetic background of C57BL/6 is known to have a significant impact on study results. Even though both models are susceptible to diet-induced obesity, the 6J mouse, which is also used in our study, shows more severely impacted glucose clearance than 6N, thereby potentially further driving progression of metabolic disease.[141]

But multiple studies compared the two strains and were not able to provide data, about which strain is best to use in metabolic studies, making it an ongoing debate.[142]

The extent to which genetic background also influences the severity of liver damage and thus elevated serum ALT markers remains speculative. However, this comparison of different studies clearly shows why proper internal control animals are of great importance. External or inappropriate controls may contribute to misinterpretation of observed effects and results.

In general, variation of AST and ALT levels could also be due to different stages of MASLD or MASH. Further mouse housing could have an impact on the outcome of metabolic studies. For once the optimal housing temperature of mice is around 25-30 °C, yet standard conditions for most studies are done at RT around 20-22 °C.[143] To maintain their core body temperature, mice need to increase their energy expenditure by up to 30%. Interestingly, mice receiving HFD do not adapt their food intake to the increased energy demand, why housing temperature can directly affect the body weight and indirectly the severity of MASLD or MASH manifestation.[143]

In-depth analysis of liver on histological level, was able to show severe steatosis in all animals receiving high caloric diet but to a more sever extent in WT animals of each cohort (Figure 13). Compared to the clear increase of steatosis, markers for inflammation upon diet were upregulated relatively little, shown by a slight increase of liver infiltrating immune cells (Figure 18). Ectopically stored LDs are able to trigger a variety of negative effects within the cells, such as the production of ROS, inflammatory processes or even cell death.[144]

The MetALD cohort did further show slightly increased levels of Sirius red staining, thereby implying a mild form of fibrosis. Animals on WD did not show any signs of fibrosis compared to that. In any case, the amount of fibrosis was too little for evaluation using an Image J script (Figure 14). These results are in agreement with Preston *et al.* who used a HFD model for 24 weeks (most comparable to WD alone).[112]

The liver is one of the metabolically most active organs, also responsible for detoxification processes and is thereby exposed to toxins such as metabolic waste products, drugs or alcohol. Thereby the additive effects of alcohol show especially in the gene expression of pro-inflammatory pathways. While serum markers are comparable between MASH and MetALD cohorts, pro-inflammatory signaling is severely upregulated in livers of MetALD (Figure 20). Elevated levels of TNF-α, CCL2, IL-6 and IL-1β can be seen especially in patients with chronic alcohol consumption and can be seen as marker of severe liver inflammation in ALD.[145] Even though IL1-α is not a classical driver of ALD alone, it does show clear upregulation in WT animals of the MetALD cohort, while it shows significant reduction in $MLKL^{K219R}$ animals.[146] IL-1α acts as Alarmin and is produced by Kupffer cells and hepatocytes, thereby contributing to liver inflammation and exacerbates it further.[147] In combination with the slight reduction of the earlier mentioned cytokines these changes could add to overall reduced inflammation and improved metabolic state of the liver. Partially contrary to these findings, Wu *et al.* investigated the role of MLKL in myeloid cells in an ALD model and found, that MLKL deficiency in immune cells, Kupffer cells particularly, impairs their phagocytic potential. Thereby, bacterial clearance within the liver is impaired, increasing its burden and further increasing inflammatory cytokines.[148] The MASH cohort does show only

a very mild increase of pro-inflammatory signaling compared to animals on NCD, suggesting that animals are in an early stage of MASH with little inflammatory signaling. But when using the NAS-scoring system (Figure 5) all animals fulfilled criteria for MASH (score > 5).[108] These results alone highlight the severe impact of alcohol as additional driver of liver disease, and why it is important to be included in future animal studies.

Furthermore, the liver has a crucial role in lipid metabolism, which is severely altered and impaired in MASLD and obesity.[63] Concerning the expression of genes involved in lipid metabolism of the liver, expression patterns were rather cohort than genotype specific. For the MASH cohort genes like Fasn, PPARα , Cidea and Cpt1 do show upregulation. Fasn and Cidea upregulation can both be associated with the increased LD formation and steatosis in liver and in general drive these processes further.[13] Fabp4 shows also a slight upregulation and is known to be associated with steatosis progression and MASLD.[149] Even though these steatosis related genes (Fasn, Fabp4, Cidea) are higher upregulated in the MetALD when compared to the MASH cohort, MLKL animals show reduced upregulation concerning these genes in both cohorts. These data would align with histologically determined steatosis, which was reduced in MLKL^{K219R} animals of both dietary cohorts (Figure 13).

However, in our setup, *in vitro* experiments could not show any differences in FA uptake in primary hepatocytes from WT and MLKL^{K219R} animals. Furthermore, western blot analysis of hepatocytes treated with high concentrations of palmitic acid (highly lipotoxic), did neither show signal for (phosphorylated) RIPK3 nor for phosphorylation of MLKL. In summary, these findings align in many parts with Tye et al., who conducted a conclusive study on MLKL in a metabolic context together with an in-depth analysis of lipid metabolism.[91] They also showed that MLKL acts in a RIPK3-independent manner and that cell death in FA treated Hepa cells (hepatoma cell line) is further independent of RIPK3 and MLKL. Furthermore, they suggest that intrahepatic MLKL is involved in lipid uptake, transport and synthesis. They also suggest, that MLKL plays a crucial regulatory role in the synthesis and transport of mono- and polyunsaturated di- and triglycerides in the liver, that are associated with progression of MASLD and obesity.

In summary, our findings show that livers of MLKL^{K219R} animals show ameliorated steatosis, reduced liver damage associated serum markers as well as a reduction in total cholesterol levels. Meanwhile inflammatory signaling does only show slight variations compared to WT animals, analysis of lipid metabolism suggests multiple improvements that align with the overall improved metabolic state of MLKL^{K219R} animals.

4.4 Involvement of MLKL in the gut

As previously mentioned, there are multiple studies reporting conflicting results, not being able to deliver a conclusive result on the role of MLKL in a metabolic context. While this study employed a point mutation that showed protective effects, Ohene-Marfo *et al.* e.g. were having the most protective effects in heterozygous animals and not in the complete KO animals.[119] While the heterozygous animals were not only protected from diet-induced obesity and IR, like the KO animals, but also from liver fibrosis. This further contributes to the indecisive data around MLKL, by adding the factor of dose-dependency.

Genetic composition as well as genetic background, as discussed earlier can severely impact experimental outcomes, particularly in control groups. Beyond genetics, the hosts meta genome, comprising microbial communities across the skin and gut for most parts, plays a crucial role in physiological responses.

Many studies were able to show the importance of the intestinal microbiota in human health. Microbes living in the human gut can aid in fiber digestion, probiotic intake, lipid metabolism, antioxidant production and regulation of gut inflammation. Dysbiosis and lack of microbial diversity of the gut microbiome have been linked to various diseases like gut inflammation, inflammatory bowl disease, IR and CVD.[150]

Microbiome research, however, faces a variety of challenges. While sequencing technologies like Illumina have improved affordability and accessibility, biases can arise at multiple stages, including sample collection, library preparation, sequencing platform choice, and alignment strategy. Like this the results from different studies are not always aligning with previous ones. Moreover, the microbiome observed in sequencing data may not accurately reflect the true underlying microbiome due to the accumulation of multiple errors along the sequencing pipeline.[151] Microbial composition can already vary significantly within one facility, making comparability of experiments from different studies even more complicated.[152] In this study we did not collect the gut tissue nor fecal samples of our experimental animals, making the analysis of the gut microbiome impossible. Yet there are hints for the involvement of the microbiota within our experiment. Notably, weight fluctuations were observed both between animals and across batches. Given the microbiota´s role in nutrient uptake, its impact on weight gain cannot be underestimated. A study of Nemoto *et al.* showed that germ-free mice that received fecal microbiota transplants gained more body weight than their germ-free control group independent of the diet.[142] While speculative, microbiome variations may have contributed to the weight differences in our study and should be considered in future research.

Many studies before showed the importance of MLKL in disease models of the gut, *e.g.* Yu *et al.* showed that MLKL expression is of importance for the intestinal mucosal barrier by enhancing inflammasome activation, thereby limiting Salmonella infection.[153] They further could show that MLKL KO animals exhibited higher bacterial burdens in the liver and spleen. In line, a study performed by Wu *et al.* was able to show, that MLKL deficiency in myeloid cells is exacerbating ethanol-induced bacterial burden and immune cell infiltration in the liver. Further, Won *et al.* showed that gut microbes can translocate to the liver through the portal vein, triggering the immune response through TLR-receptors.[154] Aligning with the results of Yu *et al.* and Wu *et al.* we observed increased immune cell infiltration in livers of $MLKL^{K219R}$ animals across both dietary cohorts in the IHC analysis. Furthermore, alcohol consumption exacerbated immune cell infiltration in both genotypes of the MetALD cohort, to an even higher extent in $MLKL^{K219R}$ animals. This aligns with the known effects of alcohol, which compromises gut barrier integrity by inducing oxidative stress and cell death in epithelial and connective tissue. The resulting gut permeability allows microbial translocation, increasing microbial burden in the bloodstream and liver, thereby amplifying the immune response.[155] Dysregulation along the gut-liver axis is a well-recognized driver of MASLD progression to its inflammatory form MASH.

In conclusion, the findings from this study, in conjunction with existing literature, strongly

suggest a role of MLKL in maintaining gut homeostasis. Future studies should further explore the gut-liver axis to better understand its implications in metabolic disease.

4.5 Protective effects observed in MLKL^{K219R} model are RIPK1 independent

RIPK1 can be seen as a master regulator deciding between cell survival and cell death by either leading to NF-κB activation or induction of apoptosis and necroptosis (section 1.4.1). Necroptosis activation is dependent on RIPK1 kinase activity which initiates the phosphorylation of RIPK3 what further leads to MLKL phosphorylation, activation and cell death execution. Previous studies showed that the systemic inhibition of RIPK1 either by small interfering RNA (siRNA) silencing or by inhibitor RIPA-56 were able to reduce body weight gain and inflammatory signaling after receiving a HFD.[156,157]

Another study by Kanurakaran *et al.* was able to show similar results by reducing RIPK1 concentration within the gut, by creating an intestine-specific RIPK1$^{IEC+/-}$ mouse model, what reduced body weight gain in female but not in male mice.[158] In summary these studies suggest involvement of RIPK1 in the metabolic response to HFD and that its inhibition does have positive impact on glucose response as well as body weight gain. That is why we applied another point mutation model of RIPK1 in our MASH and MetALD models. The RIPK1^{D138N} mutant, expresses a kinase inactive form, that is viable and protected from TNF-induced necroptosis unlike complete RIPK1 deficient animals that die perinatally due to abnormally high levels of cell death.[159,160]

Considering literature and the results from the MLKL^{K219R} animals, we expected a positive impact by impairing the TNF-α response and cell death by the RIPK1^{D138N} mutation, acting upstream of MLKL, when applying a WD alone or WD with additional alcohol. Surprisingly after initial analyses there were no obvious metabolic improvements seen in RIPK1^{D138N} animals when comparing to the respective controls . Body weight gain and cumulative food intake are comparable across both genotypes and feeding cohorts without any reduction. The glucose uptake from the blood serum is even significantly slowed in RIPK1^{D138N} compared to control animals (Figure 27). Macroscopically and microscopically livers do not show genotype-specific differences. Further blood serum analysis did not reveal any significant reduction of liver damage markers such as ALT and AST (Figure 28). In summary, these results are rather unexpected, because through the RIPK1 mutation the activation of MLKL and thereby the execution of necroptosis is also suppressed, why a similar outcome to the MLKL^{K219R} model was expected. A similar study performed by Tao *et al.* applied another kinase dead RIPK1 mutation, the RIPK1^{K45A}, in an HFD-model and were able to show significant protection from liver damage and steatosis as well as fibrosis.[161] Analysis from patients could show upregulation of RIPK1 and RIPK3 in NASH livers, thereby suggesting their negative association with the diseases outcome.[161] When applying the WD in our study, we were not able to find protective effects on steatosis manifestation and progression in RIPK1^{D138N} animals.

In our hands these findings suggest a necroptosis- and RIPK1-independent function of MLKL due to RIPK1^{D138N} not having any microscopically protective effects within the different

dietary cohorts. Especially the analysis of inflammatory signal pathways would be needed to evaluate this phenotype further and to bring it to conclusive results.

Lastly previous work of our group by Gautheron *et al.* showed, that the deletion of RIPK3, the last key player in necroptosis, does have a negative impact on diet-induced obesity and glucose response.[76]

All these studies together show, how different the outcomes of experiments can be even though they all impairing the same signal pathway. It further highlights the importance of the analysis of pathways on different levels in order to verify their potential impact beyond the specific researched area .

Chapter 5

Conclusion and Outlook

5.1 Conclusion

In conclusion, our study was able to show that the blockage of MLKL oligomerization, which completely prevents necroptosis execution, introduces a variety of improvements in animals receiving a WD alone or with additional alcohol. Both diet cohorts show an overall reduction in body weight, mainly due to a reduction in adipose tissue, specifically iWAT. *In vitro* experiments showed, that primary adipocytes from iWAT of $MLKL^{K219R}$ animals show reduced lipid accumulation upon differentiation, possibly explaining impairment of adipose tissue *in vivo*. Even though, gene expression anylsis of both WATs did not reveal any significant reduction in pro-inflammatory signaling, histological analysis of eWAT showed that $MLKL^{K219R}$ animals display a reduced number of CLS, suggesting reduced adipose tissue inflammation. Furthermore, $MLKL^{K219R}$ animals show improved glucose uptake and decreased fasting insulin levels, further adding to the metabolic improvements.

Analysis of livers revealed, that $MLKL^{K219R}$ animals show protection from liver steatosis and hepatocellular ballooning, whilst showing increased immune cell infiltration. Even though we did not investigate the effects of MLKL impairment in the gut, studies show that MLKL deficient mice have increased bacterial burden within the liver, thereby driving immune cell infiltration. Concerning pro-inflammatory signaling within the liver, analyses did not reveal clear genotype-specific effects, suggesting that MLKL most likely is not directly involved in the analyzed pathways. Furthermore, we could not detect pMLKL nor RIPK3 within the liver, suggesting that the necroptosis-dependent functions of these molecules are not essential for MASLD progression. Yet in line with earlier studies, the lipid metabolism of $MLKL^{K219R}$ animals is slightly altered. In our study we could show that genes usually associated with progression of steatosis (Fasn, Fabp4, Cidea) are clearly reduced in $MLKL^{K219R}$ animals when compared to control animals. But *in vivo* experiments with primary hepatocyte were not able to show any differences in uptake of FAs, like others did.

Lastly, animals on NCD did show increased SPA from an age of 15-weeks on. Even though SPA was not investigated in animals of MASH and MetALD cohorts, it could essentially cause increase energy expenditure and lead to increased fat burning, thereby adding to metabolic improvements seen in $MLKL^{K219R}$ animals.

At this point, the role of MLKL in a metabolic context is still poorly understood and further

investigation is needed. Up to now this and other studies show that MLKL has a variety of necroptosis-independent as well as tissue-specific functions. Even though we cannot yet decipher all mechanisms in which MLKL acts tissue-specific, this study adds important insights on the matter. It further highlights the importance to include alcohol as addition for future animal studies.

5.2 Outlook

This study contributes to the existing body of literature by emphasizing the role of MLKL in the development and progression of diet-induced MASLD and obesity. While the precise mechanisms and functions of MLKL remain to be fully elucidated, certain differences were identified. However, this study also has limitations, particularly in the scope of experiments required to further characterize this phenotype.

One major limitation is the lack of metabolic cage experiments, which are essential for a comprehensive assessment of metabolic changes. The investigation of animals on a WD using metabolic cages would provide deeper insights into key metabolic parameters, including respiratory exchange rates, physical activity, and indirect calorimetry. Additionally, the analysis of feces and urine could help determine potential differences in lipid or bile acid excretion. Of particular importance is a more detailed evaluation of physical activity and associated muscle tissue characteristics, as these could reveal relevant metabolic disparities.

Another critical gap in this study is the absence of intestinal tract analysis, despite the fact that MLKL is highly expressed in intestinal and endothelial cells and has been reported to exert protective effects against intestinal tumorigenesis.[162,163] Given the intestine's pivotal role in nutrient uptake and distribution, MLKL may have significant functions in these processes that were not explored in this study.

Although mitochondrial experiments were initially considered (data not included in this thesis), these investigations were ultimately de-prioritized due to technical challenges associated with mitochondrial analyses. However, given previous studies indicating a role for MLKL in mitophagy, future research should further explore these aspects.

The study's analysis of inflammatory and metabolic signaling was predominantly based on qPCR data. However, mRNA expression levels do not always correlate with functional protein activity, particularly for cytokines such as IL-1β, which require post-translational cleavage for activation. Thus, ELISA-based assays would provide a more accurate assessment of inflammatory states by directly quantifying cytokine protein levels. Moreover, ELISA assays targeting adipokines commonly dysregulated in obesity could further enhance the characterization of adipose tissue function in MLKL-deficient models.

Further, the usage of advanced techniques such as single-cell sequencing could provide better in-depth analysis of adipose tissue and its changes introduced by MLKL impairment. Also, tissue-specific KO or mutation models, especially of the adipose tissue, could provide important insight about the actual driver of the observed phenotype of $MLKL^{K219R}$ animals.

References

[1] V. Martin and WHO. Obesity and overweight, 2025. https://www.who.int/news-room/fact-sheets/detail/obesity-and-overweight [Accessed: 2025-07-29].

[2] T. Scheers, R. Philippaerts, and J. Lefevre. Patterns of physical activity and sedentary behavior in normal-weight, overweight and obese adults, as measured with a portable armband device and an electronic diary. *Clinical Nutrition*, 31(5):756–764, 2012.

[3] M. Bastien, P. Poirier, I. Lemieux, and J.-P. Després. Overview of epidemiology and contribution of obesity to cardiovascular disease. *Progress in Cardiovascular Diseases*, 56(4):369–381, 1 2014.

[4] M. A. Roomy, K. Hussain, H. M. Behbehani, J. Abu-Farha, R. Al-Harris, A. M. Ambi, M. A. Abdalla, F. Al-Mulla, M. Abu-Farha, and J. Abubaker. Therapeutic advances in obesity management: an overview of the therapeutic interventions. *Frontiers in Endocrinology*, Volume 15 - 2024, 2024.

[5] E. Moreno-Mendez, S. Quintero-Fabian, C. Fernandez-Mejia, and M.-L. Lazo de-la Vega-Monroy. Early-life programming of adipose tissue. *Nutrition Research Reviews*, 33(2):244–259, 12 2020.

[6] J. M. Stephens. The fat controller: adipocyte development. *PLoS Biology*, 10(11):e1001436, 2012.

[7] N. Alkhouli, J. Mansfield, E. Green, J. Bell, B. Knight, N. Liversedge, J. C. Tham, R. Welbourn, A. C. Shore, K. Kos, and C. P. Winlove. The mechanical properties of human adipose tissues and their relationships to the structure and composition of the extracellular matrix. *American Journal of Physiology-Endocrinology and Metabolism*, 305(12):E1427–E1435, 2013.

[8] S. S. Choe, J. Y. Huh, I. J. Hwang, J. I. Kim, and J. B. Kim. Adipose tissue remodeling: Its role in energy metabolism and metabolic disorders. *Frontiers in Endocrinology*, 7, 4 2016.

[9] M. Rosell, M. Kaforou, A. Frontini, A. Okolo, Y.-W. Chan, E. Nikolopoulou, S. Millership, M. E. Fenech, D. MacIntyre, J. O. Turner, J. D. Moore, E. Blackburn, W. J. Gullick, S. Cinti, G. Montana, M. G. Parker, and M. Christian. Brown and white adipose tissues: intrinsic differences in gene expression and response to cold exposure in mice. *American Journal of Physiology. Endocrinology and Metabolism*, 306(8):E945–E964, 4 2014.

[10] A. M. Cypess, A. P. White, C. Vernochet, T. J. Schulz, R. Xue, C. A. Sass, T. L. Huang, C. Roberts-Toler, L. S. Weiner, C. Sze, A. T. Chacko, L. N. Deschamps, L. M. Herder, N. Truchan, A. L. Glasgow, A. R. Holman, A. Gavrila, P.-O. Hasselgren, M. A. Mori, M. Molla, and Y.-H. Tseng. Anatomical localization, gene expression profiling and functional characterization of adult human neck brown fat. *Nature Medicine*, 19(5):635–639, 5 2013.

[11] S. A. Machado, G. Pasquarelli do Nascimento, D. S. da Silva, G. R. Farias, I. de Oliveira Santos, L. B. Baptista, and K. G. Magalhães. Browning of the white adipose tissue regulation: new insights into nutritional and metabolic relevance in health and diseases. *Nutrition & Metabolism*, 19(1):61, sep 2022.

[12] L. Scheja and J. Heeren. The endocrine function of adipose tissues in health and cardiometabolic disease. *Nature Reviews Endocrinology*, 15(9):507–524, 9 2019.

[13] J. Boucher, A. Kleinridders, and C. R. Kahn. Insulin receptor signaling in normal and insulin-resistant states. *Cold Spring Harbor Perspectives in Biology*, 6(1):a009191–a009191, 1 2014.

[14] P. Ježek, M. Jabůrek, B. Holendová, and L. Plecitá-Hlavatá. Fatty acid-stimulated insulin secretion vs. lipotoxicity. *Molecules (Basel, Switzerland)*, 23(6), 6 2018.

[15] M. Skelin Klemen, J. Dolenšek, M. Slak Rupnik, and A. Stožer. The triggering pathway to insulin secretion: Functional similarities and differences between the human and the mouse β cells and their translational relevance. *Islets*, 9(6):109–139, 11 2017.

[16] R. Liu and B. S. Nikolajczyk. Tissue immune cells fuel obesity-associated inflammation in adipose tissue and beyond. *Frontiers in Immunology*, 10:1587, 2019.

[17] K. Man, A. Kallies, and A. Vasanthakumar. Resident and migratory adipose immune cells control systemic metabolism and thermogenesis. *Cellular & Molecular Immunology*, 19(3):421–431, 3 2022.

[18] A. Sakers, M. K. De Siqueira, P. Seale, and C. J. Villanueva. Adipose-tissue plasticity in health and disease. *Cell*, 185:419–446, 2 2022.

[19] I. Wernstedt Asterholm, C. Tao, T. S. Morley, Q. A. Wang, F. Delgado-Lopez, Z. V. Wang, and P. E. Scherer. Adipocyte inflammation is essential for healthy adipose tissue expansion and remodeling. *Cell Metabolism*, 20(1):103–118, 7 2014.

[20] V. Azzu, M. Vacca, S. Virtue, M. Allison, and A. Vidal-Puig. Adipose tissue-liver cross talk in the control of whole-body metabolism: Implications in nonalcoholic fatty liver disease. *Gastroenterology*, 158(7):1899–1912, 5 2020.

[21] P. Chakrabarti, T. English, S. Karki, L. Qiang, R. Tao, J. Kim, Z. Luo, S. R. Farmer, and K. V. Kandror. Insulin inhibits lipolysis in adipocytes via the evolutionarily conserved mtorc1-egr1-atgl-mediated pathway. *Molecular and Cellular Biology*, 33(18):3659–66, 9 2013.

[22] R. Stinkens, G. H. Goossens, J. W. E. Jocken, and E. E. Blaak. Targeting fatty acid metabolism to improve glucose metabolism. *Obesity Reviews*, 16(9):715–757, 9 2015.

[23] F. Haczeyni, K. S. Bell-Anderson, and G. C. Farrell. Causes and mechanisms of adipocyte enlargement and adipose expansion. *Obesity Reviews*, 19(3):406–420, March 2018.

[24] V. Pellegrinelli, S. Carobbio, and A. Vidal-Puig. Adipose tissue plasticity: how fat depots respond differently to pathophysiological cues. *Diabetologia*, 59(6):1075–1088, June 2016.

[25] S. Carobbio, V. Pellegrinelli, and A. Vidal-Puig. *Adipose Tissue Function and Expandability as Determinants of Lipotoxicity and the Metabolic Syndrome*, pages 161–196. Springer Nature, 2017.

[26] X. Hildebrandt, M. Ibrahim, and N. Peltzer. Cell death and inflammation during obesity: "know my methods, wat(son)". *Cell Death & Differentiation*, 30(2):279–292, February 2023.

[27] G. Frühbeck, V. Catalán, A. Rodríguez, and J. Gómez-Ambrosi. Adiponectin-leptin ratio: A promising index to estimate adipose tissue dysfunction. relation with obesity-associated cardiometabolic risk. *Adipocyte*, 7(1):57–62, January 2018.

[28] N. Ouchi, J. L. Parker, J. J. Lugus, and K. Walsh. Adipokines in inflammation and metabolic disease. *Nature Reviews Immunology*, 11(2):85–97, February 2011.

[29] T. Kakuma, Y. Lee, M. Higa, Z. Wang, W. Pan, I. Shimomura, and R. H. Unger. Leptin, troglitazone, and the expression of sterol regulatory element binding proteins in liver and pancreatic islets. *Proceedings of the National Academy of Sciences*, 97(15):8536–8541, July 2000.

[30] H. Tilg and A. R. Moschen. Adipocytokines: mediators linking adipose tissue, inflammation and immunity. *Nature Reviews Immunology*, 6(10):772–783, October 2006.

[31] T. Adolph, C. Grander, F. Grabherr, and H. Tilg. Adipokines and non-alcoholic fatty liver disease: Multiple interactions. *International Journal of Molecular Sciences*, 18(8):1649, July 2017.

[32] N. Martínez-Sánchez. There and back again: Leptin actions in white adipose tissue. *International Journal of Molecular Sciences*, 21(17):6039, August 2020.

[33] N. Halberg, T. Khan, M. E. Trujillo, I. Wernstedt-Asterholm, A. D. Attie, S. Sherwani, Z. V. Wang, S. Landskroner-Eiger, S. Dineen, U. J. Magalang, R. A. Brekken, and P. E. Scherer. Hypoxia-inducible factor 1α induces fibrosis and insulin resistance in white adipose tissue. *Molecular and Cellular Biology*, 29(16):4467–4483, 8 2009.

[34] V. A. Guerreiro, D. Carvalho, and P. Freitas. Obesity, adipose tissue, and inflammation answered in questions. *Journal of Obesity*, 2022:1–11, 1 2022.

[35] K. G. Stenkula and C. Erlanson-Albertsson. Adipose cell size: importance in health and disease. *American Journal of Physiology-Regulatory, Integrative and Comparative Physiology*, 315(2):R284–R295, 8 2018.

[36] V. Mitra and J. Metcalf. Metabolic functions of the liver. *Anaesthesia & Intensive Care Medicine*, 10(7):334–335, 7 2009.

[37] Z. Fu, E. R. Gilbert, and D. Liu. Regulation of insulin synthesis and secretion and pancreatic beta-cell dysfunction in diabetes. *Current diabetes reviews*, 9(1):25–53, 1 2013.

[38] O. Schmitz, J. Rungby, L. Edge, and C. B. Juhl. On high-frequency insulin oscillations. *Ageing Research Reviews*, 7(4):301–305, 12 2008.

[39] J. T. Gonzalez, C. J. Fuchs, J. A. Betts, and L. J. C. van Loon. Liver glycogen metabolism during and after prolonged endurance-type exercise. *American Journal of Physiology-Endocrinology and Metabolism*, 311(3):E543–E553, 9 2016.

[40] M. Hargreaves and L. L. Spriet. Skeletal muscle energy metabolism during exercise. *Nature Metabolism*, 2(9):817–828, 8 2020.

[41] X. Zhang, S. Yang, J. Chen, and Z. Su. Unraveling the regulation of hepatic gluconeogenesis. *Frontiers in Endocrinology*, 9:802, 1 2019.

[42] Z. Z. Alamri. The role of liver in metabolism: an updated review with physiological emphasis. *International Journal of Basic & Clinical Pharmacology*, 7(11):2271, 10 2018.

[43] E. Trefts, M. Gannon, and D. H. Wasserman. The liver. *Current Biology*, 27(21):R1147–R1151, 11 2017.

[44] M. Merkel, R. H. Eckel, and I. J. Goldberg. Lipoprotein lipase. *Journal of Lipid Research*, 43(12):1997–2006, 12 2002.

[45] L. P. Bechmann, R. A. Hannivoort, G. Gerken, G. S. Hotamisligil, M. Trauner, and A. Canbay. The interaction of hepatic lipid and glucose metabolism in liver diseases. *Journal of Hepatology*, 56(4):952–964, 4 2012.

[46] B. A. Neuschwander-Tetri. Hepatic lipotoxicity and the pathogenesis of nonalcoholic steatohepatitis. *Hepatology*, 52(2):774–788, 8 2010.

[47] D. B. Savage, K. F. Petersen, and G. I. Shulman. Disordered lipid metabolism and the pathogenesis of insulin resistance. *Physiological Reviews*, 87(2):507–520, 4 2007.

[48] J. Lee, J. Choi, E. S. S. Alpergin, L. Zhao, T. Hartung, S. Scafidi, R. C. Riddle, and M. J. Wolfgang. Loss of hepatic mitochondrial long-chain fatty acid oxidation confers resistance to diet-induced obesity and glucose intolerance. *Cell Reports*, 20(3):655–667, 7 2017.

[49] P. M. Coen and B. H. Goodpaster. Role of intramyocelluar lipids in human health. *Trends in Endocrinology & Metabolism*, 23(8):391–398, 8 2012.

[50] M. Qatanani and M. A. Lazar. Mechanisms of obesity-associated insulin resistance: many choices on the menu. *Genes & Development*, 21(12):1443–1455, 6 2007.

[51] M. E. Rinella, J. V. Lazarus, V. Ratziu, S. M. Francque, A. J. Sanyal, F. Kanwal, D. Romero, M. F. Abdelmalek, Q. M. Anstee, J. P. Arab, M. Arrese, R. Bataller, U. Beuers, J. Boursier, E. Bugianesi, C. D. Byrne, G. E. Castro Narro, A. Chowdhury, H. Cortez-Pinto, D. R. Cryer, K. Cusi, M. El-Kassas, S. Klein, W. Eskridge, J. Fan, S. Gawrieh, C. D. Guy, S. A. Harrison, S. U. Kim, B. G. Koot, M. Korenjak, K. V. Kowdley, F. Lacaille, R. Loomba, R. Mitchell-Thain, T. R. Morgan, E. E. Powell, M. Roden, M. Romero-Gómez, M. Silva, S. P. Singh, S. C. Sookoian, C. W. Spearman, D. Tiniakos, L. Valenti, M. B. Vos, V. W. S. Wong, S. Xanthakos, Y. Yilmaz, Z. Younossi, A. Hobbs, M. Villota-Rivas, and P. N. Newsome. A multisociety delphi consensus statement on new fatty liver disease nomenclature. *Annals of Hepatology*, 29(1):101133, 1 2024.

[52] M. Israelsen, S. Francque, E. A. Tsochatzis, and A. Krag. Steatotic liver disease. *The Lancet*, 404(10464):1761–1778, 11 2024.

[53] Z. M. Younossi, A. B. Koenig, D. Abdelatif, Y. Fazel, L. Henry, and M. Wymer. Global epidemiology of nonalcoholic fatty liver disease—meta□analytic assessment of prevalence, incidence, and outcomes. *Hepatology*, 64(1):73–84, 7 2016.

[54] L. Miao, G. Targher, C. D. Byrne, Y.-Y. Cao, and M.-H. Zheng. Current status and future trends of the global burden of masld. *Trends in Endocrinology & Metabolism*, 35(8):697–707, 8 2024.

[55] Z. M. Younossi, P. Golabi, J. M. Paik, A. Henry, C. Van Dongen, and L. Henry. The global epidemiology of nonalcoholic fatty liver disease (nafld) and nonalcoholic steatohepatitis (nash): a systematic review. *Hepatology*, 77(4):1335–1347, 4 2023.

[56] J. M. Paik, L. Henry, Y. Younossi, J. Ong, S. Alqahtani, and Z. M. Younossi. The burden of nonalcoholic fatty liver disease (nafld) is rapidly growing in every region of the world from 1990 to 2019. *Hepatology Communications*, 7(10), 10 2023.

[57] E. En Li Cho, C. Z. Ang, J. Quek, C. E. Fu, L. K. E. Lim, Z. E. Q. Heng, D. J. H. Tan, W. H. Lim, J. N. Yong, R. Zeng, D. Chee, B. Nah, C. R. A. Lesmana, A. H. Bwa, K. M. Win, C. Faulkner, M. B. Aboona, M. C. Lim, N. Syn, A. V. Kulkarni, H. Suzuki, H. Takahashi, N. Tamaki, K. Wijarnpreecha, D. Q. Huang, M. Muthiah, C. H. Ng, and R. Loomba. Global prevalence of non-alcoholic fatty liver disease in type 2 diabetes mellitus: an updated systematic review and meta-analysis. *Gut*, 72(11):2138–2148, 11 2023.

[58] F. Barrera, J. Uribe, N. Olvares, P. Huerta, D. Cabrera, and M. Romero-Gómez. The janus of a disease: Diabetes and metabolic dysfunction-associated fatty liver disease. *Annals of Hepatology*, 29(4):101501, 7 2024.

[59] N. Chalasani, Z. Younossi, J. E. Lavine, M. Charlton, K. Cusi, M. Rinella, S. A. Harrison, E. M. Brunt, and A. J. Sanyal. The diagnosis and management of nonalcoholic fatty

liver disease: Practice guidance from the american association for the study of liver diseases. *Hepatology (Baltimore, Md.)*, 67(1):328–357, 1 2018.

[60] K. Staufer and R. E. Stauber. Steatotic liver disease: Metabolic dysfunction, alcohol, or both? *Biomedicines*, 11, 7 2023.

[61] R. Sandireddy, S. Sakthivel, P. Gupta, J. Behari, M. Tripathi, and B. K. Singh. Systemic impacts of metabolic dysfunction-associated steatotic liver disease (masld) and metabolic dysfunction-associated steatohepatitis (mash) on heart, muscle, and kidney related diseases. *Frontiers in cell and developmental biology*, 12:1433857, 2024.

[62] H. Tilg, T. E. Adolph, and A. R. Moschen. Multiple parallel hits hypothesis in nonalcoholic fatty liver disease: Revisited after a decade. *Hepatology (Baltimore, Md.)*, 73:833–842, 2 2021.

[63] F. Carli, G. Della Pepa, S. Sabatini, A. Vidal Puig, and A. Gastaldelli. Lipid metabolism in masld and mash: From mechanism to the clinic. *JHEP Reports*, 6:101185, 12 2024.

[64] R. Loomba, S. L. Friedman, and G. I. Shulman. Mechanisms and disease consequences of nonalcoholic fatty liver disease. *Cell*, 184:2537–2564, 5 2021.

[65] H. Leal-Lassalle, O. Estévez-Vázquez, F. J. Cubero, and Y. A. Nevzorova. Metabolic and alcohol-associated liver disease (metald): a representation of duality. *npj Gut and Liver*, 2:1, 1 2025.

[66] F.-R. Sun and B.-Y. Wang. Alcohol and metabolic-associated fatty liver disease. *Journal of clinical and translational hepatology*, 9:719–730, 10 2021.

[67] H. Yanai, H. Adachi, M. Hakoshima, S. Iida, and H. Katsuyama. Metabolic-dysfunction-associated steatotic liver disease—its pathophysiology, association with atherosclerosis and cardiovascular disease, and treatments. *International Journal of Molecular Sciences*, 24:15473, 10 2023.

[68] S. Pouwels, N. Sakran, Y. Graham, A. Leal, T. Pintar, W. Yang, R. Kassir, R. Singhal, K. Mahawar, and D. Ramnarain. Non-alcoholic fatty liver disease (nafld): a review of pathophysiology, clinical management and effects of weight loss. *BMC Endocrine Disorders*, 22:63, 3 2022.

[69] G. Semmler, C. Datz, T. Reiberger, and M. Trauner. Diet and exercise in nafld/nash: Beyond the obvious. *Liver International*, 41:2249–2268, 10 2021.

[70] S. A. Harrison, A. M. Allen, J. Dubourg, M. Noureddin, and N. Alkhouri. Challenges and opportunities in nash drug development. *Nature Medicine*, 29:562–573, 3 2023.

[71] S. J. Song, J. C.-T. Lai, G. L.-H. Wong, V. W.-S. Wong, and T. C.-F. Yip. Can we use old nafld data under the new masld definition? *Journal of Hepatology*, 80:e54–e56, 2 2024.

[72] V. Ratziu, J. Boursier, V. de Ledinghen, R. Anty, C. Costentin, and C. Bureau. Confirmatory biomarker diagnostic studies are not needed when transitioning from nafld to masld. *Journal of Hepatology*, 80:e51–e52, 2 2024.

[73] H. Tilg and A. R. Moschen. Evolution of inflammation in nonalcoholic fatty liver disease: The multiple parallel hits hypothesis. *Hepatology*, 52:1836–1846, 11 2010.

[74] L. Shojaie, A. Iorga, and L. Dara. Cell death in liver diseases: A review. *International Journal of Molecular Sciences*, 21:9682, 12 2020.

[75] S. Zhao, Y. Guo, and X. Yin. Autophagy, ferroptosis, apoptosis and pyroptosis in metabolic dysfunction-associated steatotic liver disease. *Frontiers in Bioscience-Landmark*, 29, 1 2024.

[76] J. Gautheron, M. Vucur, A. T. Schneider, I. Severi, C. Roderburg, S. Roy, M. Bartneck, P. Schrammen, M. B. Diaz, J. Ehling, F. Gremse, F. Heymann, C. Koppe, T. Lammers, F. Kiessling, N. Van Best, O. Pabst, G. Courtois, A. Linkermann, S. Krautwald, U. P. Neumann, F. Tacke, C. Trautwein, D. R. Green, T. Longerich, N. Frey, M. Luedde, M. Bluher, S. Herzig, M. Heikenwalder, and T. Luedde. The necroptosis-inducing kinase ripk3 dampens adipose tissue inflammation and glucose intolerance. *Nature Communications*, 7:11869, 6 2016.

[77] S. Kumar, Q. Duan, R. Wu, E. N. Harris, and Q. Su. Pathophysiological communication between hepatocytes and non-parenchymal cells in liver injury from nafld to liver fibrosis. *Advanced Drug Delivery Reviews*, 176:113869, 9 2021.

[78] K. Segawa and S. Nagata. An apoptotic ‘eat me’ signal: Phosphatidylserine exposure. *Trends in Cell Biology*, 25:639–650, 11 2015.

[79] O.-H. Kim, G.-H. Kang, J. Hur, J. Lee, Y. Jung, I.-S. Hong, H. Lee, S.-Y. Seo, D. H. Lee, C. S. Lee, I.-K. Lee, S. Bonner-Weir, J. Lee, Y. J. Park, H. Kim, S. E. Shoelson, and B.-C. Oh. Externalized phosphatidylinositides on apoptotic cells are eat-me signals recognized by cd14. *Cell Death & Differentiation*, 29:1423–1432, 7 2022.

[80] J. D. Webster and D. Vucic. The balance of tnf mediated pathways regulates inflammatory cell death signaling in healthy and diseased tissues. *Frontiers in Cell and Developmental Biology*, 8, 5 2020.

[81] P. Gough and I. A. Myles. Tumor necrosis factor receptors: Pleiotropic signaling complexes and their differential effects. *Frontiers in Immunology*, 11, 11 2020.

[82] R. F. Schwabe and T. Luedde. Apoptosis and necroptosis in the liver: a matter of life and death. *Nat. Rev. Gastroenterol. Hepatol.*, 15(12):738–752, dec 2018.

[83] M. Najjar, D. Saleh, M. Zelic, S. Nogusa, S. Shah, A. Tai, J. N. Finger, A. Polykratis, P. J. Gough, J. Bertin, M. Whalen, M. Pasparakis, S. Balachandran, M. Kelliher, A. Poltorak, and A. Degterev. Ripk1 and ripk3 kinases promote cell-death-independent inflammation by toll-like receptor 4. *Immunity*, 45:46–59, 7 2016.

[84] K. Ye, Z. Chen, and Y. Xu. The double-edged functions of necroptosis. *Cell Death & Disease*, 14:163, 2 2023.

[85] L. R. Garcia, T. Tenev, R. Newman, R. O. Haich, G. Liccardi, S. W. John, A. Annibaldi, L. Yu, M. Pardo, S. N. Young, C. Fitzgibbon, W. Fernando, N. Guppy, H. Kim, L.-Y. Liang, I. S. Lucet, A. Kueh, I. Roxanis, P. Gazinska, M. Sims, T. Smyth, G. Ward, J. Bertin, A. M. Beal, B. Geddes, J. S. Choudhary, J. M. Murphy, K. Aurelia Ball, J. W. Upton, and P. Meier. Ubiquitylation of mlkl at lysine 219 positively regulates necroptosis-induced tissue injury and pathogen clearance. *Nature Communications*, 12:3364, 6 2021.

[86] M. E. Choi, D. R. Price, S. W. Ryter, and A. M. K. Choi. Necroptosis: a crucial pathogenic mediator of human disease. *JCI Insight*, 4, 8 2019.

[87] Z.-H. Yang, X.-N. Wu, P. He, X. Wang, J. Wu, T. Ai, C.-Q. Zhong, X. Wu, Y. Cong, R. Zhu, H. Li, Z.-Y. Cai, W. Mo, and J. Han. A non-canonical pdk1-rsk signal diminishes pro-caspase-8-mediated necroptosis blockade. *Molecular Cell*, 80:296–310.e6, 10 2020.

[88] D. Yang, Y. Liang, S. Zhao, Y. Ding, Q. Zhuang, Q. Shi, T. Ai, S.-Q. Wu, and J. Han. Zbp1 mediates interferon-induced necroptosis. *Cellular & molecular immunology*, 17:356–368, 4 2020.

[89] Z. Liu, S. Wang, W. Wang, R. Lv, and C. Sun. Necroptosis in obesity: a complex cell death event. *Apoptosis*, 12 2024.

[90] M. Yang, W. Chen, L. He, D. Liu, L. Zhao, and X. Wang. A glimpse of necroptosis and diseases. *Biomedicine & Pharmacotherapy*, 156:113925, 12 2022.

[91] H. Tye, S. A. Conos, T. M. Djajawi, T. A. Gottschalk, N. Abdoulkader, I. Y. Kong, H. L. Kammoun, V. K. Narayana, T. Kratina, M. Speir, J. Emery, D. S. Simpson, C. Hall, A. J. Vince, S. Russo, R. Crawley, M. Rashidi, J. M. Hildebrand, J. M. Murphy, L. Whitehead, D. P. De Souza, S. L. Masters, A. L. Samson, N. Lalaoui, E. D. Hawkins, A. J. Murphy, J. E. Vince, and K. E. Lawlor. Divergent roles of ripk3 and mlkl in high-fat diet–induced obesity and mafld in mice. *Life Science Alliance*, 8:e202302446, 1 2025.

[92] H. Xu, X. Du, G. Liu, S. Huang, W. Du, S. Zou, D. Tang, C. Fan, Y. Xie, Y. Wei, Y. Tian, and X. Fu. The pseudokinase mlkl regulates hepatic insulin sensitivity independently of inflammation. *Molecular Metabolism*, 23:14–23, 5 2019.

[93] X. Wu, K. L. Poulsen, C. Sanz-Garcia, E. Huang, M. R. McMullen, S. Roychowdhury, S. Dasarathy, and L. E. Nagy. Mlkl-dependent signaling regulates autophagic flux in a murine model of non-alcohol-associated fatty liver and steatohepatitis. *Journal of hepatology*, 73:616–627, 9 2020.

[94] H. Flores-Romero, U. Ros, and A. J. Garcia-Saez. Pore formation in regulated cell death. *The EMBO Journal*, 39, 12 2020.

[95] Z. Cai, S. Jitkaew, J. Zhao, H.-C. Chiang, S. Choksi, J. Liu, Y. Ward, L. g. Wu, and Z.-G. Liu. Plasma membrane translocation of trimerized mlkl protein is required for tnf-induced necroptosis. *Nature Cell Biology*, 16:55–65, 1 2014.

[96] B. Xia, S. Fang, X. Chen, H. Hu, P. Chen, H. Wang, and Z. Gao. Mlkl forms cation channels. *Cell Research*, 26:517–528, 5 2016.

[97] S. Liu, H. Liu, A. Johnston, S. Hanna-Addams, E. Reynoso, Y. Xiang, and Z. Wang. Mlkl forms disulfide bond-dependent amyloid-like polymers to induce necroptosis. *Proceedings of the National Academy of Sciences*, 114, 9 2017.

[98] S. Yoon, K. Bogdanov, and D. Wallach. Site-specific ubiquitination of mlkl targets it to endosomes and targets listeria and yersinia to the lysosomes. *Cell Death & Differentiation*, 29:306–322, 2 2022.

[99] S. Yoon, A. Kovalenko, K. Bogdanov, and D. Wallach. Mlkl, the protein that mediates necroptosis, also regulates endosomal trafficking and extracellular vesicle generation. *Immunity*, 47:51–65.e7, 7 2017.

[100] J. Dai, C. Zhang, L. Guo, H. He, K. Jiang, Y. Huang, X. Zhang, H. Zhang, W. Wei, Y. Zhang, L. Lu, and J. Hu. A necroptotic-independent function of mlkl in regulating endothelial cell adhesion molecule expression. *Cell Death & Disease*, 11:282, 4 2020.

[101] S. A. Conos, K. W. Chen, D. De Nardo, H. Hara, L. Whitehead, G. Núñez, S. L. Masters, J. M. Murphy, K. Schroder, D. L. Vaux, K. E. Lawlor, L. M. Lindqvist, and J. E. Vince. Active mlkl triggers the nlrp3 inflammasome in a cell-intrinsic manner. *Proceedings of the National Academy of Sciences*, 114, 2 2017.

[102] S. Martens, J. Bridelance, R. Roelandt, P. Vandenabeele, and N. Takahashi. Mlkl in cancer: more than a necroptosis regulator. *Cell Death and Differentiation*, 28:1757–1772, 6 2021.

[103] J. Taylor, J. Sellin, L. Kuerschner, L. Krähl, Y. Majlesain, I. Förster, C. Thiele, H. Weighardt, and E. Weber. Generation of immune cell containing adipose organoids for in vitro analysis of immune metabolism. *Scientific Reports*, 10:21104, 12 2020.

[104] M. Khan and S. Gasser. Generating primary fibroblast cultures from mouse ear and tail tissues. *Journal of Visualized Experiments*, 2016, 1 2016.

[105] M. Charni-Natan and I. Goldstein. Protocol for primary mouse hepatocyte isolation. *STAR Protocols*, 1:100086, 2020.

[106] J. T. Auman, G. A. Boorman, R. E. Wilson, G. S. Travlos, and R. S. Paules. Heat map visualization of high-density clinical chemistry data. *Physiological Genomics*, 31:352–356, 10 2007.

[107] U. Ros, A. Peña-Blanco, K. Hänggi, U. Kunzendorf, S. Krautwald, W. W.-L. Wong, and A. J. García-Sáez. Necroptosis execution is mediated by plasma membrane nanopores independent of calcium. *Cell Reports*, 19:175–187, 4 2017.

[108] D. E. Kleiner, E. M. Brunt, M. Van Natta, C. Behling, M. J. Contos, O. W. Cummings, L. D. Ferrell, Y.-C. Liu, M. S. Torbenson, A. Unalp-Arida, M. Yeh, A. J. McCullough, and A. J. Sanyal. Design and validation of a histological scoring system for nonalcoholic fatty liver disease†. *Hepatology*, 41:1313–1321, 6 2005.

[109] I. Murano, G. Barbatelli, V. Parisani, C. Latini, G. Muzzonigro, M. Castellucci, and S. Cinti. Dead adipocytes, detected as crown-like structures, are prevalent in visceral fat depots of genetically obese mice. *Journal of Lipid Research*, 49:1562–1568, 7 2008.

[110] M. Guerre-Millo. Adipose tissue and adipokines: for better or worse. *diabetes & metabolism*, 30:13–19, 2 2004.

[111] R. Gallego-Durán, J. Ampuero, D. Maya-Miles, H. Pastor-Ramírez, R. Montero-Vallejo, J. Rivera-Esteban, L. Álvarez Amor, M. J. Pareja, M. C. Rico, R. Millán, M. J. Robles-Frías, R. Aller, Á. Rojas, R. Muñoz-Hernández, A. Gil-Gómez, S. Gato, M. García-Lozano, M. T. Arias-Loste, J. Abad, J. L. Calleja, R. J. Andrade, J. Crespo, Á. González-Rodríguez, C. García-Monzón, F. Andreola, J. M. Pericás, R. Jalan, F. Martín-Bermudo, and M. Romero-Gómez. Fibroblast growth factor 21 is a hepatokine involved in masld progression. *united european gastroenterology journal*, 12:1056–1068, 10 2024.

[112] S. P. Preston, M. D. Stutz, C. C. Allison, U. Nachbur, Q. Gouil, B. M. Tran, V. Duvivier, P. Arandjelovic, J. P. Cooney, L. Mackiewicz, Y. Meng, J. Schaefer, S. M. Bader, H. Peng, Z. Valaydon, P. Rajasekaran, C. Jennison, S. Lopaticki, A. Farrell, M. Ryan, J. Howell, C. Croagh, D. Karunakaran, C. Schuster-Klein, J. M. Murphy, T. Fifis, C. Christophi, E. Vincan, M. E. Blewitt, A. Thompson, J. A. Boddey, M. Doerflinger, and M. Pellegrini. Epigenetic silencing of ripk3 in hepatocytes prevents mlkl-mediated necroptosis from contributing to liver pathologies. *gastroenterology*, 163:1643–1657.e14, 12 2022.

[113] K. J. Hintze, A. D. Benninghoff, C. E. Cho, and R. E. Ward. Modeling the western diet for preclinical investigations. *advances in nutrition*, 9:263–271, 5 2018.

[114] K. J. Hintze, A. D. Benninghoff, and R. E. Ward. Formulation of the total western diet (twd) as a basal diet for rodent cancer studies. *journal of agricultural and food chemistry*, 60:6736–6742, 7 2012.

[115] P. Lang, S. Hasselwander, H. Li, and N. Xia. Effects of different diets used in diet-induced obesity models on insulin resistance and vascular dysfunction in c57bl/6 mice. *scientific reports*, 9:19556, 12 2019.

[116] WHO. Harmful use of alcohol kills more than 3 million people each year, most of them men, 9 2018. https://www.who.int/news/item/21-09-2018-harmful-use-of-alcohol-kills-more-than-3-million-people-each-year--most-of-them-men [Accessed: 2025-08-20].

[117] R. J. W. Wilkin, P. F. Lalor, R. Parker, and P. N. Newsome. Murine models of acute alcoholic hepatitis and their relevance to human disease. *the american journal of pathology*, 186:748–760, 4 2016.

[118] J. Fletcher. What is heterogeneity and is it important? *bmj*, 334:94–96, 1 2007.

[119] P. Ohene-Marfo, H. V. M. Nguyen, S. Mohammed, N. Thadathil, A. Tran, E. H. Nicklas, D. Wang, R. Selvarani, J. W. Farriester, R. Varshney, M. Kinter, A. Richardson, M. C. Rudolph, and S. S. Deepa. Non-necroptotic roles of mlkl in diet-induced obesity, liver pathology, and insulin sensitivity: Insights from a high-fat, high-fructose, high-cholesterol diet mouse model. *International Journal of Molecular Sciences*, 25:2813, 2 2024.

[120] J. L. Steiner, K. T. Crowell, and C. H. Lang. Impact of alcohol on glycemic control and insulin action. *Biomolecules*, 5:2223–46, 9 2015.

[121] S.-J. Kim and D.-J. Kim. Alcoholism and diabetes mellitus. *Diabetes & Metabolism Journal*, 36:108–15, 4 2012.

[122] Y. Diao, J. Nie, P. Tan, Y. Zhao, T. Zhao, J. Tu, H. Ji, Y. Cao, Z. Wu, H. Liang, H. Huang, Y. Li, X. Gao, and L. Zhou. Long-term low-dose ethanol intake improves healthspan and resists high-fat diet-induced obesity in mice. *Aging*, 12:13128–13146, 7 2020.

[123] M. Babuta, C. Morel, M. de Carvalho Ribeiro, A. A. Datta, C. Calenda, C. Copeland, I. Nasser, and G. Szabo. A novel experimental model of metald in male mice recapitulates key features of severe alcohol-associated hepatitis. *Hepatology Communications*, 8, 7 2024.

[124] M. You, R. V. Considine, T. C. Leone, D. P. Kelly, and D. W. Crabb. Role of adiponectin in the protective action of dietary saturated fat against alcoholic fatty liver in mice. *Hepatology*, 42:568–577, 9 2005.

[125] F. Ziemke and C. S. Mantzoros. Adiponectin in insulin resistance: lessons from translational research. *The American Journal of Clinical Nutrition*, 91:258S–261S, 1 2010.

[126] M. You and C. Q. Rogers. Adiponectin: A key adipokine in alcoholic fatty liver. *Experimental Biology and Medicine*, 234:850–859, 8 2009.

[127] J. L. Steiner and C. H. Lang. Alcohol, adipose tissue and lipid dysregulation. *Biomolecules*, 7, 2 2017.

[128] A. Pérez-Pérez, F. Sánchez-Jiménez, T. Vilariño-García, and V. Sánchez-Margalet. Role of leptin in inflammation and vice versa. *International Journal of Molecular Sciences*, 21:5887, 8 2020.

[129] P. J. Scarpace and Y. Zhang. Leptin resistance: a prediposing factor for diet-induced obesity. *American Journal of Physiology-Regulatory, Integrative and Comparative Physiology*, 296:R493–R500, 3 2009.

[130] G. Traversy and J.-P. Chaput. Alcohol consumption and obesity: An update. *Current Obesity Reports*, 4:122–130, 3 2015.

[131] T. Kawai, M. V. Autieri, and R. Scalia. Adipose tissue inflammation and metabolic dysfunction in obesity. *American Journal of Physiology-Cell Physiology*, 320:C375–C391, 3 2021.

[132] J. J. Fuster, N. Ouchi, N. Gokce, and K. Walsh. Obesity-induced changes in adipose tissue microenvironment and their impact on cardiovascular disease. *Circ. Res.*, 118(11):1786–1807, may 2016.

[133] J. Magusto, C. Beaupère, M. B. Afonso, M. Auclair, J.-L. Delaunay, P.-A. Soret, G. Courtois, T. Aït-Slimane, C. Housset, I. Jéru, B. Fève, V. Ratziu, C. M. P. Rodrigues, and J. Gautheron. The necroptosis-inducing pseudokinase mixed lineage kinase domain-like regulates the adipogenic differentiation of pre-adipocytes. *iScience*, 25(10), oct 2022.

[134] D. B. Ballak, R. Stienstra, C. J. Tack, C. A. Dinarello, and J. A. van Diepen. IL-1 family members in the pathogenesis and treatment of metabolic disease: Focus on adipose tissue inflammation and insulin resistance. *Cytokine*, 75(2):280–290, October 2015.

[135] J. J. Fuster, N. Ouchi, N. Gokce, and K. Walsh. Obesity-induced changes in adipose tissue microenvironment and their impact on cardiovascular disease. *Circ. Res.*, 118(11):1786–1807, May 2016.

[136] B. Klop, J. W. F. Elte, and M. C. Cabezas. Dyslipidemia in obesity: mechanisms and potential targets. *Nutrients*, 5(4):1218–1240, apr 2013.

[137] Z. Michailidou, M. Gomez-Salazar, and V. I. Alexaki. Innate immune cells in the adipose tissue in health and metabolic disease. *J. Innate Immun.*, 14(1):4–30, 2022.

[138] W. K. Saeed, D. W. Jun, K. Jang, J. H. Oh, Y. J. Chae, J. S. Lee, D. H. Koh, and H. T. Kang. Decrease in fat de novo synthesis and chemokine ligand expression in non-alcoholic fatty liver disease caused by inhibition of mixed lineage kinase domain-like pseudokinase. *Journal of Gastroenterology and Hepatology*, 34(12):2206–2218, 2019.

[139] V. Schirinzi, C. Poli, C. Berteotti, and A. Leone. Browning of adipocytes: A potential therapeutic approach to obesity. *Nutrients*, 15(9), May 2023.

[140] A. Ferdouse and R. D. Clugston. Pathogenesis of alcohol-associated fatty liver: Lessons from transgenic mice. *Front. Physiol.*, 13:940974, jul 2022.

[141] A. Nicholson, P. C. Reifsnyder, R. D. Malcolm, C. A. Lucas, G. R. MacGregor, W. Zhang, and E. H. Leiter. Diet-induced obesity in two c57bl/6 substrains with intact or mutant nicotinamide nucleotide transhydrogenase (nnt) gene. *Obesity (Silver Spring)*, 18(5):982–985, may 2010.

[142] S. Nemoto, T. Kubota, and H. Ohno. Metabolic differences and differentially expressed genes between c57bl/6j and c57bl/6n mice substrains. *PLOS ONE*, 17(12):e0271651, dec 2022.

[143] L. M. John, N. Petersen, M. K. Gerstenberg, L. Torz, K. Pedersen, B. Ø. Christoffersen, and R. E. Kuhre. Housing-temperature reveals energy intake counter-balances energy expenditure in normal-weight, but not diet-induced obese, male mice. *Communications Biology*, 5(1):946, sep 2022.

[144] M. Danielli, L. Perne, E. Jarc Jovičić, and T. Petan. Lipid droplets and polyunsaturated fatty acid trafficking: Balancing life and death. *Front. Cell Dev. Biol.*, 11:1104725, January 2023.

[145] M. G. Neuman, Y. Maor, R. M. Nanau, E. Melzer, H. Mell, M. Opris, L. Cohen, and S. Malnick. Alcoholic liver disease: Role of cytokines. *Biomolecules*, 5(3):2023–2034, August 2015.

[146] H. Tilg, A. R. Moschen, and G. Szabo. Interleukin-1 and inflammasomes in alcoholic liver disease/acute alcoholic hepatitis and nonalcoholic fatty liver disease/nonalcoholic steatohepatitis. *Hepatology*, 64(3):955–965, September 2016.

[147] M. N. de Menezes, É. M. Salles, F. Vieira, E. P. Amaral, V. Zuzarte-Luís, A. Cassado, S. Epiphanio, J. M. Alvarez, J. C. Alves-Filho, M. M. Mota, and M. R. D'Império-Lima. IL-1α promotes liver inflammation and necrosis during blood-stage plasmodium chabaudi malaria. *Sci. Rep.*, 9(1):7575, May 2019.

[148] X. Wu, X. Fan, M. R. McMullen, T. Miyata, A. Kim, V. Pathak, J. Wu, L. Z. Day, J. E. Hardesty, N. Welch, J. Dasarathy, D. S. Allende, A. J. McCullough, J. M. Jacobs, D. M. Rotroff, S. Dasarathy, and L. E. Nagy. Macrophage-derived MLKL in alcohol-associated liver disease: Regulation of phagocytosis. *Hepatology*, 77(3):902–919, March 2023.

[149] C. Zhuang, F. Cui, J. Chen, D. He, T. Sun, and P. Wang. Rbm39 ameliorates metabolic dysfunction-associated steatotic liver disease by regulating apob and fabp4. *Biochim. Biophys. Acta Mol. Basis Dis.*, 1871(5):167815, June 2025.

[150] A. M. Valdes, J. Walter, E. Segal, and T. D. Spector. Role of the gut microbiota in nutrition and health. *BMJ*, page k2179, jun 2018.

[151] J. T. Nearing, A. M. Comeau, and M. G. I. Langille. Identifying biases and their potential solutions in human microbiome studies. *Microbiome*, 9(1):113, may 2021.

[152] K. D. McCoy, M. B. Geuking, and F. Ronchi. Gut microbiome standardization in control and experimental mice. *Current Protocols in Immunology*, 117(1), apr 2017.

[153] S.-X. Yu, W. Chen, Z.-Z. Liu, F.-H. Zhou, S.-Q. Yan, G.-Q. Hu, X.-X. Qin, J. Zhang, K. Ma, C.-T. Du, J.-M. Gu, X.-M. Deng, W.-Y. Han, and Y.-J. Yang. Non-hematopoietic mlkl protects against salmonella mucosal infection by enhancing inflammasome activation. *Frontiers in Immunology*, 9, feb 2018.

[154] S.-M. Won, E. Park, J.-J. Jeong, R. Ganesan, H. Gupta, Y. A. Gebru, S. Sharma, D.-J. Kim, and K.-T. Suk. The gut microbiota-derived immune response in chronic liver disease. *International journal of molecular sciences*, 22(15), aug 2021.

[155] F. Bishehsari, E. Magno, G. Swanson, V. Desai, R. M. Voigt, C. B. Forsyth, and A. Keshavarzian. Alcohol and gut-derived inflammation. *Alcohol research : current reviews*, 38(2):163–171, 2017.

[156] A. Majdi, L. Aoudjehane, V. Ratziu, T. Islam, M. B. Afonso, F. Conti, T. Mestiri, M. Lagouge, F. Foufelle, F. Ballenghien, T. Ledent, M. Moldes, A. Cadoret, L. Fouassier, J.-L. Delaunay, T. Aït-Slimane, G. Courtois, B. Fève, O. Scatton, C. Prip-Buus, C. M. P. Rodrigues, C. Housset, and J. Gautheron. Inhibition of receptor-interacting protein kinase 1 improves experimental non-alcoholic fatty liver disease. *Journal of Hepatology*, 72:627–635, 4 2020.

[157] D. Karunakaran, A. W. Turner, A.-C. Duchez, S. Soubeyrand, A. Rasheed, D. Smyth, D. P. Cook, M. Nikpay, J. W. Kandiah, C. Pan, M. Geoffrion, R. Lee, L. Boytard, H. Wyatt, M.-A. Nguyen, P. Lau, M. Laakso, B. Ramkhelawon, M. Alvarez, K. H. Pietiläinen, P. Pajukanta, B. C. Vanderhyden, P. Liu, S. B. Berger, P. J. Gough, J. Bertin, M.-E. Harper, A. J. Lusis, R. McPherson, and K. J. Rayner. Ripk1 gene variants associate with obesity in humans and can be therapeutically silenced to reduce obesity in mice. *Nature Metabolism*, 2:1113–1125, 9 2020.

[158] Y. Yuan, X. Hu, C. Guo, Y. Xu, S. Li, W. Wen, X. Hu, F. Zeng, W. Cui, W. Chen, X. Sun, N. Hou, J. Wang, R.-P. Xiao, and X. Zhang. Reduction of intestinal ripk1 ameliorates hfd-induced metabolic disorders in female mice. *iScience*, 28:111906, 2 2025.

[159] A. Polykratis, N. Hermance, M. Zelic, J. Roderick, C. Kim, T.-M. Van, T. H. Lee, F. K. M. Chan, M. Pasparakis, and M. A. Kelliher. Cutting edge: Ripk1 kinase inactive mice are viable and protected from tnf-induced necroptosis in vivo. *J. Immunol.*, 193(4):1539–1543, 2014.

[160] M. A. Kelliher, S. Grimm, Y. Ishida, F. Kuo, B. Z. Stanger, and P. Leder. The death domain kinase rip mediates the tnf-induced nf-κb signal. *Immunity*, 8:297–303, 3 1998.

[161] L. Tao, Y. Yi, Y. Chen, H. Zhang, P. Orning, E. Lien, J. Jie, W. Zhang, Q. Xu, Y. Li, Z. Ding, C. Wu, Q. Ding, J. Wang, J. Zhang, and D. Weng. Rip1 kinase activity promotes steatohepatitis through mediating cell death and inflammation in macrophages. *Cell Death & Differentiation*, 28:1418–1433, 4 2021.

[162] Q. Zhao, X. Cheng, J. Guo, Y. Bi, L. Kuang, J. Ren, J. Zhong, L. Pan, X. Zhang, Y. Guo, Y. Liu, S. Jin, Y. Tan, and X. Yu. Mlkl inhibits intestinal tumorigenesis by suppressing stat3 signaling pathway. *International Journal of Biological Sciences*, 17(3):869–881, 2021.

[163] J. Wu, Z. Huang, J. Ren, Z. Zhang, P. He, Y. Li, J. Ma, W. Chen, Y. Zhang, X. Zhou, Z. Yang, S.-Q. Wu, L. Chen, and J. Han. Mlkl knockout mice demonstrate the indispensable role of mlkl in necroptosis. *Cell Research*, 23(8):994–1006, aug 2013.

Chapter 6

Appendix

6.1 List of Figures

6.2 List of Tables

6.3 Supplementary Information

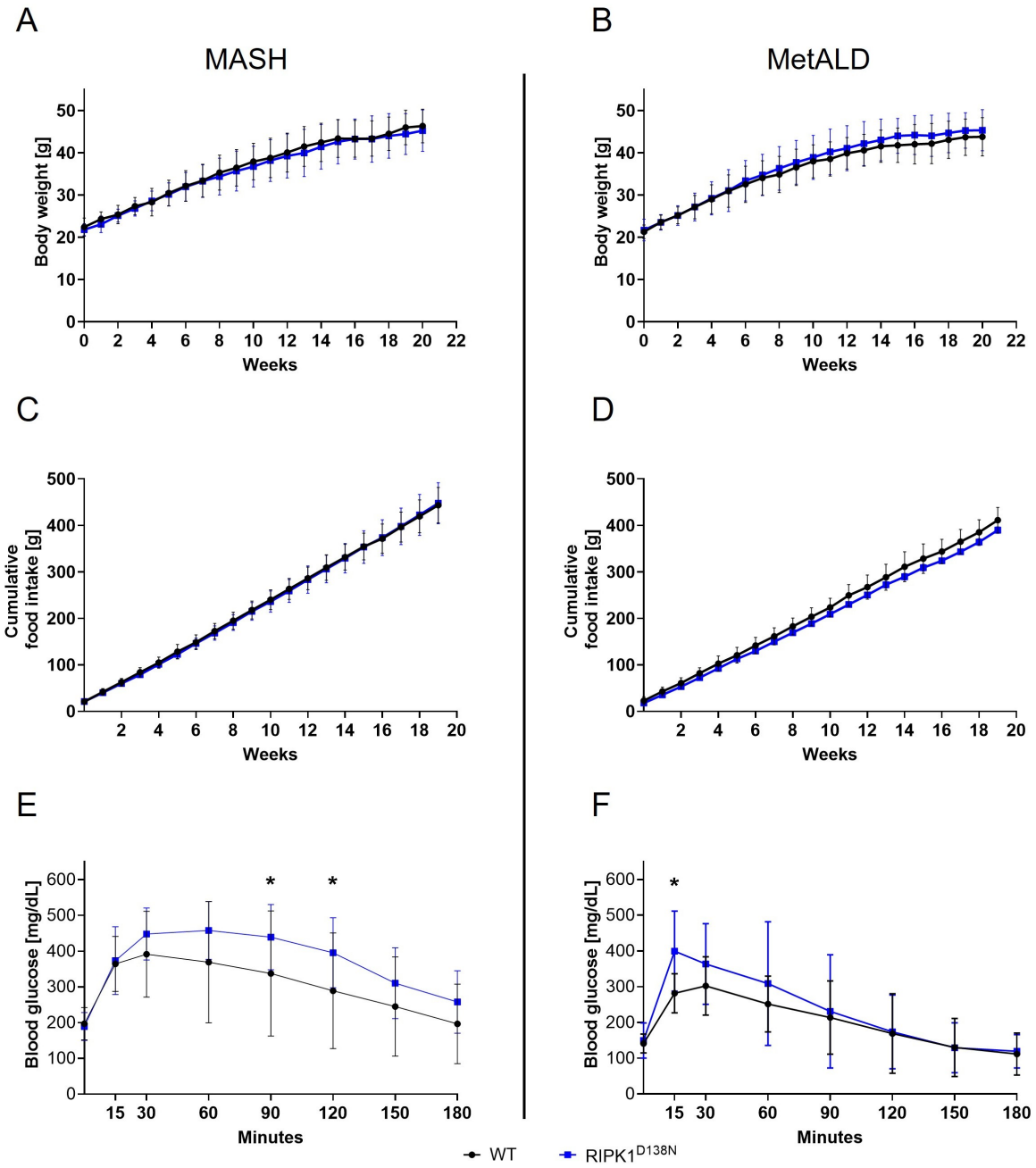

Figure 27: Inhibition of RIPK1 kinase activity through genetic mutation has no impact on body weight gain or glucose response in MASH or MetALD cohort. Body weight gain of WT and RIPK^{D138N} receiving (A) a WD (MASH cohort) or (B) a WD with 10% (v/v) alcohol (MetALD cohort) for 20 weeks with according cumulative food intake in (C) and (D). Results of glucose tolerance test of animals 16 weeks on (E) WD or (F) WD + 10% (v/v) alcohol. Values are mean ± SD. Statistical analyses were done by an ordinary two-way ANOVA test with an uncorrected Fisher´s LSD.

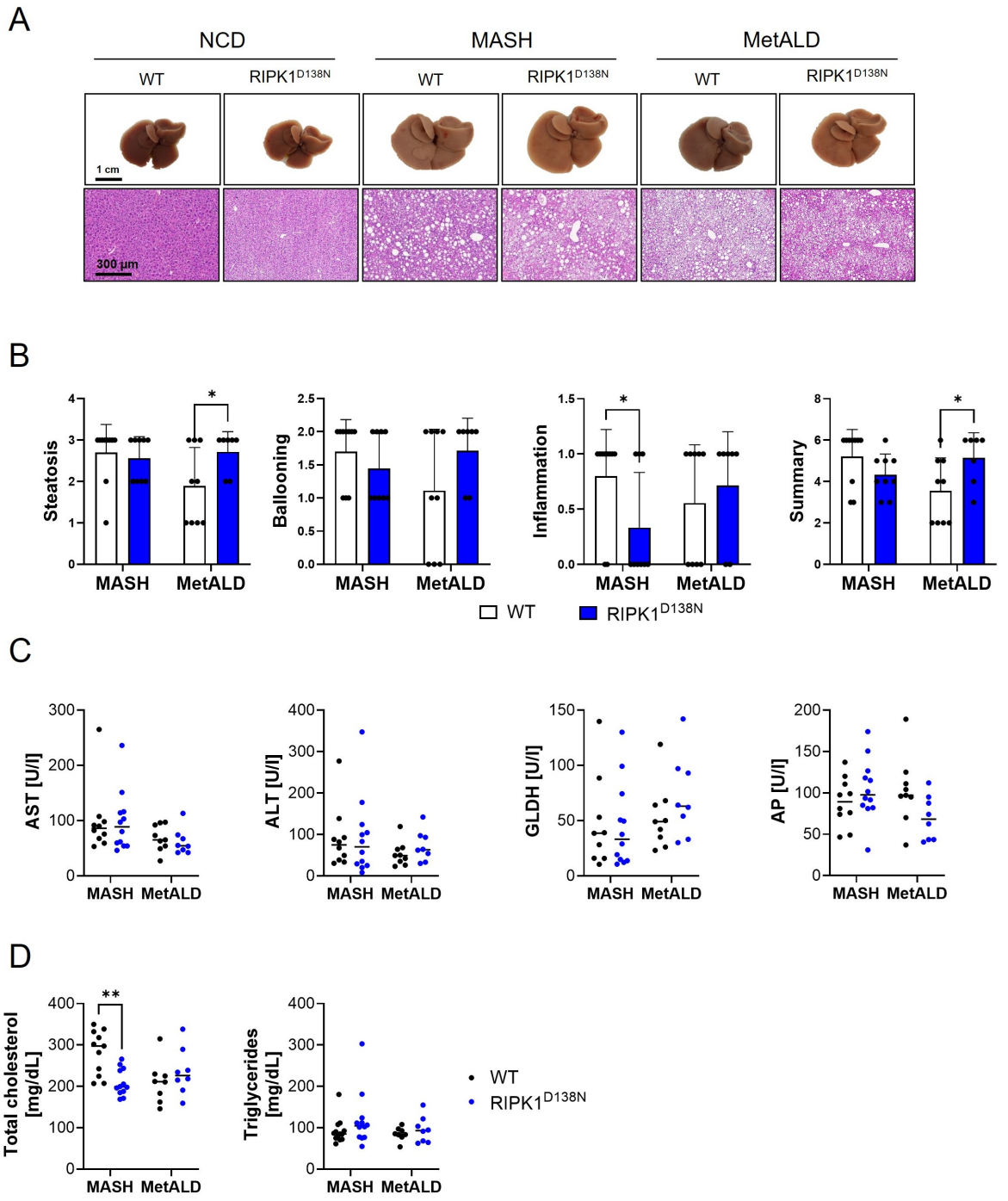

Figure 28: RIPK1 kinase dead animals show no protective effect on liver damage. (A) Exemplary macroscopic pictures of livers of 26-28 week-old animals with corresponding H&E staining liver. (B) Single parameters and summary of NAS score from livers of 26-28 week-old experimental animals. (C) Liver damage markers AST, ALT, GLDH and AP in [U/l] measured in blood serum. (D) Analysis of lipid metabolism markers total cholesterol and triglycerides in [mg/dL] in blood serum of experimental animals. Values are mean ± SD. Statistical analyses was done by an ordinary two-way ANOVA test with an uncorrected Fisher´s LSD. *p<0.05; **p<0.01

6.4 List of contributions

The following results presented were conducted partially by my former master´s student and mostly by myself, as shown in Table 19.

Table 19: List of people contributing to experiments in this thesis. If not declared otherwise, the experiments were performed by the author himself. **MTS**: M.Sc. Michael Thaddäus Singer (author), **AY**: M.Sc. Lea Aylin Yücel.

Figure	Experiment	Performed by
Figure 10A	Live cell imaging of Fibroblasts	AY
Figure 24	qPCR analysis of MASH cohort (liver)	AY
Figure 25A,B	FA uptake assay in primary hepatocytes	AY, MTS

6.5 Eidesstattliche Erklärung

Ich, Michael Thaddäus Singer, erkläre hiermit, dass diese Dissertation und die darin dargelegten Inhalte die eigenen sind und selbstständig, als Ergebnis der eigenen originären Forschung, generiert wurden.

Hiermit erkläre ich an Eides statt:

1. Diese Arbeit wurde vollständig oder größtenteils in der Phase als Doktorand dieser Fakultät und Universität angefertigt.
2. Sofern irgendein Bestandteil dieser Dissertation zuvor für einen akademischen Abschluss oder eine andere Qualifikation an dieser oder einer anderen Institution verwendet wurde, wurde dies klar angezeigt.
3. Wenn immer andere eigene oder Veröffentlichungen Dritter herangezogen wurden, wurden diese klar benannt.
4. Wenn aus anderen eigenen oder Veröffentlichungen Dritter zitiert wurde, wurde stets die Quelle hierfür angegeben. Diese Dissertation ist vollständig meine eigene Arbeit, mit der Ausnahme solcher Zitate.
5. Alle wesentlichen Quellen von Unterstützung wurden benannt.
6. Wenn immer ein Teil dieser Dissertation auf der Zusammenarbeit mit anderen basiert, wurde von mir klar gekennzeichnet, was von anderen und was von mir selbst erarbeitet wurde.
7. Kein Teil dieser Arbeit wurde vor deren Einreichung veröffentlicht.

Düsseldorf, den 16.03.2026

Michael Thaddäus Singer

6.6 Acknowledgements

Zu guter Letzt möchte ich mich bei allen bedanken, die mich über die Jahre auf dieser Reise begleitet haben.

Zu allererst geht mein Dank an Prof. Dr. med Tom Lüdde, der mir durch die Aufnahme in seine Arbeitsgruppe die Möglichgkeit gegeben hat diese Arbeit anzufertigen und über die Jahre hinweg die Wissenschaft mit all seinen Facetten kennenlernen zu dürfen. Vielen Danke für fünf spannende Jahre.

Des Weiteren geht mein Dank an Univ. Prof. Dr. med Mathias Hornef für die Übernahme des Erstgutachtens meiner Doktorarbeit.

Auch meinen direkten BetreurInnen PD Dr. Mihael Vucur und Dr. Anne Theres Schneider möchte ich für die Betreuung der Arbeit im Labor herzlich danken. Ob mehrfachen Umzug des ganzen Labors oder der direkte Notfall an der Bench, man konnte immer auf helfende Hände zählen.

In diesem Zuge danke ich auch nochmals allen KollegInnen der ganzen Abteilung der Gastroenterologie, Hepatologie und Infektiologie. Ob Raucherpäuschen, Fütterungssession, Revierkampf um die Mittagszeit oder doch mal beim gemeinsamen Bierchen trinken. Immer habe ich mich willkommen gefühlt und gewusst, dass man immer auf euch zählen kann, wenn die Bude brennt. Das gilt natürlich auch ganz besonders meinen beiden Masterandinnen Aylin und Parisa. Dank euch konnte ich die Wissenschaft nochmals von einer ganz anderen Seite kennenlernen und bin sehr dankbar, euch ein Stück auf eurer erfolgreichen Reise, die noch vor euch steht, begleitet haben zu dürfen. Ein ganz besonderer Dank geht natürlich auch an Lena und Veronika. Von Aachen bis Düsseldorf, und vielleicht noch viel weiter. Danke für die tollen und vielen Stunden in Labor, Büro und drüber hinaus.

Auch an meine liebgewonnene Frühbesprechung: Anna, Carolin, Leonie und Matthias. Morgenstund hat Gold im Mund, oder vielleicht auch einfach nur ein Eierbrötchen mit ein klein wenig zu viel Remmo. Auch ohne euch wäre es nicht das Gleiche gewesen.

Am Ende des Tages geht ein riesiges Dankeschön an alle FreundInnen, die in den langen Jahren wahrscheinlich nicht unbedingt nur von Erfolgen und Höhenflügen zu hören bekommen haben. Danke, dass ihr dann doch immer da wart und mir zur Seite standet.

Besonders dankbar bin ich auch dir, Tobi, der Ruhepol und der kühle Kopf der mich in vielerlei Hinsicht immer wieder auf den Boden zurückgeholt hat und mir immer wieder die ein oder andere Alternativkarriere ausgeredet hat.

Zu guter Letzt möchte ich mich bei meiner Mutter bedanken. Ohne dich, deinen imaginären Schuh, deine Arbeitsmoral, Fleiß und den gewissen Schneid den du mir mit auf den Weg gegegen hast, wäre ich wohl auch nie dort gelandet, wo ich es jetzt bin. Vielen, vielen Dank dir, dass du uns immer alles ermöglichst und viel zu oft selbst dafür zurückgesteckt hast.

DANKE!